


8-2014

# Impedance Biosensors for the Rapid Detection of Viral and Bacterial Pathogens Using Avian Influenza Virus Subtypes H5N1 and H7N2 and Escherichia coli O157:H7 as Model Targets

Jacob David Lum

*University of Arkansas, Fayetteville*

Follow this and additional works at: <http://scholarworks.uark.edu/etd>

 Part of the [Biomedical Devices and Instrumentation Commons](#), [Cell Biology Commons](#), [Pathogenic Microbiology Commons](#), and the [Virology Commons](#)

---

## Recommended Citation

Lum, Jacob David, "Impedance Biosensors for the Rapid Detection of Viral and Bacterial Pathogens Using Avian Influenza Virus Subtypes H5N1 and H7N2 and Escherichia coli O157:H7 as Model Targets" (2014). *Theses and Dissertations*. 2213.  
<http://scholarworks.uark.edu/etd/2213>

This Dissertation is brought to you for free and open access by ScholarWorks@UARK. It has been accepted for inclusion in Theses and Dissertations by an authorized administrator of ScholarWorks@UARK. For more information, please contact [scholar@uark.edu](mailto:scholar@uark.edu), [ccmiddle@uark.edu](mailto:ccmiddle@uark.edu).

Impedance Biosensors for the Rapid Detection of Viral and Bacterial Pathogens Using Avian Influenza Virus Subtypes H5N1 and H7N2 and *Escherichia coli* O157:H7 as Model Targets

Impedance Biosensors for the Rapid Detection of Viral and Bacterial Pathogens Using Avian Influenza Virus Subtypes H5N1 and H7N2 and *Escherichia coli* O157:H7 as Model Targets

A dissertation submitted in partial fulfilment  
of the requirements for the degree of  
Doctor of Philosophy in Cell and Molecular Biology

By

Jacob David Lum  
University of Arkansas- Monticello  
Bachelor of Science in Biology, 2008  
University of Arkansas  
Master of Science in Cell and Molecular Biology, 2010

August 2014  
University of Arkansas

This dissertation is approved for Recommendation to the Graduate Council

---

Dr. Yanbin Li  
Dissertation Director

---

Dr. Gisela Erf  
Committee Member

---

Dr. David McNabb  
Committee Member

---

Dr. Billy Hargis  
Committee Member

---

Dr. Byung-Whi Kong  
Committee Member

## Abstract

This research investigated impedance biosensors for the rapid detection of viral and bacterial pathogens using avian influenza virus (AIV) subtypes H5N1 and H7N2 and *Escherichia coli* O157:H7 as the model targets, which were chosen due to their impact on the agricultural and food industries. For the detection of AIV H7N2, a single stranded DNA aptamer was selected using systematic evolution of ligands by exponential enrichment (SELEX). The selected aptamer and a previously selected aptamer against AIV H5N1 were used in a microfluidics chip with an embedded interdigitated array microelectrode to fabricate an impedance biosensor for specific detection of AIV H7N2 and H5N1. The developed label-free biosensor was capable of detecting AIV H7N2 and H5N1 at a concentration down to  $2^7 \times 10^{-4}$  hemagglutination units (HAU) in 30 min without sample pre-treatment, comparable to previously designed biosensors though with the advantage of DNA aptamers. Two impedance biosensors based on the use of screen-printed interdigitated electrodes were developed for the detection of *E. coli* O157:H7. The first was a label-free biosensor based on magnetic separation and concentration of target bacteria using antibody-labelled magnetic nanobeads and Faradic impedance measurement. It was capable of detecting 1400 cells or more of *E. coli* O157:H7 in a total detection time of 1 h. COMSOL Multiphysics software was used to analyze the biosensor using a simplified model and determine the role of the magnetic nanobeads in the impedance measurement. The second biosensor for detection of *E. coli* O157:H7 was based on aptamer-labeled magnetic nanobeads and glucose oxidase/Concanavalin A-coated gold nanoparticle labels. This biosensor was capable of detecting 8 cells or more of *E. coli* O157:H7 in 1.5 h. The lower detection limit of the developed impedance biosensor was comparable to the most sensitive biosensors published for the detection of *E. coli* O157:H7 and was also more rapid and more practical for in-field tests.

Multiple impedance biosensor designs were developed in this research. The developed biosensor for AIV could conceivably be adapted for detection of other AIV subtypes and the developed *E. coli* O157:H7 biosensors could easily be adapted to detect different bacterial pathogens.

**Keywords:** Impedance biosensor; avian influenza; *E. coli*; aptamers; magnetic nanoparticles

## **Acknowledgements**

I would like to begin by thanking my advisor, Dr. Yanbin Li, for his support and encouragement throughout my graduate education. He allowed me the freedom and space to grow as a researcher though was never too far away to provide constructive feedback and advice. I also thank him for sharing his research experience and insights with me. During my graduate studies he has always led by example through his dedication and passion for research. The lessons he has taught me will always be with me throughout my career.

I also want to thank my advisory committee members, Dr. Billy Hargis, Dr. Gisela Erf, Dr. David McNabb and Dr. Byung-Whi Kong. I appreciate the advice and help that they were always able to find time for.

I want to thank the research groups that collaborated with us throughout the research: Dr. Steve Tung and his research group at the University of Arkansas for fabrication of the microfluidics chips; Dr. Huaguang Lu of Penn State University for providing non-target viruses; and Aibit, LLC for providing the screen-printed electrodes.

Also I thank the research group for their support: Dr. Ronghui Wang for her knowledge and advice on all things research related; Lisa Kelso for her help in taking EM pictures; Dr. Yingchun Fu for his advice and friendship; Zach Callaway for his help with the COMSOL software; and Kentu Lassiter, who has not only taught me everything I know about lab work and continues to do so, but also has provided me with an invaluable friendship. I also want to thank the rest of the research group whose friendship and camaraderie will never be forgotten.

I want to thank the Department of Biological and Agricultural Engineering, Department of Poultry Science and the Cell and Molecular Biology Program for supporting my graduate studies. I would also like to thank the Center of Excellence for Poultry Science and all who work there for providing the infrastructure and support for my graduate career. I want to especially thank Donna Delozier, whose frequent lunches and snacks made the days so much better.

This research was made possible by a grant from USDA/NRI (project #2009-35603-05063) and Arkansas Biosciences Institute. They have my deepest gratitude for their financial support.

I want to thank my grandparents, whose support and never-ending faith in me has motivated me to be the best I can be.

Finally and most importantly, I thank my parents for everything they have done for me. Their love, support and encouragement has been unending my entire life and I know I would have never made it this far without them. I am lucky to have such amazing parents and the credit and thanks they deserve is more than can be put into words.

## Table of Contents

<b>Chapter 1 Introduction.....</b>	<b>1</b>
<b>Chapter 2 Objectives.....</b>	<b>4</b>
<b>Chapter 3 Review of Literature.....</b>	<b>6</b>
3.1 Detection methods for viral and bacterial pathogens.....	6
3.1.1 Conventional methods for detection of avian influenza virus.....	6
3.1.2 Conventional methods for detection of <i>E. coli</i> O157:H7.....	9
3.2 Biosensors.....	11
3.2.1 Impedance biosensors.....	16
3.2.1.1 Interdigitated microelectrode arrays in impedance biosensors.....	19
3.2.2 Impedance biosensors for detection of avian influenza virus.....	20
3.2.2 Impedance biosensors for detection of <i>E. coli</i> O157:H7.....	21
3.3 Nucleic acid aptamers.....	23
3.3.1 Aptamer selection.....	26
3.3.2 Aptamers used in the detection of avian influenza virus.....	30
3.3.3 Aptamers used in the detection of <i>E. coli</i> O157:H7.....	31
3.4 Aptamer-based biosensors.....	31



3.4.1 Aptamer-based biosensors for the detection of avian influenza virus.....	32
3.4.2 Aptamer-based biosensors for the detection of <i>E .coli</i> O157:H7.....	32
3.5 Magnetic nanoparticles and immunomagnetic separation.....	33
3.6 References.....	34
<b>Chapter 4 In vitro selection of DNA aptamers against avian influenza subtype H7.....</b>	<b>40</b>
4.1 Abstract.....	40
4.2 Introduction.....	41
4.3 Materials and methods.....	43
4.3.1 Target protein and viruses.....	43
4.3.2 DNA library.....	44
4.3.3 In vitro selection of aptamers.....	44
4.3.4 PCR amplification and regeneration of ssDNA library.....	45
4.3.5 Dot blot analysis.....	46
4.3.6 Plasmid cloning and sequencing.....	47
4.4 Results and discussion.....	48
4.4.1 Aptamer pool affinity and specificity during selection using dot blot analysis.....	48
4.4.2 Aptamer cloning and sequencing.....	50

4.4.3 Evaluation of DNA aptamers using Dot blot analysis.....	52
4.5 Conclusion.....	52
4.6 References.....	54
<b>Chapter 5 An impedance aptasensor with microfluidic chips for rapid and specific detection of avian influenza viruses H5N1 and H7N2.....</b>	<b>55</b>
5.1 Abstract.....	55
5.2 Introduction.....	56
5.3 Materials and methods.....	59
5.3.1 Materials.....	59
5.3.2 Microfluidics biochips with embedded interdigitated microelectrodes.....	60
5.3.3 Aptamer immobilization.....	61
5.3.4 AIV detection.....	64
5.3.5 Electron microscopy.....	64
5.3.6 Statistical analysis.....	65
5.4 Results and discussion.....	65
5.4.1 Characterization of impedance data.....	65
5.4.2 Detection of AIV H7N2 and H5N1.....	73

5.4.3 Specificity of the aptasensor in detection of AIV H7N2 and H5N1.....	79
5.5. Conclusion.....	81
5.6 References.....	82
<b>Chapter 6 A label-free impedance biosensor using screen-printed interdigitated electrodes and magnetic nanobeads for the detection of <i>E. coli</i> O157:H7.....</b>	<b>85</b>
6.1 Abstract.....	85
6.2 Introduction.....	86
6.3 Materials and methods.....	88
6.3.1 Bacterial culture.....	88
6.3.2 Biological and chemical reagents.....	88
6.3.3 Screen-printed interdigitated electrodes and magnetic nanobeads.....	88
6.3.4 Impedance measurement.....	91
6.3.5 Immunomagnetic separation of <i>E. coli</i> O157:H7.....	91
6.3.6 Detection of <i>E. coli</i> O157:H7.....	91
6.3.7 Equivalent circuit modeling and statistical analysis.....	93
6.3.8 Electron microscopy.....	93
6.4 Results and discussion.....	93

6.4.1 Characterization of impedance spectrum data.....	93
6.4.2 Detection of <i>E. coli</i> O157:H7.....	98
6.5 Conclusion.....	105
6.6 References.....	105
<b>Chapter 7 An impedance aptasensor for rapid detection of <i>E. coli</i> O157:H7 using screen-printed interdigitated electrodes and GOx/Con A-labeled gold nanoparticles.....</b>	<b>107</b>
7.1 Abstract.....	107
7.2 Introduction.....	108
7.3 Materials and methods.....	111
7.3.1 Culture and plating of bacteria.....	111
7.3.2 Materials.....	111
7.3.3 Screen-printed interdigitated electrodes.....	112
7.3.4 Preparation of GOx/ConA gold nanoparticles.....	114
7.3.5 Magnetic separation of <i>E. coli</i> O157:H7 with aptamer-coated beads.....	114
7.3.6 Detection of <i>E. coli</i> O157:H7 using GOx/ConA gold nanoparticle labels.....	115
7.3.7 Environmental scanning electron microscopy.....	117
7.4 Results and discussion.....	118

7.4.1 Characterization of impedance spectrum data.....	118
7.4.2 Detection of <i>E. coli</i> O157:H7.....	122
7.4.3 Specificity of the aptasensor.....	126
7.5 Conclusion.....	127
7.6 References.....	128
<b>Chapter 8 Conclusion.....</b>	<b>130</b>
<b>Chapter 9 Recommendations for Future Research.....</b>	<b>135</b>

**List of Tables**

**Table 5.1.** Contributions of the elements in the equivalent circuit to the impedance magnitude. Impedance magnitude values were calculated using simulated data from fitting the equivalent circuit to measured data gathered in the detection of  $2^7 \times 10^{-1}$  HAU of AIV H5N1 and H7N2.....72

**Table 7.1.** Contributions of the elements in the equivalent circuit to the impedance magnitude. Impedance magnitude values were calculated using simulated data from fitting the equivalent circuit to measured data gathered in the detection of an *E. coli* O157:H7 sample containing  $10^5$  cfu ml<sup>-1</sup> cells.....122

## List of Figures

<b>Fig. 3.1.</b> Secondary structures of DNA aptamers against avian influenza virus H5N1 (Wang et al., 2013).....	24
<b>Fig. 4.1.</b> Aptamer pool affinity after the (a) 4 <sup>th</sup> and (b) 12 <sup>th</sup> SELEX rounds.....	49
<b>Fig. 4.2.</b> Aptamer pool specificity at round (a) 4 and (b) 12.....	50
<b>Fig. 4.3.</b> Secondary structures of (a) aptamer #1, (b) aptamer #2, and aptamer #3 as given by UNAFold software.....	51
<b>Fig 5.1.</b> (a) Microfluidics biochip with an embedded gold interdigitated array with electrode connections and sample injection port. (b) Close up of interdigitated microelectrode array with PDMS microfluidics flow chamber.....	61
<b>Fig. 5.2.</b> Design of the impedance aptasensors for the detection of AIV subtype H7N2 and AIV H5N1. (a) The microelectrode surface was modified using streptavidin. (b) Biotin-labelled aptamer was then immobilized through biotin-streptavidin binding. (c) Target AIV was captured and the impedance was measured. After each step the flow cell was washed to remove unbound particles.....	63
<b>Fig. 5.3.</b> Typical impedance magnitude data of the tests on (a) AIV H7N2 and (b) AIV H5N1. Typical phase angle data of the tests on (c) AIV H7N2 and (d) AIV H5N1. Data labels correspond to serial dilution value of 2 <sup>7</sup> HAU virus sample ( $2^7 \times 10^{-1}$ ... $2^7 \times 10^{-5}$ ). Frequency range was from 1 Hz to 1 MHz. Amplitude of voltage, 100 mV.....	67

**Fig. 5.4.** Typical phase angle data of the tests on (c) AIV H7N2 and (d) AIV H5N1. Data labels correspond to serial dilution value of  $2^7$  HAU virus sample ( $2^7 \times 10^{-1} \dots 2^7 \times 10^{-5}$ ). Frequency range was from 1 Hz to 1 MHz. Amplitude of voltage, 100 mV.....68

**Fig. 5.5.** (a) Equivalent circuit used for data analysis. The equivalent circuit components were resistance of the solution ( $R_s$ ), resistance of PDMS ( $R_{pdms}$ ), double layer capacitance ( $C_{dl}$ ), and geometrical capacitance ( $C_g$ ). (b) Bode diagram of measured impedance data and simulated impedance data generated by curve fitting of equivalent circuit. Measured data taken with  $2^7 \times 10^{-1}$  HAU H5N1 virus sample.....70

**Fig. 5.6.** Average impedance change caused by different concentrations of (a) AIV H7N2 and (b) AIV H5N1. The values of horizontal axis correspond to serial dilution value of  $2^7$  HAU virus sample ( $2^7 \times 10^{-1} \dots 2^7 \times 10^{-5}$ ). Error bars based on the standard deviation of means in triplicate tests. LDL line was determined by signal/noise ratio of 3. The impedance was measured at the frequency of 25.8 kHz.....75

**Fig. 5.7.** ESEM micrographs of the electrode surface with immobilized aptamers (a) before and (b) after AIV capture.....78

**Fig. 5.8.** Average impedance change caused by  $2^7 \times 10^{-1}$  HAU target and three non-target virus at 25.8 kHz in the detection of (a) H7N2 and (b) H5N1. Error bars based on the standard deviation of means in triplicate tests. LDL line was determined by signal/noise ratio of 3.....80

**Fig. 6.1.** (a) A photograph of the screen printed electrode and (b) drawing of the interdigitated electrode. Dimensions are given in millimeters.....90



<b>Fig. 6.2.</b> Immunomagnetic separation of <i>E. coli</i> O157:H7 from media using the antibody-coated nanobeads and the concentration of bacteria on the electrode surface using a magnetic field.....	92
<b>Fig. 6.3.</b> A typical Bode plot of the measured impedance data of the control and <i>E. coli</i> O157:H7 at a concentration of $10^7$ cfu ml <sup>-1</sup> . (a) Impedance magnitude and (b) Phase angle. Frequency range was 10 Hz to 100 kHz. The amplitude of voltage applied was 50 mV.....	95
<b>Fig. 6.4.</b> (a) Equivalent circuit used for data analysis. The equivalent circuit components were bulk electrolyte ( $R_{sol}$ ), electron transfer resistance ( $R_{et}$ ), resistance due to surface roughness ( $R_{sur}$ ), double layer capacitance ( $C_{dl}$ ), capacitance of bacterial cells ( $C_{mem}$ ), and a Warburg impedance element ( $Z_w$ ). (b) Bode diagram of measured impedance data and simulated impedance data generated by curve fitting of equivalent circuit. Measured data was taken with a sample containing $10^7$ cfu ml <sup>-1</sup> <i>E. coli</i> O157:H7.....	97
<b>Fig. 6.5.</b> Average impedance change between the control and bacteria measurements at 100 Hz for <i>E. coli</i> O157:H7. Error bars were based on the standard deviation of means in triplicate tests. LDL line was determined by signal/noise ratio of 3.....	99
<b>Fig. 6.6.</b> ESEM photographs of (a) free <i>E. coli</i> O157:H7 cells and an <i>E. coli</i> O157:H7 cell captured by antibody-coated nanobeads.....	100
<b>Fig. 6.7.</b> Capture efficiency of $10^5$ cfu ml <sup>-1</sup> <i>E. coli</i> O157:H7 using different amounts of antibody-coated magnetic nanobeads.....	101
<b>Fig. 6.8.</b> Average impedance change between the pure redox probe and pure antibody-coated nanobeads under a magnetic field and pure <i>E. coli</i> O157:H7 and average impedance change	

between a control sample and *E. coli* O157:H7 and nanobeads with a magnetic field at 100 Hz. Error bars were based on the standard deviation of means in triplicate tests. LDL line was determined by signal/noise ratio of 3, where noise was defined as the standard deviation of the pure redox probe measurements. ....102

**Fig. 6.9.** (a) COMSOL model of simplified biosensor system with a pair of electrodes and 100 cells of *E. coli* evenly distributed on the electrode surfaces and the space between and (b) simulated impedance magnitude percent changes at different distances between the electrode surface and the *E. coli* cells.....104

**Fig. 7.1.** (a) A photograph of the screen printed electrode and (b) drawing of the interdigitated electrode. Dimensions are given in millimeters.....113

**Fig. 7.2.** Diagram of the (a) magnetic separation with aptamer-coated beads, (b) labeling of *E. coli* O157:H7 cells with GOx/ConA gold nanoparticles, and (c) impedance measurement.....116

**Fig. 7.3.** Bode plot of impedance measurement of *E.coli* O157:H7 sample containing  $10^5$  cfu ml<sup>-1</sup> cells. 38 points were measured at frequencies from 100 kHz to 10 Hz. The voltage amplitude was 5 mV.....119

**Fig. 7.4.** (a) Equivalent circuit model for impedance aptasensor. The equivalent circuit components were bulk electrolyte resistance ( $R_{sol}$ ), double layer capacitance ( $C_{dl}$ ), capacitance of solution ( $C_g$ ). (b) Bode plot of measured and fitted data. Measured data was taken using *E. coli* O157:H7 sample containing  $10^5$  cfu ml<sup>-1</sup> cells.....120

**Fig. 7.5.** Average impedance change at 1 kHz between 0 min and 30 min after introduction of glucose solution for detection of *E. coli* O157:H7. Error bars were based on the standard deviation of means in triplicate tests. LDL line was determined by signal/noise ratio of .....123

**Fig. 7.6.** Average impedance change at 1 kHz between 0 min and 30 min after introduction of glucose solution for specificity tests. Error bars based on the standard deviation of means in triplicate tests. LDL line was determined by a signal/noise ratio of 3.....127

## 1. Introduction

Traditional methods for microbial detection and identification, such as culturing, serological tests, microscopy, and polymerase chain reaction, are time and resource consuming and require specialized laboratories and facilities. In the past decade biosensors have become a promising alternative to these traditional methods due to their ability to rapidly, sensitively, and specifically detect a large number of targets such as cells, bacteria, viruses, organic molecules, and many other analytes. Biosensors consist of a transducer, a signal processor, and a biological sensing element, which can include antibodies, aptamers, enzymes, or even whole cells. Impedance biosensors, a class of electrochemical biosensors, rely on changes in the electrochemical makeup around an electrode to detect a target. They show promise in point-of-care applications due to their ease of miniaturization, low cost, and low power requirements.

Many previously designed biosensors rely on antibodies as the biological recognition element, which have several drawbacks. Antibodies are sensitive to thermal and chemical degradation, must be made in animals over the course of several months, and can only be made against immunogenic compounds. Nucleic acid aptamers are artificial oligonucleotides (DNA or RNA) that can bind to a broad range of targets. In diagnostic and detection assays, aptamers represent an alternative to antibodies as recognition agents due to their greater thermal and chemical stability, lower cost, and simpler production. When used in conjunction with impedance biosensors they also have added advantages such as greater uniformity and smaller size, leading to greater sensitivity and higher repeatability.

In this research, impedance biosensors were developed for the detection of viral and bacterial pathogens using avian influenza viruses H5N1 and H7N2 for the model virus targets

and *E. coli* O157:H7 as the model bacterial target. The model targets were chosen for their significant impact on the agricultural and food safety fields.

Avian influenza viruses have a large impact on the poultry each year and also represent a threat to human health. Rapid in-field detection or screening is necessary to prevent future outbreaks and monitor and control current outbreaks. Traditional detection methods, such as RT-PCR and virus isolation, are time consuming and require specialized personnel and facilities. Current biosensors for AIV lack specificity, sensitivity, or require labels to amplify the signal. Also most developed biosensors rely on antibodies, which suffer from low thermal and chemical stability. For this reason, aptamer-based biosensor (aptasensor) would be superior to an antibody-based sensor (immunosensor) for potential in-field tests. A DNA aptamer was developed for avian influenza virus hemagglutinin subtype H7 in this research and used along with a previously developed aptamer for avian influenza virus H5N1 in developing an impedance biosensor based on a microfluidics chip with an embedded interdigitated array microelectrode. The developed biosensor was capable of detecting AIV H5N1 and AIV H7N2 at a lower detection limit of  $2^7 \times 10^{-4}$  hemagglutination units (HAU) in 30 min with no labels or signal amplification.

The bacteria *E. coli* O157:H7 is one of the most dangerous foodborne pathogens, having a low infectious dose (~10 cells) and causing an estimated 63,000 illnesses a year in the United States. In addition to the health impact, *E. coli* O157:H7 also has a large economic impact, causing food product recalls each year that result in millions of dollars of direct costs plus income loss due to lost consumer trust. Current methods for *E. coli* O157:H7 detection may take days to get results, during which time production may have to be shut down or contaminated food products may be shipped out. Two rapid, specific, and inexpensive biosensors based on screen-printed interdigitated electrodes were developed. The first was a Faradic impedance

biosensor using antibody-coated magnetic nanobeads to capture *E. coli* O157:H7 cells and concentrate them on the electrode surface. This biosensor had a lower detection limit of ~1400 cells and could detect them in 30 min. The second biosensor developed for the detection of *E. coli* O157:H7 was non-Faradic and based on the use of aptamer-coated magnetic nanobeads and glucose oxidase/Concanavalin A gold nanoparticle labels. The glucose oxidase/Concanavalin A labels were used to oxidize a 10 mM glucose solution, reducing the impedance of the system. The biosensor was capable of detecting 8 cells of *E. coli* O157:H7 in 1.5 h.

The biosensors developed in this research have the potential to be adapted to detect other viral and bacterial pathogens. The biosensors could also be fully developed into a portable biosensor for in-field tests.

## 2. Objectives

The overall goal of this research is to develop impedance biosensors for the rapid detection of viral and bacterial pathogens using avian influenza virus subtypes H5N1 and H7N2 and *Escherichia coli* O157:H7 as model targets. The objective of this research concerning viral pathogens was to select a ssDNA aptamer against avian influenza virus hemagglutinin subtype H7 and use the developed aptamer along with a previously developed aptamer against avian influenza virus H5N1 in a microfluidics based impedance biosensor for detection of avian influenza H5N1 and H7.

The objective of the bacterial pathogen section of this research was to develop two biosensors based on the use of inexpensive and reusable screen-printed interdigitated electrodes for the detection of *E. coli* O157:H7.

The specific objectives of this project were as follows:

1. To develop an impedance biosensor for the detection of avian influenza H5N1 and H7N2 based on the use of aptamers and microfluidics chips with embedded interdigitated array microelectrodes.

The specific sub-objectives of this research were:

- a. Develop an ssDNA aptamer against avian influenza virus hemagglutinin subtype H7.
- b. Use the developed H7 aptamer and a previous developed aptamer against H5N1 to develop an impedance aptasensor for avian influenza virus.

2. To develop an impedance biosensor based on the use of screen-printed interdigitated electrodes for the detection of *E. coli* O157:H7.

The specific sub-objectives of the research were:

- a. Develop a Faradic impedance biosensor based on immunomagnetic separation and concentration for *E. coli* O157:H7.
- b. Develop a non-Faradic impedance biosensor based on aptamer-coated magnetic nanobeads and glucose oxidase/Concanavalin A gold nanoparticle labels for the detection of *E. coli* O157:H7.



### **3. Review of the Literature**

#### **3.1 Detection methods for viral and bacterial pathogens**

Traditionally, detection and identification methods of viral and bacterial pathogens have depended on classification of phenotypic and physiological typing. These methods often involve culturing of the pathogen in a variety of conditions, such as specific cell lines, agar plates, or nutrient broths, followed by immunological tests and microscopy. While these methods have proven themselves to be powerful and are often still considered the gold standard detection method for many pathogens, they are often time- and labor-intensive and the results can often be subject to the user's interpretation. Modern molecular methods, such as polymerase chain reaction (PCR), enzyme-linked immunoassay (ELISA), and direct sequencing, are considerably more rapid, allow for many more samples to be tested at one time, and often result in more specific identification of the pathogen. A disadvantage of many molecular methods is that they do not allow for detection of unknown pathogens and, therefore, may miss pathogens closely related to the intended detection target.

##### **3.1.1 Conventional methods for detection of avian influenza virus**

Early identification of influenza viruses is essential for reducing the spread of avian influenza and controlling outbreaks (MacKay et al., 2008). The effectiveness of a detection technique depends on the specificity, sensitivity and time for detection. Cost, ease of use and portability are also factors in determining the practicality of a rapid detection method. Some of the current methods used in influenza detection include viral isolation culture, immunochromatographic strips, direct immunofluorescent assay, enzyme-linked immunoassay,

complement fixation, hemagglutinin-inhibition, and reverse-transcription-polymerase chain reaction (Amano and Cheng, 2005).

Viral isolation (VI) culture with immunological antigen conformation is considered the gold standard method for virus detection to which all other detection methods are compared (Leland and Ginocchio, 2007). Viral isolation for influenza viruses involves inoculating specific pathogen free (SPF) embryonated chicken eggs or cell cultures with a virus sample. Inoculation of eggs or tissue culture allows for the measurement of virus infectivity in either 50% Egg Infectious Dose per ml ( $EID_{50} \text{ ml}^{-1}$ ) or 50% Tissue Culture Infectious Dose per ml ( $TCID_{50} \text{ ml}^{-1}$ ). Viral isolation is followed by hemagglutination inhibition or serological tests for subtyping of the virus. Hemagglutination inhibition is based on antibody binding of hemagglutinin which hinders the ability to agglutinate of erythrocytes. The test consists of mixing a standard quantity of HA with serially diluted antisera and added erythrocytes to determine specific subtype of the HA antigen. Serological tests involve identifying the antibodies in blood serum which are secreted in response to challenge with avian influenza virus. Though viral isolation with immunological tests provides good sensitivity and is relatively inexpensive, it also requires long incubation times, specialized eggs or cell cultures, a high level of technical expertise, and is only useful for live viruses (Charlton et al., 2009).

Molecular detection techniques have begun to overcome the disadvantages of cell cultures, shortening detection times and decreasing the level of expertise required to use them. Reverse transcription-polymerase chain reaction (RT-PCR) is one molecular method which offers fast detection times and high sensitivity. RT-PCR amplifies segments of viral RNA for isolation and identification to determine the phylogeny of a virus and whether it is pathogenic strain or not. Because DNA is needed for PCR amplification the genomic RNA must first be

converted to DNA. This is done by using an enzyme called reverse transcriptase to convert the RNA segments into DNA copies (cDNA). The cDNA segments are then amplified using polymerase activity. DNA primers can be picked to allow for the detection of a selected HA by picking a well-conserved region of the HA gene (Dawson et al., 2006). Real time RT-PCR (rRT-PCR) is a method based on RT-PCR which utilizes fluorescent probes to detect specific gene fragments at the same time as gene amplification. Because the probes only report the DNA with the desired sequence, the specificity of rRT-PCR is significantly better than traditional RT-PCR. Also multiple fluorescent probes can be used to detect multiple genes simultaneously. Multiplex rRT-PCR assays can provide virus subtype information for both HA and NA antigens (Fereidouni et al., 2009; Yang et al., 2010). While rapid, specific and sensitive, RT-PCR methods have the disadvantages of being expensive, requiring specialized equipment and labs, high false positive rates, and consist of complicated procedures requiring extensive training (Ellis and Zambon, 2002). Other nucleic acid-based techniques, such as oligonucleotide hybridization and microarrays, have also shown promise in providing subtype identification (Fesenko et al., 2007; Gall et al., 2009a; Gall et al., 2009b).

Immunochromatographic strips rely on enzyme-labeled antibodies to influenza nucleoprotein bound to a membrane and reagents to cause a color change on a strip signifying the presence of virus. Immunochromatographic strip tests allow for simple and rapid detection (<30 min), but do not provide subtype information for the virus and have low sensitivity, requiring lab confirmation for any negative samples.

### **3.1.2 Conventional methods for detection of *E. coli* O157:H7**

Conventional bacterial identification methods typically rely on analysis of the bacterial biochemistry combined with morphological features of individual bacterial cells and bacterial colony morphology. The morphology of individual bacterial cells is usually done with simple light microscopy, often with the aid of various dyes and stains. These dyes and stains often serve a second purpose, such as giving clues to the biochemical makeup of the cell or highlighting certain morphological features that would go unnoticed without the stain. The most prominent example of these stains is the Gram stain, which can be used to divide bacteria into two groups, Gram-positive and Gram-negative, based on the presence or absence of a peptidoglycan layer in the cell wall (Budin et al., 2012). In situations where a more in-depth analysis of the bacterial morphology is needed, scanning electron microscopy (SEM) or atomic force microscopy (AFM) can be used. Though SEM and AFM are exceptionally more powerful than standard light microscopy, the sample preparation involved with both is time consuming and often alters the morphology of the bacteria cells being prepared (Trinidad et al., 2010).

While morphological analysis of bacteria is typically rapid and simple, it only provides a limited amount of information about a bacterial sample and is only an aid in bacterial identification, not an endpoint. Morphological analysis of an *E. coli* O157:H7 sample would only result in the knowledge that the bacteria are rod-shaped and Gram-negative. To further identify any bacteria, biochemical analysis has to be done. Growing bacterial cultures in selective or indicator media has been the gold standard method for biochemical analysis of bacteria for years. Selective media tests involve growing bacteria in selective broths or agars in which only the desired or suspected bacteria grow well. These selective media may contain antibiotics that certain bacteria are resistant to, or energy sources which only the desired bacteria are capable of

utilizing. Indicator media tests involve growing the bacteria on a substrate-containing compounds that can be broken down by certain bacterial enzymes. This normally results in a visible color change in the bacterial colonies or the surrounding media. Knowledge about where a bacterial sample was gathered and the likely bacterial suspects can help decide which selective or indicator media types would result in the most knowledge gathered. When using multiple selective media tests, it is possible to identify a bacterial culture or at least narrow down the range of possible bacterial suspects. Commercialized tests such as analytical profile index (API) strips provide an easy-to-read format for multiple biochemical tests, such as sugar fermentation, amino acid synthesis, and utilization of secondary carbon sources. Also other factors such as optimum growth temperature and aerobic/anaerobic requirements can help identify an unknown bacterial sample. Sorbitol-MacConkey agar (SMAC) is the most prevalent selective media used to identify *E. coli* O157:H7. It is a variant of the standard MacConkey agar, which is used to differentiate Gram-negative bacteria that are capable of lactose fermentation from those that are not capable. In SMAC the lactose is replaced with sorbitol, which is fermented by most *E. coli* species but not *E. coli* O157:H7. Sorbitol-fermenting *E. coli* species will produce colonies with a pink color while *E. coli* O157:H7 colonies will be colorless. The fermentation of sorbitol by the non-O157:H7 species reduces the pH resulting in the pink color of sorbitol-fermenting colonies. Since *E. coli* O157:H7 cannot utilize sorbitol it relies on the peptone in the growth media for sustenance, which increases the pH, resulting in yellow or no coloration. Selective and indicator media tests can also be followed up with serological tests to reach an even more specific identification of a bacterial sample. Though bacterial plating followed by serological tests is still considered the gold standard for bacterial identification, the culturing methods required are time-consuming and labor and resource intensive.

Modern molecular methods such as polymerase chain reaction (PCR) and 16S ribosomal sequencing offer much more rapid and specific results. PCR involves using DNA polymerase enzymes to amplify a small amount of DNA. A pair of short oligonucleotides known as primers is used to identify the target sequence to be amplified. The amplified DNA can then be further analyzed for sequence or size determination. The disadvantage of PCR is that the target must already be known so that specific primers can be used to amplify the DNA. Multiplex PCR can somewhat resolve this problem by having multiple primer pairs in each PCR reaction, though this is still limited to around 10 primer pairs (Hirota et al., 2011). Sequencing of the 16S ribosomal RNA can result in rapid and simple bacterial identification but it still has several drawbacks. Closely related species can be difficult to differentiate and misidentification can be a problem. Also for both PCR and 16S sequencing, a pure and clean sample is required and several hours of highly technical processing and preparation must be done (Spratt, 2004).

### **3.2 Biosensors**

The International Union of Pure and Applied Chemistry defines a biosensor as “a device that uses specific biochemical reactions mediated by isolated enzymes, immunosystems, tissues, organelles or whole cells to detect chemical compounds usually by electrical, thermal, or optical signals” (IUPAC, 2006). A biosensor consists of three components: biological element, transducing element, and a signal processing element.

Biosensors are able to detect a chemical or biological target through the reaction of the target with a specific biological recognition molecule. The biological material acts as the functional group of the sensor and may be an enzyme, antibody, protein, cell, virus, phage, organelle or nucleic acid probe. The interaction between the biological recognition material and

target analyte produces a biochemical change in the environment that the transducing element is able to detect through electrochemical, piezoelectric, mechanical, optical, thermal or magnetic measurements (Nayak et al., 2009). The signal from the transducer is sent to a signal processor to be turned into useable data. A biosensor can be categorized by their biological element (cell-based biosensor), transducing element (piezoelectric biosensor) or a combination of both (antibody-based electrochemical biosensor).

The biosensor research field began in the 1960s when the first biosensor, a glucose sensor, was proposed by Clark and Lyons at Children's Hospital in Cincinnati. Their device consisted of a layer of glucose oxidase enzyme immobilized over an oxygen sensor. The sensor would measure the amount of oxygen consumed by the enzymatic reaction and compare the measurement with a control electrode to determine the amount of glucose in a whole blood sample (Wang, 2001). Since their first development biosensor applications have expanded throughout the medical diagnosis field and also into the fields of environmental monitoring, agriculture, food safety, pharmaceutical screening, biodefense and even explosives detection (Rodriguez-Mozaz et al., 2004; Skottrup et al., 2008; Wang et al., 2009; Han et al., 2007; Smith et al., 2008). Biosensors offer the advantages of targeted specificity, fast response times, continuous data collection, simplified sample preparation and the capability to reproduce units (Deisingh and Thompson, 2004).

While biosensors of a wide variety of types have been developed for use in a range of applications three main biosensor types have been studied for use in microbial detection: piezoelectric, optical and electrochemical.

Piezoelectric biosensors utilize crystals capable of generating a piezoelectric field to detect mass changes in the sensing environment (Amano and Cheng, 2005). The crystal is sandwiched between two excitation electrodes which apply an electrical field that causes the crystal to undergo dimensional changes, or oscillations, at the crystals natural resonant frequency. An increase in the mass on the surface of the crystal, such as antibody immobilization or capture of antigen, decreases the resonant frequency. Piezoelectric biosensors are useful because they are low-cost, label-free, sensitive, and have extremely low detection levels (Amano and Cheng, 2005).

The most intensively studied piezoelectric biosensor is the quartz crystal microbalance, or QCM, which uses a thin wafer of quartz as the transducing crystal. Quartz crystals have the advantages of being widely available, relatively inexpensive, and durable (Bunde et al., 1998). QCM biosensors have been well studied for the detection of bacteria, viruses, cells, proteins and nucleic acids. Other techniques are often coupled with QCM to increase the performance and capability of the biosensor. QCM has been used to detect avian influenza label-free in nasal washings with a lower detection limit of  $10^4$  pfu ml<sup>-1</sup>, though with the addition of a gold nanoparticle conjugate the detection limit was reduced to  $10^3$  pfu ml<sup>-1</sup> which is comparable to the sensitivity and specificity of viral isolation techniques (Peduru Hewa et al., 2009). QCM DNA sensors have not been able to reach the lower detection limit or sensitivity of traditional gold standard methods but the use of mass enhancing nanoparticle labels have been shown to improve both the lower detection limit and the sensitivity of *E. coli* O157:H7 DNA detection (Mao et al., 2006). A detection method combining QCM and magnetic separation was shown effective in detecting biotin-streptavidin binding and demonstrated the feasibility of QCM as an on-line detection technique (Tsai et al., 2008).



Optical biosensors rely on visual phenomenon to detect the interaction between the biological element and the target analyte. Examples of optical biosensors include surface plasmon resonance (SPR), absorption, luminescence, and fluorescent sensors. Detection by optical biosensors can occur in two ways: by the analyte directly affecting the optical properties of the sensing environment, such as in SPR or absorption methods, or by the analyte being tagged with a label that produces an optical phenomenon, such as in fluorescence methods.

Of the optical methods requiring labels for detection, fluorescence is the most widely studied. Commonly used labels in fluorescent biosensors are dyes, quantum dots and fluorescent proteins, with the latter two becoming more popular as they are further researched (Medintz et al., 2005). Quantum dots are a type of semiconductor with a diameter typically between 2 to 10 nm whose excitons are confined in three spatial dimensions, giving them properties of both unconfined semiconductors and discrete molecules. Hahn et al. was able to use quantum dots in a flow cytometer to detect *E. coli* O157:H7 cells in a heterogeneous cell mixture of 1% *E. coli* O157:H7 (Hahn et al., 2008). Simultaneous detection of separate bacterial pathogens has been performed with the use of quantum dots, taking advantage of their narrow emission range and single excitation wavelength (Yang and Li, 2006). Fluorescent protein labels, such as green fluorescent protein (GFP) and its derivatives, have mainly been confined to the fields of proteomics and functional genomics though some research has been conducted using them in pathogen detection (VanEngelenburg and Palmer, 2008). In one study, the GFP gene was inserted into *Listeria monocytogenes* for the detection of bacteria inside of cells (Fortineau et al., 2000).

Label-free optical biosensors overcome some of the disadvantages of fluorescent labels, such as requiring extra steps and time and false positives and negatives (Cooper, 2002). SPR

biosensors measure the change in refractive index due to binding of biomolecules near the sensor surface. SPR biosensors have been shown to be effective in detecting bacteria, viruses and proteins rapidly, in real time and label-free (Phillips and Cheng, 2007). Estmer-Nilsson et al. (2010) was able to utilize SPR to quantify influenza virus for vaccine production via an antibody inhibition assay using HA proteins immobilized on the sensor surface.

Electrochemical biosensors use changes in the electrical properties caused by biochemical reactions to detect an analyte (Grieshaber et al., 2008). Electrochemical transducers offer several advantages: low cost, ease of miniaturization, low power requirements and simplicity of use (Pejcic et al., 2006). Electrochemical biosensors can be divided by the electrical parameter that they measure: amperometric, potentiometric, conductimetric, and impedimetric. Amperometric biosensors work by applying a constant potential across an electrode and measuring the current associated with either the reduction or oxidation of an electroactive species created by the interaction of the biological element and the analyte. Amperometric biosensors are often used with an enzyme capable of catalyzing the production of an ionic product, increasing the selectivity and the sensitivity (Lojou and Bianco, 2006). Potentiometric biosensors gather data by converting a biological reaction into a potential signal with the use of ion-selective electrodes (Koncki, 2007). Conductimetric biosensors simply measure the conductivity change in a medium caused by the analytes. Impedimetric biosensors measure a combination of the resistive and capacitive or inductive properties of a material in response to a small amplitude sinusoidal excitation signal (Varshney and Li, 2009).

Electrochemical biosensors have been well researched for detection of cells, bacteria, viruses, proteins, nucleic acid and chemicals. Electrochemical biosensors are showing promise in point-of-care cancer diagnosis, being able to detect cancer cells, cancer-related proteins and

specific mutations in DNA (Wang, 2006). Another research field in which electrochemical biosensors are prominent is food safety, which often requires working with complex media (Abu-Rabeah et al., 2009). Pohlmann successfully detected bacterial ribosomal RNA in a meat juice solution at a bacterial concentration equivalent to 500 cfu ml<sup>-1</sup> (Pohlmann et al., 2009). Electrochemical biosensors have also been used to inspect milk products for the presence of antibiotics (Davis and Higson, 2010). The most commonly used electrochemical biosensor is the glucose sensor, which is used by millions of diabetics everyday (Wang, 2008).

### **3.2.1 Impedance biosensors**

Impedance biosensors are a class of electrical biosensors that measure the electrical impedance of an interface in AC steady state with constant DC bias conditions. This is accomplished by imposing a sinusoidal voltage at a given frequency and measuring the current. This measurement can be done over a range of frequencies or at a given frequency (Daniels and Pourmand, 2007). Many impedance biosensors utilize a capture probe on the detecting surface to hold the target molecule, thereby stabilizing the point of detection. Due to the ease of miniaturization, low energy usage and relatively low cost impedance biosensors show promise for point-of-care applications.

Impedance ( $Z$ ) is defined as the total opposition a circuit offers to the flow of an alternating current at a given frequency. Four electrical parameters determine the value of impedance: resistance, capacitance, inductance, and angular frequency. The impedance is usually represented as a vector consisting of the resistance (real component,  $R$ ), which is not dependent on frequency, and the reactance (imaginary component,  $X$ ), which is dependent on frequency. The reactance portion of impedance consists of the capacitance ( $C$ ) and inductance ( $L$ )

parameters, though for electrochemical measurements the inductance parameter is often ignored due to its insignificant effect. The effect of capacitance on impedance will increase as the frequency decreases and this effect is measured as the phase angle shift ( $\phi$ ).

Impedance data is often presented in one of two forms: Nyquist plot or Bode plot. A Nyquist plot shows the real component (X axis) versus the imaginary component (Y axis). Nyquist plots are used when measuring Faradic impedance, which requires the use of a redox probe. A Bode plot is better suited to representing a non-Faradic impedance measurement, which relies on direct detection of the analyte and no redox probe. In a Bode plot the log of the frequency is plotted on the X axis with both the log of the impedance magnitude and the phase angle shift plotted on the Y axis (Barsoukov and Macdonald, 2005). Impedance magnitude ( $|Z|$ ) can be calculated by the formula:

$$|Z| = \sqrt{R^2 + (X_L - X_C)^2} \quad 3.1$$

where  $R$  is the resistance,  $X_C$  is the impedance due to capacitance, and  $X_L$  is the impedance due to inductance (usually negligible in biological systems). The phase angle can be calculated using the formula:

$$\phi = \text{Tan}^{-1}\left[\frac{X_L - X_C}{R}\right] \quad 3.2$$

While the real component of impedance is independent of frequency, the imaginary component is a function of frequency. The contribution of capacitance on the impedance value can be calculated using the formula:

$$X_C = 1/(2\pi fC) \quad 3.3$$

where  $f$  is the frequency in Hz and  $C$  is the value of the capacitor in F.

Impedance biosensors can use a variety of biological sensing elements but the most commonly used are antibodies. When using antibodies as the biological element the biosensor is often referred to as an impedance immunosensor. Impedance immunosensors rely on the interaction of the antibody and the antigen to generate a detectable signal for the transducing element. This allows the immunosensor to detect either indirect or direct impedance measurements. Direct impedance measurement, or label-free detection, is dependent on monitoring the changes in the electrical properties of the sensing environment caused by the antibody-antigen interaction. A label-free detection method has several advantages over an indirect detection method, including reduced detection time, lower cost, and simpler detection protocol.

Impedance biosensors have been shown to be capable of detecting eukaryotic cells, bacteria and viruses (Houssin et al., 2010; Varshney and Li, 2009; Wang et al., 2009; Garcia-Aljaro et al., 2009). Many current tests for infectious pathogens require expensive equipment and facilities, highly trained expertise, and clean laboratory settings. Impedance biosensor research has begun to move towards making pathogen detection more mobile, inexpensive, and require less training. Also many pathogen detection methods require pure samples for detection, which involve time-consuming and expensive pretreatment procedures. Impedance biosensors in combination with immunomagnetic separation techniques have the ability to rapidly and specifically detect a target pathogen from complex matrices, such as blood, food, or environmental samples (Ivnitski et al., 1999).

### **3.2.1.1 Interdigitated array microelectrodes in impedance biosensors**

In traditional impedance biosensors macrosized electrodes would have to be submerged into the detection medium to measure the impedance. This method required large amount of media and reagents. Microelectrodes were seen as promising due to the decrease in amount of reagents and sample required and they require lower concentrations of ions for double layer capacitor formation, increasing sensitivity.

Interdigitated array microelectrodes (IDAM) offer the advantages of low ohmic drop, fast establishment of steady-state, rapid reaction kinetics, and increased signal to noise ratio. IDAMs consist of a series of parallel microelectrode fingers in which alternating fingers are connected, with the distance between the fingers being in the micrometer range. As with other microelectrodes, IDAMs reduce the required sample size needed and increase sensitivity. IDAMs also decrease detection times due to their low response time (Varshney and Li, 2009).

Several parameters of the IDAM affect the sensitivity. Width, height, length, gap, material, and number of electrodes have been looked at to determine the effect on electrode performance. Many of these parameters, when changed, have a positive effect in one aspect and a negative effect in another. For example, an increase in the area of the array increases the signal value but at the same time also increases the background noise and while a large surface area increases the area for target binding though decrease in the electrode width increases the signal to noise ratio (Stulik et al., 2000).

### 3.2.2 Impedance biosensors for detection of avian influenza virus

Several impedance biosensors have previously been developed for the detection of AIV subtype H5 or H5N1. A non-Faradic impedance biosensor was investigated in combination with a microfluidic flow cell containing an embedded interdigitated microelectrode array and immunomagnetic separation using anti-H5 antibody-coated magnetic nanobeads, and a lower detection limit of  $10^3 \text{ EID}_{50} \text{ ml}^{-1}$  was achieved specific for the H5 subtype (Li et al., 2006; Wang et al., 2011). The second non-Faradic biosensor developed for the detection of AIV H5N1 used immunomagnetic separation with anti-H5 antibody-coated magnetic nanobeads, a microfluidic flow cell with an embedded interdigitated microelectrode that was coated in anti-N1 antibody and chicken red blood cell (RBC) labels for amplification (Lum et al., 2012). This biosensor was capable of specifically detecting AIV subtype H5N1 at  $10^3 \text{ EID}_{50} \text{ ml}^{-1}$  but had a detection time of 2 h and required multiple steps in the detection protocol. A Faradic impedance biosensor was developed using an open interdigitated microelectrode array with immobilized polyclonal antibody against H5, and when RBC amplification was used the sensor had a lower detection limit of  $10^3 \text{ EID}_{50} \text{ ml}^{-1}$  (Wang et al., 2009).

A miniaturized biosensor was developed by Diouani et al. (2008) for the detection of H7N1. Polyclonal antibodies against AIV H7N1 were attached to a gold electrode using a self-assembled monolayer. The impedance measurement was carried out in the presence of a redox probe and inside a Faraday cage. The lower detection limit of this biosensor was determined to be  $5 \mu\text{g ml}^{-1}$  of specific antigen. Though the biosensor was miniaturized for portable in-field detection the electrode preparation protocol was time-consuming and labor-intensive, making the biosensor impractical for in-field use.

Hassen et al. (2011) developed an impedance biosensor capable of quantifying Influenza A virus in a media comprised of numerous other proteins and viruses. The biosensor had a lower detection limit of  $8 \text{ ng ml}^{-1}$ , even in the presence of non-specific viruses and proteins. The biosensor was only capable of detecting Influenza A viruses and not able to provide any subtype specificity. Also a time-consuming electrode preparation reduced the usefulness of the biosensor.

Though impedance biosensors for avian influenza detection have mostly been used for whole virus detection, a few groups have developed biosensors for the detection of avian influenza nucleic acid sequences. These biosensors are based on the use of nucleic acid probes which bind to specific sequence in the influenza genome. Kukol et al. (2008) was able to detect 30 to 100 fmol of the target sequence without the use of labels. Bonanni et al. (2010) used gold nanoparticle amplification to achieve a lower detection of 7.5 fmol of the target. Both of these biosensors were developed as proof-of-designs, targeting artificially made DNA sequences instead of actual Influenza A RNA sequences.

### **3.2.3 Impedance biosensors for detection of *E. coli* O157:H7**

Due to the large impact of *E. coli* O157:H7, it has been the target of many developed impedance biosensors. (Chowdhury et al., 2012; Radke and Alocilja, 2005; Varshney and Li, 2007; Varshney et al., 2007; Varshney and Li, 2008). An impedance biosensor based on a polyaniline and monoclonal antibody functionalized electrode was able to detect  $10^2 \text{ cfu ml}^{-1}$  of *E. coli* O157:H7 in 10 min (Chowdhury et al., 2012). A high density microelectrode array biosensor developed by Radke and Alocilja (2005) was able to detect  $10^4 \text{ cfu ml}^{-1}$  *E. coli* O157:H7. The novelty of the biosensor was in the dimensions of the microelectrode array used.



The finger width and spacing were 3 and 4  $\mu\text{m}$ , respectively. This increased the contribution each captured bacteria had on the measured impedance.

Several impedance biosensors have incorporated magnetic nanoparticles in their design. Varshney et al. (2007) combined magnetic nanoparticle-antibody conjugates with a microfluidic flow cell with embedded gold interdigitated array microelectrode to detect *E. coli* O157:H7 in 35 min at a lower detection limit of  $1.6 \times 10^2$  cfu ml<sup>-1</sup> and  $1.2 \times 10^3$  cfu ml<sup>-1</sup> in pure and ground beef samples, respectively. The magnetic nanoparticles were used to isolate and concentrate the bacterial cells before impedance measurement, increasing the sensitivity of the biosensor. Varshney and Li (2007) used magnetic nanoparticles not only to isolate a bacterial sample but to also concentrate the bacteria on the electrode surface using a magnetic field. The biosensor was able to detect  $7.4 \times 10^4$  and  $8.0 \times 10^5$  CFU ml<sup>-1</sup> in pure and ground beef samples, respectively, in 35 min.

Several of the previously developed impedance biosensors have been shown to be capable of extreme sensitivity. Chan et al. (2013) were able to detect 10 *E. coli* O157:H7 cells using immunomagnetic separation and concentration and a nanoporous alumina membrane coated with antibody. As with Varshney and Li (2007), magnetic nanobeads were used to concentrate the bacterial cells on the sensing surface. Santos et al. (2013) developed a highly sensitive biosensor based on antibody-coated electrodes and impedance measurement in the presence of a redox probe that was able to detect 2 *E. coli* O157:H7 cells. While the developed biosensors were highly sensitive, the fabrication and use of the biosensors was complex and time consuming, making them impractical for rapid in-field use. Escamilla-Gomez et al. (2009) were able to detect 3.3 cfu ml<sup>-1</sup> wild type *E. coli* in an impedance biosensor based on self-assembled monolayer-modified gold screen printed electrodes, though strain specificity was not

looked at. An amperometric biosensor developed by Settingington and Alcocilja (2011) used screen-printed carbon electrodes, immunomagnetic separation, and electroactive polyaniline labels to detect *E. coli* O157:H7 at a lower detection level of 7 cells in 70 min. Their biosensor was highly sensitive, easy to use, and reusable, though it was limited in that the detection was not quantitative.

### **3.3 Nucleic acid aptamers**

Nucleic acid aptamers are artificial short single stranded oligonucleotides that can bind to a wide range of targets including proteins, carbohydrates, lipids, small organic and inorganic molecules, and metal ions. Aptamer/target binding is based on hydrogen binding, the specificity of which is based on the secondary structure of the aptamer. An example of several aptamer secondary structures is shown in Fig. 3.1. Since the development of an aptamer selection technique in 1990 (Ellington and Szostak, 1990), aptamers has seen use in a number of different fields including biodetection, therapeutics, microscopy, and drug development (Song et al., 2008; Ni et al., 2011; Cui et al., 2011; Mayer and Jenne, 2004).

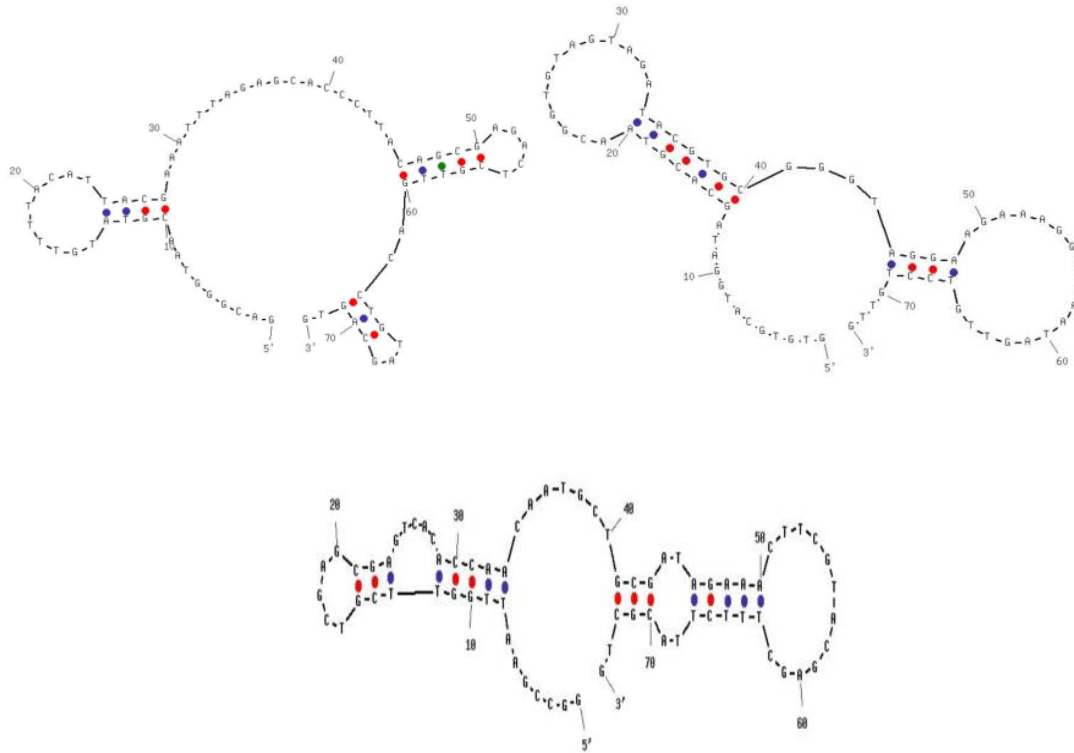


Fig. 3.1. Secondary structures of DNA aptamers against avian influenza virus H5N1 (Wang et al., 2013).

Nucleic acid aptamers can be either DNA or RNA. There are no differences between RNA and DNA aptamers except for DNA aptamers are inherently more stable and less susceptible to degradation by nucleases (Gold et al., 1995). Developing DNA aptamers also requires fewer steps than RNA aptamers and as such DNA is the primary nucleic acid used for aptamers.

In recent years aptamers have been looked at as alternatives to antibodies due to a number of advantages that aptamers have over antibodies. Aptamers, being composed of nucleic acids instead of amino acids, are inherently more stable than antibodies, which are proteins composed of amino acids. While high temperature or temperature swings may denature both

proteins and nucleic acid aptamers, aptamers will resume their secondary structure and retain their binding affinity and specificity while proteins are irreversibly denatured, losing their binding function. Nucleic acid aptamers also exhibit high chemical stability. Chemical environments that might irreversibly denature a protein, such as a high salt concentration, will only affect a nucleic acid aptamer as long as the aptamer is in the solution. Once the aptamer is removed from the harsh chemical environment it will regain its secondary structure and binding ability.

In addition to higher thermal and chemical stability compared to antibodies, nucleic acid aptamers are also faster and less expensive to develop. Nucleic acid development is based on an in vitro chemical selection method, whereas antibody development is dependent on an in vivo immune reaction in an animal. Due to the use of an animal immune system for development, antibodies can only be developed for molecules which trigger an immune response. Also the environmental conditions are limited to physiological temperature, pH, and salt concentrations and as such antibodies are typically only functional at or near physiological conditions. Furthermore, it is difficult to develop antibodies to molecules which may harm or kill an animal. Nucleic acid aptamer development is an in vitro chemical process that can be tailored to specific needs. The temperature at which the aptamer binds can be selected for along with pH or salt concentration. It is also possible to select for molecules which have low or no immunogenicity.

Development of high affinity and high specificity antibodies may take 6-12 months during which the animals must be housed and fed and personnel must be assigned to care for them. The time and economic investments for antibodies are substantial and therefore only a few specialized laboratories or facilities undertake the effort. Because aptamers are developed by an in vitro chemical process using skills and equipment found in most molecular biology labs, they

are much more convenient for most laboratories to develop. Also the time investment for developing aptamers is far less than that for antibodies, often taking only several weeks to a few months. Because aptamer development requires less time and does not rely on animals the cost of aptamer development is far less than antibodies. Aptamer development also avoids the legal complications caused by animal use.

Though aptamers have numerous advantages over antibodies, they are more susceptible to degradation in an environmental sample due to the presence of nucleases. This problem can be alleviated in several ways. Substitution of 2' fluoro, amino, or methoxy groups is a common method to stabilize aptamers. The use of spiegelmers (L-enantiomeric oligonucleotides) greatly increases the lifetime of an aptamer, though this requires a specialized development process. The problem of nuclease degradation seems to be limited when the aptamers are immobilized on a surface such as an electrode or nanoparticle. It is thought that the high concentration of nucleic acids creates a high ion concentration which interferes with the activity of nucleases, providing some protection to the aptamers (Xiao and Farokhzad, 2012).

### **3.3.1 Aptamer selection**

Aptamer selection is done by a method known as systematic evolution of ligands by exponential enrichment or SELEX. SELEX is an in vitro chemical selection method based on mixing a library of randomized oligonucleotides with a target such as a protein or organic molecule. The oligonucleotide sequences bound to the target are then isolated and amplified through polymerase chain reaction. The amplified sequences are then mixed with the target to repeat the selection. This is done for multiple cycles, typically 10-15 cycles, until only high affinity, high specificity aptamer sequences are left.

The SELEX process is begun by designing the starting oligonucleotide library. The library will have at least part of its sequence randomized with equal incorporation of A, G, C, and T or U. Two factors are taken into consideration at this point: oligonucleotide length and primer/primerless design. The typical oligonucleotide length is between 50-120 nucleotides long. The length of the oligonucleotide has an effect on the final product. A shorter length will be cheaper to produce and likely have greater stability, though it is suggested that the affinity and specificity of a shorter aptamer may be less than that of a longer aptamer. Though a longer aptamer will have a higher number of possible sequences and therefore secondary structures, resulting in higher possible affinity and specificity, they will also be susceptible to nucleases and be more expensive to produce.

The oligonucleotide must be able to be amplified to be used in the SELEX process and therefore has to have primer regions for use in PCR. One method of dealing with this is to simply include the primer sequences in the oligonucleotide. This method is by far the simplest, requiring no special procedures to prepare the oligonucleotides for PCR amplification. The alternative to including the primer regions in the oligonucleotide designs it to use a primerless library. In this method the entire oligonucleotide sequence is randomized and primer regions are glued to the sequences after each binding cycle using a ligase enzyme to allow for PCR amplification. After PCR the primer regions are then cut off using a restriction enzyme and the next binding cycle is begun. It is thought that including the primer regions in the oligonucleotide sequence may negatively affect the final aptamer specificity and affinity though the convenience of this method is typically considered to outweigh any possible gain in final aptamer quality.

After the starting library has been prepared it is mixed with the target. As the SELEX process is gone through it is common for the binding time to be decreased and library/target

molar ratio to be increased to increase the selection pressure. This increase in selection pressure results in higher quality aptamers though if the selection is too stringent some high affinity and specificity aptamer may be lost. Negative selection pressure can be accomplished at this stage by mixing the aptamer library with non-targets and saving only those aptamer sequences that do not bind. This is especially useful when developing aptamers meant to differentiate between two closely related molecules, such as phosphorylated and non-phosphorylated versions of the same protein (Tombelli et al., 2005).

After the binding step the bound aptamer sequences must be isolated and the unbound sequences washed away. This can be accomplished by filtration or by affinity chromatography. In both of these methods it is usually required that the starting aptamer library is passed through the filter or column before ever mixing with the target. This aptamers that are passed through the filter or column are saved to be used in the actual SELEX process. The removal of any aptamer sequences which non-specifically bind to the filter or column prevents them from being amplified in the SELEX process, which could eventually lead to them outnumbering and masking the sequences that bind to the intended target. A few research groups have used magnetic nanobeads or nanoparticles labeled with the target to isolate bound aptamers. While the method is as effective as filtering or affinity chromatography the added cost of the nanobeads means that it is likely to be more useful for the automation of the SELEX process.

Once the bound aptamers are isolated they are removed from the target using an elution buffer and amplified using polymerase chain reaction (PCR). The final product of PCR is double stranded DNA (dsDNA) so this dsDNA library must be regenerated to a single stranded DNA (ssDNA) library. This can either be accomplished by enzymatic digestion of one strand of the dsDNA or through asymmetric PCR. The most prominent method of regenerating the ssDNA

library is to use Lambda exonuclease. This is done by using one PCR primer labeled with a 5' phosphate group. Lambda exonuclease targets the phosphate labeled strand and degrades it, leaving ssDNA for the next SELEX cycle. Assymmetric PCR involves using unequal amounts of one PCR primer to get a final PCR product that consists mainly of ssDNA. This technique is far less efficient than enzymatic digestion and requires extensive optimization of the PCR reaction (Svobodova et al., 2012). One other method that has been looked at is physical separation of the DNA strands using magnetic nanoparticles. This involves having a biotin label on one of the DNA strands which is captured by streptavidin-coated nanobeads. The non-biotin labeled strand is then released by either thermal or alkaline treatment. This method is fast and simple but has several drawbacks. First the thermal and alkaline treatments can result in the biotin labeled strand being released from the streptavidin, leaving the DNA strand double stranded. Also the streptavidin can become detached from the nanobeads and cause problems downstream if special precautions are not taken (Wilson, 2012). Overall method of ssDNA regeneration does not seem to affect the final SELEX product and the decision of which method is used should simply be based on convenience and cost (Marimuthu et al., 2012).

After regeneration of the ssDNA library the SELEX cycle is repeated. The number of times is often up to the discretion of the scientist though some the research team of Nitsche et al. (2007) claim that only one SELEX cycle (called MonoLEX) is needed to develop high quality aptamers, though a search of the literature shows that only one use of this procedure has been done, though a company, Aptares, has been formed around it.

Once the enough SELEX cycles are finished the aptamer library is inserted into a plasmid and cloned inside bacteria. The individual clones are then sequenced. The number of final aptamers sequences depends on the complexity of the target molecule and the stringency of the



selection pressure. A large complex target such as a whole virus is likely to have many binding aptamer sequences, whereas a small molecule such as ATP is likely to have only a few (Ellington and Conrad, 1995). After the aptamers are sequenced the secondary structures can be determined using software such as mFold (The RNA Institute, University at Albany, Albany, NY) or UNAFold (Integrated DNA Technologies, Coralville, IA). These free internet-based programs calculate the secondary structures of ssDNA aptamers using free energy minimization algorithms.

To further investigate the individual aptamer sequences, surface plasmon resonance (SPR) can be used. With an SPR such as Biacore (GE Healthcare Biosciences, Pittsburg, PA) the association and dissociation rate, equilibrium dissociation constant, and regeneration ability can all be determined. Knowledge of these properties can help optimize conditions for future aptamer use (Misono and Kumar, 2005).

### **3.3.2 Aptamers used in detection of avian influenza virus**

The majority of aptamers developed for avian influenza viruses have focused on inhibition of the hemagglutinin protein preventing viral infection. A DNA aptamer has been developed that prevents influenza infection by efficiently blocking receptor binding region of the viral HA (Jeon et al., 2004). RNA aptamers that inhibit membrane fusion of AIV H3N2 and Influenza B virus hemagglutinin have also been developed (Gopinath et al., 2006a, b). DNA and RNA aptamers that targeted to HA1 proteins of influenza virus hemagglutinin subtype H5 were developed in two different studies (Cheng et al., 2008; Park et al., 2011). These aptamers were developed to inhibit function of the hemagglutinin protein and prevent or treat influenza

infection. Based on the function and likely binding sites of these aptamers it seems unlikely these aptamers would be optimal sequences to use in a biodetection assay.

A DNA aptamer for avian influenza H5N1 was developed by Wang et al. (2013) using a combination of protein and whole virus targets. It is unique in its binding affinity in that it specifically targets the H5N1 subtype, having no binding activity with other influenza viruses containing either the H5 or N1 proteins. This suggests that the binding site is at an intersection of the H5 and N1 proteins.

### **3.3.3 Aptamers used in detection of *E. coli* O157:H7**

Only a few studies have developed aptamers against *E. coli* O157:H7, possibly due to the high availability of *E. coli* O157:H7 antibodies. Lee et al. (2012) developed an RNA aptamer by *E. coli* K12 as a negative selection target and then using whole *E. coli* O157:H7 cells as the target. Wu et al. (2012a, b) describe the use of DNA aptamers for *E. coli* O157:H7 though the actual aptamer selection is not described. A presentation at the conference of the European Society of Clinical Microbiology and Infectious Diseases reports the development of a DNA against a clinical isolate of *E. coli* O157:H7 and the use of the aptamers in PCR and fluorescence-based assays (Kozyr et al., 2013).

### **3.4 Aptamer-based biosensors**

Aptamer-based biosensors, or aptasensors, utilize nucleic acid or peptide aptamers as the biological recognition element. Aptasensors have been developed based on piezoelectric, optical, and electrochemical transducer systems for a variety of different targets, such as proteins, viruses, and bacteria.

### 3.4.1 Aptamer-based biosensors for detection of avian influenza virus

Several aptamer-based biosensors have been developed for the detection of AIV. Bai et al. (2012) reported a surface plasmon resonance aptasensor for the detection of AIV H5N1. The developed aptasensor had a detection time of 1.5 h and a lower detection limit of  $2^7 \times 10^{-4}$  HAU. A hydrogel-based QCM aptasensor was able to detect AIV H5N1 at  $2^7 \times 10^{-4}$  HAU in 30 min (Wang and Li, 2013). The QCM aptasensor was based on swelling of the hydrogel after AIV H5N1 capture due to dissolution of the crosslinked aptamers and ssDNA in the hydrogel polymer. Though the developed aptasensor was both rapid and sensitive, it is not practical for in-field use due to QCM's predisposition to environmental noise (Spangler et al., 2001). Brockman et al. (2013) developed a QCM aptasensor for AIV H5N1 using magnetic nanobeads labels as mass amplifiers. The biosensor was found to have a lower detection limit of 1 HAU, though the detection time was reduced by half compared to a similar QCM biosensor using antibodies (Li et al., 2011). The biosensor Cui et al. (2011) investigated a method of labeling AIV particles with aptamer-coated quantum dots, but no detection limit or detection time was given.

### 3.4.2 Aptamer-based biosensors for detection of *E. coli* O157:H7

Only a few aptamer-based biosensors have been developed for the detection of *E. coli* O157:H7. Wu et al. (2012a) developed a colorimetric biosensor based on aptamer-labeled nanoscale polydiacetylene vesicles. Upon binding to the target *E. coli* O157:H7 the vesicles displayed a color shift that was read using absorbance spectroscopy. The detection limit of the aptasensor was  $10^4$  cfu ml<sup>-1</sup>. Wu et al. (2012b) developed a biosensor based on aptamer modified gold nanoparticles which produced a color shift upon aggregation onto the target *E. coli* O157:H7 and had a detection limit of  $10^5$  cfu ml<sup>-1</sup>. So et al. (2008) was able to detect a

concentration of  $10^3$  cfu ml<sup>-1</sup> *E. coli* using aptamer-functionalized single-walled carbon nanotube field-effect transistors, though the *E. coli* strain used was DH5 $\alpha$ , not O157:H7, and the fabrication of the biosensor was costly, time consuming, and labor intensive.

### **3.5 Magnetic nanoparticles and immunomagnetic separation**

Magnetic nanoparticles, defined as a paramagnetic material with at least one dimension being 100 nm or less, have become a staple of modern biotechnology and biomedical research. Nanoparticles can be coated in a variety of chemicals, proteins, or functional groups to be used in a wide range of applications such as cancer research and treatment, enzymatic reactions, drug delivery, molecular detection, and separation and purification techniques.

Immunomagnetic separation involves the use of magnetic micro- or nano- particles labeled with antibodies, binding agents, or aptamers to isolate a target from a clinical or environmental sample. These targets can be eukaryotic cells, bacteria, viruses, proteins, or chemicals (Oren et al., 2005; Lee et al., 2009; Wang et al., 2009; Jin et al., 2009).

Immunomagnetic separation is simple, rapid, requires no expensive equipment, and can provide high capture efficiency and specificity when using appropriate antibodies. Also immunomagnetic separation can concentrate the sample into a small volume to allow for more sensitive detection (Horak et al., 2007). Magnetic separation is suited for biological application due to the fact that most biomaterials are not susceptible to magnetic fields. The specificity is a significant advantage over traditional isolation techniques such as filtration or centrifugation. Beads with a diameter of 150 nm or below can exist as a stable colloid. When a magnetic field is applied the beads form a monolayer, allowing any waste to be separated from the beads and target (Hsing et al., 2007).

A disadvantage of using immunomagnetic separation is that the technique utilizes micro- and nano- sized particles which have been shown to have harmful effects on both eukaryotic and prokaryotic cells in lab and environmental settings (Neal, 2008; Nel et al., 2006; Goya et al., 2008; Alekseenko et al., 2008). Further research, such as modifying the coating layer, is being conducted to reduce this problem (Yang et al., 2009).

### 3.6 References

- Abu-Rabeah, K., Ashkenazi, A., Atias, D., Amir, L., Marks, R.S., 2009. *Biosens. Bioelectron.* 24, 3461-3466.
- Alekseenko, A.V., Waseem, T.V., Fedorovich, S.V., 2008. *Brain Res.* 1241, 193-200.
- Amano, Y., Cheng, Q., 2005. *Anal. Bioanal Chem.* 381, 156-164.
- Bai, H., Wang, R., Hargis, B., Lu, H., Li, Y., 2012. *Sensors (Basel)*. 12, 12506-12518.
- Barsoukov, E, Macdonald, J., 2005. *Impedance spectroscopy: theory, experiment, and applications*, 2 ed. John Wiley and Sons, Hoboken, NJ.
- Bonanni, A., Pividori, M.I., del Valle, M., 2010. *Analyst* 135, 1765-1772.
- Budin, G., Chung, H.J., Lee, H., Weissleder, R., 2012. *Angew. Chem. Int. Ed Engl.* 51, 7752-7755.
- Chan, K.Y., Ye, W.W., Zhang, Y., Xiao, L.D., Leung, P.H.M., Li, Y., Yang, M., 2013. *Biosens. Bioelectron.* 41, 532-537.
- Charlton, B., Crossley, B., Hietala, S., 2009. *Comp. Immunol. Microbiol. Infect. Dis.* 32, 341-350.
- Cheng, C., Dong, J., Yao, L., Chen, A., Jia, R., Huan, L., Guo, J., Shu, Y., Zhang, Z., 2008. *Biochem. Biophys. Res. Commun.* 366, 670-674.
- Chowdhury, A.D., De, A., Chaudhuri, C.R., Bandyopadhyay, K., Sen, P., 2012. *Sensors Actuators B: Chem.* 171-172, 916-923.
- Cooper, M.A., 2002. *Nat. Rev. Drug Discov.* 1, 515-528.

- Cui, Z.Q., Ren, Q., Wei, H.P., Chen, Z., Deng, J.Y., Zhang, Z.P., Zhang, X.E., 2011. *Nanoscale*. 3, 2454-2457.
- Daniels, J.S., Pourmand, N., 2007. *Electroanal.* 19, 1239-1257.
- Davis, F., Higson, S.P., 2010. *Pediatr. Res.* 67, 476-480.
- Dawson, E.D., Moore, C.L., Smagala, J.A., Dankbar, D.M., Mehlmann, M., Townsend, M.B., Smith, C.B., Cox, N.J., Kuchta, R.D., Rowlen, K.L., 2006. *Anal. Chem.* 78, 7610-7615.
- Deisingh, A.K., Thompson, M., 2004. *Can. J. Microbiol.* 50, 69-77.
- Diouani, M.F., Helali, S., Hafaid, I., Hassen, W.M., Snoussi, M.A., Ghram, A., Jaffrezic-Renault, N., Abdelghani, A., 2008. *Materials Sci. Engr. C.* 28, 580-583.
- dos Santos, M.B., Aguil, J.P., Prieto-Simón, B., Sporer, C., Teixeira, V., Samitier, J., 2013. *Biosens. Bioelectron.* 45, 174-180.
- Ellington, A.D., Conrad, R., 1995. *Biotechnol. Annu. Rev.* 1, 185-214.
- Ellington, A.D., Szostak, J.W., 1990. *Nature* 346, 818-822.
- Ellis, J.S., Zambon, M.C., 2002. *Rev. Med. Virol.* 12, 375-389.
- Escamilla-Gómez, V., Campuzano, S., Pedrero, M., Pingarrón, J.M., 2009. *Biosens. Bioelectron.* 24, 3365-3371.
- Estmer Nilsson, C., Abbas, S., Bennemo, M., Larsson, A., Hämäläinen, M.D., Frostell-Karlsson, Å., 2010. *Vaccine.* 28, 759-766.
- Fereidouni, S.R., Starick, E., Grund, C., Globig, A., Mettenleiter, T.C., Beer, M., Harder, T., 2009. *Vet. Microbiol.* 135, 253-260.
- Fesenko, E.E., Kireyev, D.E., Gryadunov, D.A., Mikhailovich, V.M., Grebennikova, T.V., L'vov, D.K., Zasedatelev, A.S., 2007. *Influenza Other Respi Viruses.* 1, 121-129.
- Fortineau, N., Trieu-Cuot, P., Gaillot, O., Pellegrini, E., Berche, P., Gaillard, J., 2000. *Res. Microbiol.* 151, 353-360.
- Gall, A., Hoffmann, B., Harder, T., Grund, C., Ehricht, R., Beer, M., 2009. *J. Clin. Microbiol.* 47, 2985-2988.
- Gall, A., Hoffmann, B., Harder, T., Grund, C., Ehricht, R., Beer, M., 2009. *J. Virol. Methods.* 160, 200-205.
- García-Aljaro, C., Muñoz-Berbel, X., Muñoz, F.J., 2009. *Biosens. Bioelectron.* 24, 1712-1716.

- Gold, L., Polisky, B., Uhlenbeck, O., Yarus, M., 1995. *Annu. Rev. Biochem.* 64, 763-797.
- Gopinath, S.C., Sakamaki, Y., Kawasaki, K., Kumar, P.K., 2006. *J. Biochem.* 139, 837-846.
- Gopinath, S.C., Misono, T.S., Kawasaki, K., Mizuno, T., Imai, M., Odagiri, T., Kumar, P.K., 2006. *J. Gen. Virol.* 87, 479-487.
- Grieshaber, D., MacKenzie, R., Vörös, J., Reimhult, E., 2008. *Sensors* 8, 1400-1458.
- Hahn, M.A., Keng, P.C., Krauss, T.D., 2008. *Anal. Chem.* 80, 864-872.
- Han, S., Cho, J., Cho, I., Paek, E., Oh, H., Kim, B., Ryu, C., Lee, K., Kim, Y., Paek, S., 2007. *Anal. Chim. Acta.* 587, 1-8.
- Hassen, W.M., Duplan, V., Frost, E., Dubowski, J.J., 2011. *Electrochim. Acta.* 56, 8325-8328.
- Hirota, S., Sasaki, T., Kuwahara-Arai, K., Hiramatsu, K., 2011. *J. Clin. Microbiol.* 49, 3627-3631.
- Horak, D., Babic, M., Mackova, H., Benes, M.J., 2007. *J. Sep. Sci.* 30, 1751-1772.
- Houssin, T., Follet, J., Follet, A., Dei-Cas, E., Senez, V., 2010. *Biosens. Bioelectron.* 25, 1122-1129.
- Hsing, I., Xu, Y., Zhao, W., 2007. *Electroanal.* 19, 755-768.
- Ivnitski, D., Abdel-Hamid, I., Atanasov, P., Wilkins, E., 1999. *Biosens Bioelectron.* 14, 599-624.
- Jeon, S.H., Kayhan, B., Ben-Yedidia, T., Arnon, R., 2004. *J. Biol. Chem.* 279, 48410-48419.
- Jin, H., Lin, J., Wang, X., Xin, T., Liang, S., Li, Z., Hu, G., 2009. *J. Pharm. Biomed. Anal.* 50, 891-896.
- Koncki, R., 2007. *Anal. Chim. Acta.* 599, 7-15.
- Kukol, A., Li, P., Estrela, P., Ko-Ferrigno, P., Migliorato, P., 2008. *Anal. Biochem.* 374, 143-153.
- Lee, H., Kim, B.C., Kim, K., Kim, Y.K., Kim, J., Oh, M., 2009. *Biosens. Bioelectron.* 24, 3550-3555.
- Lee, Y.J., Han, S.R., Maeng, J.S., Cho, Y.J., Lee, S.W., 2012. *Biochem. Biophys. Res. Commun.* 417, 414-420.
- Leland, D.S., Ginocchio, C.C., 2007. *Clin. Microbiol. Rev.* 20, 49-78.

- Li, D., Wang, J., Wang, R., Li, Y., Abi-Ghanem, D., Berghman, L., Hargis, B., Lu, H., 2011. *Biosens. Bioelectron.* 26, 4146-4154.
- Lojou, E., Bianco, P., 2006. *J. Electroceramics* 16, 79-91.
- Lum, J., Wang, R., Lassiter, K., Srinivasan, B., Abi-Ghanem, D., Berghman, L., Hargis, B., Tung, S., Lu, H., Li, Y., 2012. *Biosens. Bioelectron.* 38, 67-73.
- Mao, X., Yang, L., Su, X., Li, Y., 2006. *Biosens. Bioelectron.* 21, 1178-1185.
- Marimuthu, C., Tang, T.H., Tominaga, J., Tan, S.C., Gopinath, S.C., 2012. *Analyst* 137, 1307-1315.
- Mayer, G., Jenne, A., 2004. *BioDrugs* 18, 351-359.
- Medintz, I.L., Uyeda, H.T., Goldman, E.R., Mattoussi, H., 2005. *Nat. Mater.* 4, 435-446.
- Misono, T.S., Kumar, P.K.R., 2005. *Anal. Biochem.* 342, 312-317.
- Nayak, M., Kotian, A., Marathe, S., Chakravorty, D., 2009. *Biosens. Bioelectron.* 25, 661-667.
- Neal, A.L., 2008. *Ecotoxicology* 17, 362-371.
- Nel, A., Xia, T., Madler, L., Li, N., 2006. *Science* 311, 622-627.
- Ni, X., Castanares, M., Mukherjee, A., Lupold, S.E., 2011. *Curr. Med. Chem.* 18, 4206-4214.
- Nitsche, A., Kurth, A., Dunkhorst, A., Pänke, O., Sielaff, H., Junge, W., Muth, D., Scheller, F., Stöcklein, W., Dahmen, C., 2007. *BMC Biotech* 7, 48.
- Park, S.Y., Kim, S., Yoon, H., Kim, K.B., Kalme, S.S., Oh, S., Song, C.S., Kim, D.E., 2011. *Nucleic Acid Ther.* 21, 395-402.
- Peduru Hewa, T.M., Tannock, G.A., Mainwaring, D.E., Harrison, S., Fecondo, J.V., 2009. *J. Virol. Methods* 162, 14-21.
- Pejčić, B., De Marco, R., Parkinson, G., 2006. *Analyst* 131, 1079-1090.
- Phillips, K.S., Cheng, Q., 2007. *Anal. Bioanal Chem.* 387, 1831-1840.
- Pöhlmann, C., Wang, Y., Humenik, M., Heidenreich, B., Gareis, M., Sprinzl, M., 2009. *Biosens. Bioelectron.* 24, 2766-2771.
- Radke, S.M., Alocilja, E.C., 2005. *Biosens. Bioelectron.* 20, 1662-1667.



Rodriguez-Mozaz, S., Marco, M., de Alda, M., Barceló, D., 2004. *Pure Appl. Chem.* 76, 723-752.

Settingington, E.B., Alocilja, E.C., 2011. *Biosens. Bioelectron.* 26, 2208-2214.

Skottrup, P.D., Nicolaisen, M., Justesen, A.F., 2008. *Biosens. Bioelectron.* 24, 339-348.

So, H.M., Park, D.W., Jeon, E.K., Kim, Y.H., Kim, B.S., Lee, C.K., Choi, S.Y., Kim, S.C., Chang, H., Lee, J.O., 2008. *Small* 4, 197-201.

Song, S., Wang, L., Li, J., Fan, C., Zhao, J., 2008. *TrAC Trends in Anal. Chem.* 27, 108-117.

Spangler, B.D., Wilkinson, E.A., Murphy, J.T., Tyler, B.J., 2001. *Anal. Chim. Acta.* 444, 149-161.

Spratt, D.A., 2004. *Endodontic Topics* 9, 5-14.

Stulík, K., Amatore, C., Holub, K., Marecek, V., Kutner, W., 2000. *Pure Appl. Chem.* 72, 1483-1492.

Svobodova, M., Pinto, A., Nadal, P., O'Sullivan, C.K., 2012. *Anal. Bioanal Chem.* 404, 835-842.

Tombelli, S., Minunni, M., Mascini, M., 2005. *Biosens. Bioelectron.* 20, 2424-2434.

Trinidad, A., Ibanez, A., Gomez, D., Garcia-Berrocal, J., Ramírez-Camacho, R., 2010. *Microscopy: Sci.Technol.Appl.Educ.* 1, 204-210.

Tsai, H., Lin, Y., Chang, H.W., Fuh, C.B., 2008. *Biosens. Bioelectron.* 24, 485-488.

VanEngelenburg, S.B., Palmer, A.E., 2008. *Curr. Opin. Chem. Biol.* 12, 60-65.

Varshney, M., Li, Y., 2009. *Biosens. Bioelectron.* 24, 2951-2960.

Varshney, M., Li, Y., 2008. *Talanta* 74, 518-525.

Varshney, M., Li, Y., 2007. *Biosens. Bioelectron.* 22, 2408-2414.

Varshney, M., Li, Y., Srinivasan, B., Tung, S., 2007. *Sens. Actua. B: Chem.* 128, 99-107.

Wang, R., Zhao, J., Jiang, T., Kwon, Y.M., Lu, H., Jiao, P., Liao, M., Li, Y., 2013. *J. Virol. Meth.* 189, 362-369.

Wang, J., 2008. *Chem. Rev.* 108, 814-825.

Wang, J., 2006. *Biosens. Bioelectron.* 21, 1887-1892.

Wang, J., 2001. *Electroanal.* 13, 983-988.

Wang, R., Li, Y., 2013. *Biosens. Bioelectron.* 42, 148-155.

Wang, R., Wang, Y., Lassiter, K., Li, Y., Hargis, B., Tung, S., Berghman, L., Bottje, W., 2009. *Talanta* 79, 159-164.

Wilson, R., 2011. *Nucleic Acid Ther.* 21, 437-440.

Wu, W., Zhang, J., Zheng, M., Zhong, Y., Yang, J., Zhao, Y., Wu, W., Ye, W., Wen, J., Wang, Q., Lu, J., 2012. *PLoS One.* 7, e48999.

Wu, W.H., Li, M., Wang, Y., Ouyang, H.X., Wang, L., Li, C.X., Cao, Y.C., Meng, Q.H., Lu, J.X., 2012. *Nanoscale Res. Lett.* 7, 658-276X-7-658.

Xiao, Z., Farokhzad, O.C., 2012. *ACS Nano.* 6, 3670-3676.

Yang, L., Li, Y., 2006. *Analyst* 131, 394-401.

Yang, H., Liu, C., Yang, D., Zhang, H., Xi, Z., 2009. *J. Appl. Toxicol.* 29, 69-78.

Yang, Y., Gonzalez, R., Huang, F., Wang, W., Li, Y., Vernet, G., Wang, J., Jin, Q., 2010. *J. Virol. Methods.* 167, 37-44.

## **4. In vitro selection of DNA aptamers against avian influenza subtype H7**

### **4.1 Abstract**

Aptamers are artificial oligonucleotides (DNA or RNA) that can bind to a broad range of targets. In diagnostic and detection assays, aptamers represent an alternative to antibodies as recognition agents due to their greater thermal and chemical stability, lower cost, and simpler production. The objective of this study was to select and characterize single-stranded DNA (ssDNA) aptamers that can specifically bind to avian influenza virus (AIV) hemagglutinin subtype H7 using the Systematic Evolution of Ligands by Exponential enrichment (SELEX) method and surface plasmon resonance (SPR). A starting library of  $10^{14}$  ssDNA molecules with a randomized central 40 nt flanked by 20 nt conserved primer regions was used to begin the selection process. A purified H7 hemagglutinin protein (HA) from AIV H7N3 was used as the target protein. After 13 rounds of selection, DNA aptamers that bind to the H7 protein were isolated and three aptamer sequences were characterized further by sequencing and affinity binding analysis. Dot blot analysis was employed for monitoring the SELEX process and conducting the preliminary tests on the affinity and specificity of aptamers.

## 4.2 Introduction

The avian influenza virus (AIV) H7 subtype has been linked with multiple high pathogenic outbreaks in poultry and stands to have a large impact on not only the poultry industry but also human health. Until 2013 only one major documented outbreak of the H7 subtype in humans was recorded. In 2003 in the Netherlands an outbreak of H7N7 infected 89 people and killed one (Koopmans et al., 2004). In 2013 a novel H7N9 outbreak occurred in China, which at the time of writing had infected 108 people and killed 22 (WHO, 2013), sparking public fear. Rapid and specific detection of AIV H7 is crucial for controlling outbreaks not only in humans but also in poultry, where viruses may mutate to become a threat to public health. Traditional methods of influenza virus detection, viral isolation and RT-PCR, while highly sensitive and specific, are time consuming, expensive, and require specialized facilities and personnel. Commercially available direct antigen tests are used for rapid in-field diagnostics and many research groups around the world are focusing on developing biosensors for in-field detection of avian influenza (Krejcová et al., 2012). These tests rely on antibodies, which can suffer from low thermal stability, high cost, and batch-to-batch variation.

Nucleic acid aptamers are short oligonucleotides that can bind to a range of targets molecules. They are generated by a process known as systematic evolution of ligands by exponential enrichment, or SELEX (Tuerk and Gold, 1990). Aptamers have high affinity for their targets similar to that of monoclonal antibodies, in the micromolar to picomolar range. They also have several advantages over antibodies, namely higher thermal and chemical stability, short development time, reproducible synthesis, and lack of immunogenicity (Iliuk, 2011).

When unbound to the target molecule, nucleic acid aptamers exist in a secondary structure determined by complementary nucleic acid base pairing. These structures often take the shape of short helical arms and single stranded loops. These secondary structures play a role in the initial interactions between the aptamer and target molecule. Upon initial binding with the target molecule, the aptamer will form tertiary structure dependent on van der Waals forces, hydrogen bonding and electrostatic interactions with the target, forming an aptamer-target complex. The bond between the tertiary form aptamer and target is much stronger than the bond between the secondary form aptamer and target, though the secondary structure does play a role in both specificity and binding affinity.

Several DNA and RNA aptamers have been reported for AIV. The majority of aptamers developed have focused on inhibition of the hemagglutinin protein preventing viral infection. A DNA aptamer has been developed that prevents influenza infection by efficiently blocking receptor binding region of the viral HA (Jeon et al., 2004). RNA aptamers that inhibit membrane fusion of AIV H3N2 and Influenza B virus hemagglutinin have also been developed (Gopinath et al., 2006a; Gopinath et al., 2006b). DNA and RNA aptamers that targeted to HA1 proteins of influenza virus hemagglutinin subtype H5 were developed in two different studies (Cheng et al., 2008; Park et al., 2011). These aptamers were developed to inhibit function of the hemagglutinin protein and prevent or treat influenza infection. Based on the function and likely binding sites of these aptamers it seems unlikely these aptamers would be optimal sequences to use in a biodetection assay.

A DNA aptamer for avian influenza H5N1 was developed by Wang et al. (2013) using a combination of protein and whole virus targets. It is unique in its binding affinity in that it specifically targets the H5N1 subtype, having no binding activity with other influenza viruses

expressing either the H5 or N1 proteins. This suggests that the binding site is at an intersection of the H5 and N1 proteins. This aptamer was designed to be used in a biosensor system and has successfully been utilized in several different biosensor designs (Bai et al., 2012; Wang and Li, 2013; Brockman et al., 2013).

To date, no aptamer for AIV H7 has been reported. Therefore the objective of this study was to develop and characterize DNA aptamers that can specifically bind to AIV H7 to be used in a biosensor system. Twelve cycles of SELEX were completed and the most promising aptamer candidate was evaluated using a dot blot assay.

### **4.3 Materials and methods**

#### **4.3.1 Target protein and viruses**

Full-length glycosylated recombinant hemagglutinin subtype H7 (A/Netherlands/219/03) with a concentration of 218  $\mu\text{g ml}^{-1}$  from Protein Sciences Corporation (Meriden, CT). The protein was produced in insect cells using a baculovirus expression vector system and purified to 90% under conditions to preserve its biological activity and tertiary structure. The protein was diluted using phosphate buffered saline (PBS; 0.01 M; pH 7.4; Sigma Aldrich, St. Louis, MO).

The avian influenza viruses used in the tests were  $\beta$ -propiolactone-inactivated and obtained from the Animal Diagnostic Laboratory at Pennsylvania State University (University Park, PA) for the H7N2 subtype and non-target subtypes, and the USDA-APHIS National Veterinary Services Laboratory (NSVL, Ames, IA) for H5N1.

### 4.3.2 DNA library and primers

A 80nt single-stranded oligonucleotide library was synthesized with the following sequence: 5'-CCG AAT TCG AAG GAC AAG AG – (N)40 - TCT TTT ATG CTA CGT CCC GC-3' where the flanking 20 nucleotides are primer binding regions for PCR reactions and the central 40 nucleotides represent a random sequence based on equal incorporation of A, T, G, and C. Amplification by PCR was done using Forward 5'-CCG AAT TCG AAG GAC AAG AG-3' and Reverse 5'-GCG GGA CGT AGC ATA AAA GA-3'. Forward primer with a 5' biotinylation was used Dot Blot testing. Reverse primer with a 5' phosphorylation was used to regenerate the ssDNA library using lambda exonuclease digestion. Both the library and primers were obtained from Integrated DNA Technologies (Coralville, IA). All library and primer dilutions were done using sterile water.

### 4.3.3 In vitro selection of aptamers

Aptamer candidates against AIV HA subtype H7 were selected for using the SELEX technique described by Tuerk and Gold (1990). The ssDNA library was prepared by first by removing any filter binding ssDNA sequences by passing the library three times through a prewetted nitrocellulose acetate membrane (0.45  $\mu\text{m}$  HAWP filter, Millipore, Billerica, MA) held in a filter holder ("pop-top", 13 mm diameter, Millipore, Billerica, MA).

In the first selection cycle, 35.5  $\mu\text{l}$  of the ssDNA library (1  $\mu\text{g } \mu\text{l}^{-1}$ ) was added to 114.5  $\mu\text{l}$  of binding buffer (50 mM Tris-HCl, 25 mM NaCl, 5 mM MgCl<sub>2</sub>, 10 mM dithiothreitol; pH 7.5). The library of the first selection cycle contained 1.4 nmol of ssDNA oligonucleotide or  $8.7 \times 10^{14}$  oligonucleotide molecules. The ssDNA library was denatured for 10 min at 95° C and cooled at room temperature for 30 min. The denatured library was mixed with the target HA protein for 1

h and 45 min at 15 rpm. The mixture was then filtered through a HAWP filter prewetted with binding buffer, retaining ssDNAs bound to the HA protein and washed with 1 ml binding buffer. Bound ssDNAs were eluted twice from the filter using 200  $\mu$ l elution buffer (5 mM EDTA, 0.4 M sodium acetate, 7 M urea; pH 5.5). The elutes were diluted with an equal amount of deionized water (dH<sub>2</sub>O) and mixed with 0.12 mg glycogen, an equal amount or 7.5 M ammonium acetate and 1 ml of 100% ethanol. The mixture was precipitated at -80 °C for 1 h and centrifuged at 13,000 rpm at 4 °C for 1 h. the supernatant was discarded and the pellet was washed twice with 75% ethanol. After washing, the pellet was resuspended in dH<sub>2</sub>O. The selected ssDNAs were amplified using PCR (Mastercycler Gradient, Eppendorf, Hauppauge, NY) and used for the next SELEX cycle. Following rounds were conducted as described above with the exception that the selection pressure was increased in each round to select for aptamers with high binding affinity and specificity. Binding time was decreased and the molar ratio of HA /ssDNA was increased throughout the selection process.

#### **4.3.4 PCR amplification and regeneration of ssDNA library**

The eluted ssDNA was used as a template for PCR reaction using a Mastercycler Gradient thermocycler (Eppendorf, Hauppauge, NY). The reaction was carried out at a total volume of 50  $\mu$ l of standard Taq buffer (10 mM Tris-HCl, 50 mM KCl, 1.5 mM MgCl<sub>2</sub>; pH 8.3; New England Biolabs, Ipswich, MA, USA) containing 0.4  $\mu$ M of each primer, 200  $\mu$ M dNTPs, and 2.5U of standard Taq polymerase (New England Biolabs, Ipswich, MA,). The PCR thermocycler was programmed as follows: initial denaturation at 95 °C for 5 min, followed by 30 cycles of denaturation at 95 °C for 30 s, annealing at 64 °C for 45 s, and extension at 72 °C for 45 s, followed by a final extension of 72 °C for 10 min. PCR products were analyzed on non-



denaturing 6% Tris-borate EDTA polyacrylamide gels (Invitrogen, Carlsbad, CA) at 200 V for 18 min after binding SYBR Green 1 (Invitrogen, Carlsbad, CA).

The ssDNA library was then regenerated by incubation with lambda exonuclease (New England Biolabs, Ipswich, MA), which selectively digested the DNA strand with the 5' phosphorylation. The PCR product was mixed with 10U lambda exonuclease and lambda exonuclease reaction buffer (67 mM glycine-KOH, 2.5 mM MgCl<sub>2</sub>, 50 µg ml<sup>-1</sup> BSA; pH 9.4; New England Biolabs, Ipswich, MA) to a final volume of 50 µl. The reaction proceeded at 37 °C for 1 h, followed by a 10 min inactivation at 75 °C. The digested product was precipitated using the protocol described in Section 2.3 except the final resuspension was done in binding buffer not dH<sub>2</sub>O. A NanoDrop 1000 Spectrophotometer (ThermoScientific, Wilmington, DE) was used to determine the ssDNA concentration before proceeding to the next SELEX round.

#### **4.3.5 Dot blot analysis**

Dot Blot analysis was used to rapidly check specificity and affinity of the aptamer throughout the SELEX process. Forward primer with a 5' biotin label and reverse primer with a 5' phosphorylation were used to obtain dsDNA. The dsDNA PCR product was digested with Lambda exonuclease to obtain 5' biotin-labeled ssDNA.

To test aptamer affinity AIV H7N2 was spotted onto a nitrocellulose membrane (BA85 Protran, 0.45 µm; Invitrogen, Grand Island, NY, USA) and air dried. The membrane was blocked using blocking buffer (12.5 g casein, 4.5 g NaCl, 605 mg Tris, 100 mg Thimerosal; pH 7.6) for 45 min and air dried. The membrane was incubated with the biotin-labelled ssDNA aptamer library (3 µg ml<sup>-1</sup>) for 30 min. The membrane was washed three times with 1× KPL washing solution (0.002 M imidazole, 0.02% Tween-20, 0.5 mM EDTA, 160 mM NaCl; KPL Inc.,

Gaithersburg, MD) to remove any unbound aptamers and air dried. The membrane was incubated with phosphatase-labeled streptavidin ( $2 \mu\text{g ml}^{-1}$ ; KPL Inc., Gaithersburg, MD) for 30 min. Unbound enzyme was washed away by washing three times with  $1\times$  KPL washing solution. The membrane was air dried and coated in BCIP/NBT (KPL Inc., Gaithersburg, MD) and put in the dark for color development. PBS buffer was used as a negative control and biotin-labelled polyclonal antibody was used as a positive control. All incubations and drying were done at room temperature.

Dot blot analysis was also used to test for aptamer specificity. The previously described protocol was used, with non-target AIV subtypes replacing the target AIV H7N2.

#### **4.3.6 Plasmid cloning and sequencing**

After 12 rounds selection, the PCR product was cleaned using a Qiaquick PCR Purification kit (Qiagen, Valencia, CA) following the manufacturers protocol. The purified products were inserted into pGEM-T Easy vector plasmids (Promega, Madison, WI) using an insert to vector ratio of 3:1. The ligation was allowed to occur overnight at  $4^\circ\text{C}$ . JM109 High Efficiency Competent *E. coli* cells (Promega, Madison, WI) were transformed using the prepared vector according to the manufacturer's manual. The transformed cells were plated on LB agar containing X-Gal (Invitrogen, Carlsbad, CA), IPTG, and ampicillin (Calbiochem, San Diego, CA). Twenty-four white colonies were randomly chosen and streaked on new plates. Individual clones were grown in LB broth with ampicillin ( $50 \mu\text{g ml}^{-1}$ ) for 15 h at  $37^\circ\text{C}$ . The cells were centrifuged at 5,000 rpm for 7 min and plasmid DNA was isolated using a Qiaprep Miniprep kit (Qiagen, Valencia, CA). Plasmid DNA concentration was measured using a NanoDrop 1000 Spectrophotometer.

Sequencing was done by automated DNA sequencing using an ABI 7300 Sequence Detector with ABI 3130xl analyzer BigDye 3.1 chemistry (Applied Biosystems, Foster City, CA).

Sequence analysis was accomplished using ABI Sequence Scanner v1.0 (Applied Biosystems, Foster City, CA). Web-based UNAFold software (Integrated DNA Technologies, Coralville, IA) was used to predict secondary structures of sequenced aptamers based on free energy minimization calculations.

## **4.4 Results and Discussion**

### **4.4.1 Aptamer affinity and specificity during selection using Dot blot analysis**

After the 4<sup>th</sup> and 12<sup>th</sup> round of selection, the aptamer pool was tested for affinity and specificity using Dot Blot analysis as described in Section 4.3.5. Binding affinity was tested by spotting differing titers of AIV H7N2 onto the nitrocellulose membrane. Fig. 1 shows the Dot Blot membranes after the 4<sup>th</sup> and 12<sup>th</sup> rounds of selection. The 4<sup>th</sup> round product showed a clear dot at the titer of 32 HAU but only a very faint dot at 16 HAU. The final 12<sup>th</sup> round showed a clear dot at the 16 HAU concentration and a faint dot for 8 HAU.

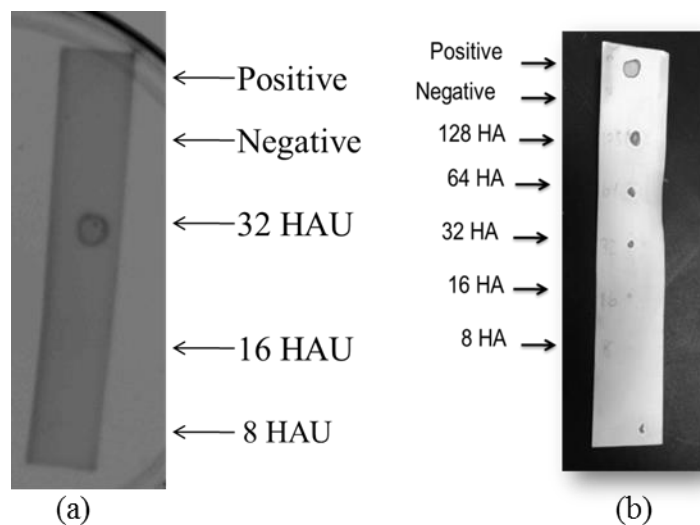


Fig. 4.2. Aptamer pool affinity after the (a) 4<sup>th</sup> and (b) 12<sup>th</sup> SELEX rounds.

The specificity of the aptamer pool was tested using non-target AIV subtypes (H5N1, H1N1, H9N2, H5N2, H5N3, and H2N2) as seen in Fig. 2. After the 4<sup>th</sup> selection round the aptamer pool showed affinity towards non-target AIV H5N1 that was equal to its affinity to AIV H7N2. A very faint dot was also seen for AIV H9N2. The aptamer pools from round 12 showed no non-specific interaction with the non-target virus subtypes.

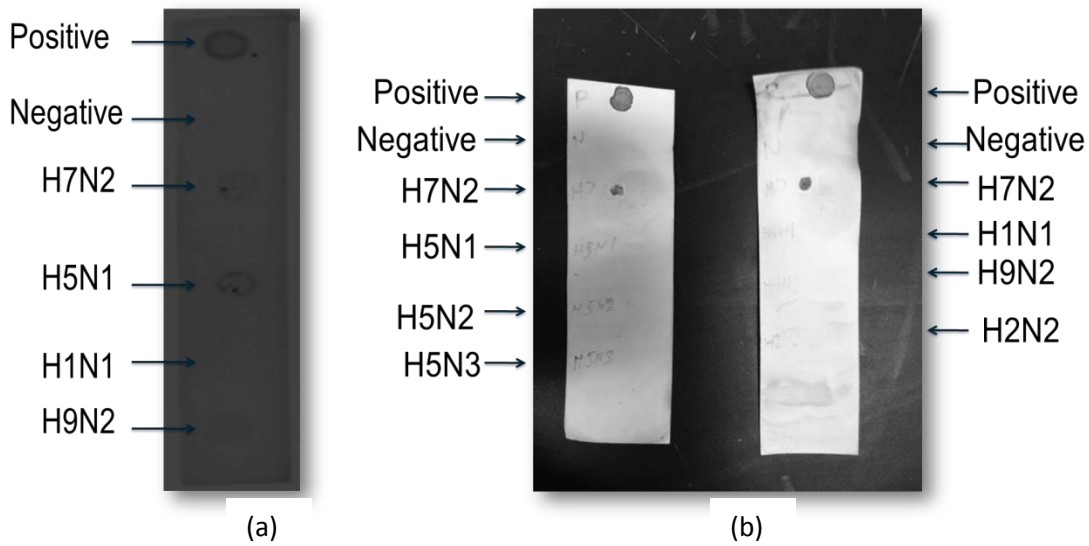


Fig. 4.2. Aptamer pool specificity at round (a) 4 and (b) 12.

#### 4.4.2 Aptamer cloning and sequencing

After the 12<sup>th</sup> round of selection the PCR product was ligated into pGEM-T Easy vectors. The pGEM-T Easy vector is linearized with a 3' thymidine at both ends, preventing self-ligation and providing an efficient hybridization site for PCR products produced by many thermostable polymerases. The pGEM-T Easy vector also contains the sequence for the  $\beta$ -galactosidase enzyme, which causes the bacterial colonies to produce a blue color when grown on certain indicator plates. Insertion of an aptamer sequence inactivates the  $\alpha$ -peptide of this enzyme, therefore a clone with a plasmid containing an insert will not produce the blue color. After transformation and plating, twenty-four randomly picked white colonies were streaked onto new plates. Single colonies from each were grown in LB broth with ampicillin. Sixteen of the colonies grew in the broth culture. After plasmid isolation, thirteen of the clones produced sufficient amounts of plasmid for sequencing. A total of three unique sequences were obtained as follows: (1) 5'-CCG AAT TCG AAG GAC AAG AGG CGA AAA GAT TTA AAG TAA TCA AAG ACT GAG CAA CTC TTA TCT TTT ATG CTA CGT CCC GC-3', (2) 5'-CCG AAT

TCG AAG GAC AAG AGA ATT AAC CCT CAC TAA AGG GCT GAG TCT CAA AAC  
 CGC AAT TCT TTT ATG CTA CGT CCC GC-3', and (3) 5'-CCG AAT TCG AAG GAC  
 AAG AGG TGA GTC GTT ACT ATC AAT ATT AGC CTA TGA CGA TAG GAA TCT TTT  
 ATG CTA CGT CCC GC-3'.

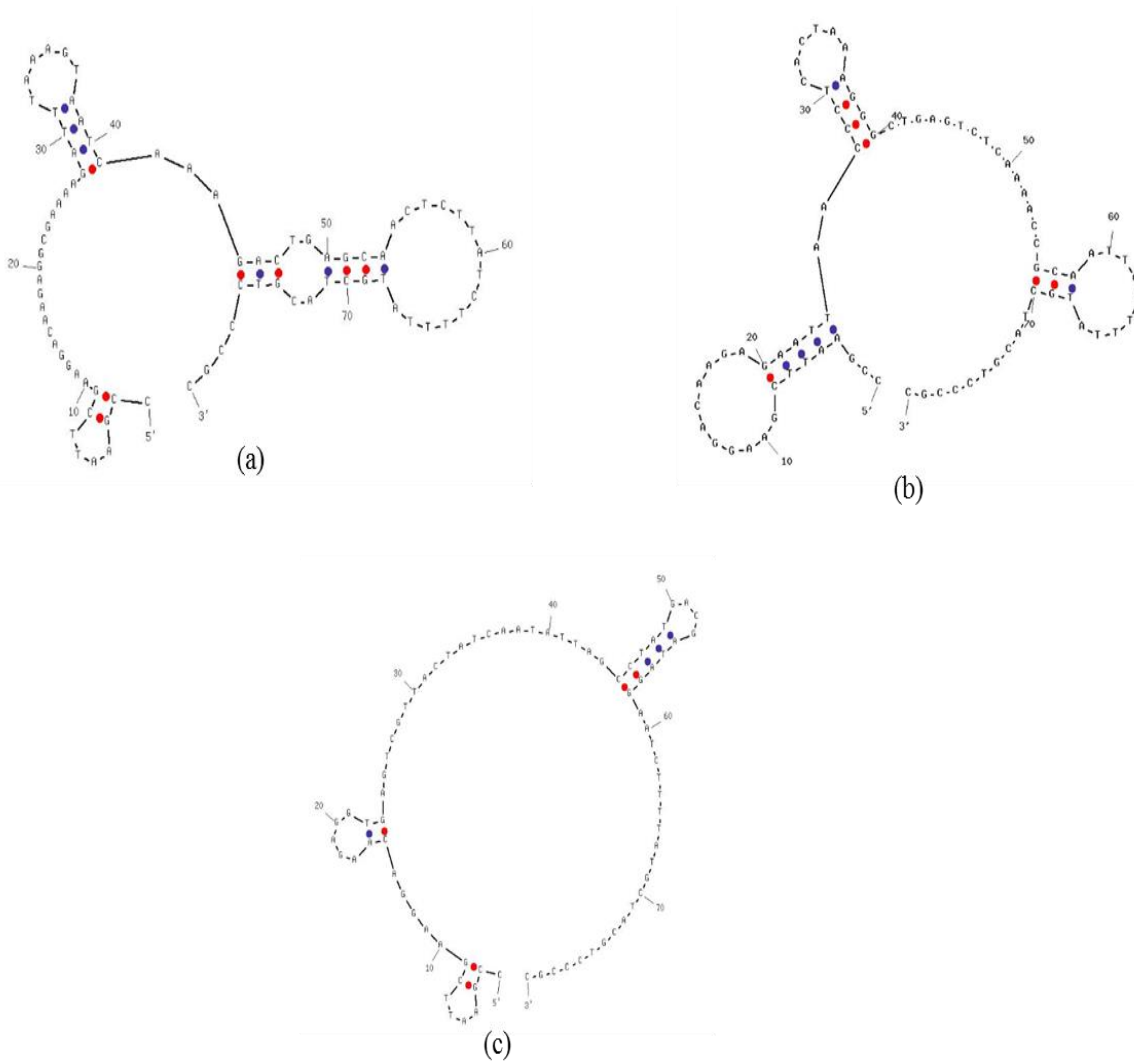


Fig. 4.3. Secondary structures of (a) aptamer #1, (b) aptamer #2, and aptamer #3 as given by UNAFold software.

Secondary structures were predicted using UNAFold software, with the folding conditions set equal to 0.01 M PBS at 25 °C. The  $T_m$  and  $\Delta G$  values were 37.2 °C, 42 °C, and 44.3 °C and -

4.58, -5.37, and -4.94, respectively. The G-C contents of the sequences were 41.3%, 46.3%, and 43.8%, respectively. The secondary structure of sequence (1) had one central loop with three hairpin loops extending from the central loop. The longest hairpin loop also had a non-hybridized section between the central loop and hairpin loop. The secondary structure of sequence (2) had one central loop with 3 hairpin loops extending from the central loop. The secondary structure of sequence (3) had one large central loop with 3 small hairpin loops.

#### **4.4.3 Evaluation of DNA aptamers using Dot blot analysis**

The three aptamer sequences were separately amplified by PCR using biotinylated forward primers and evaluated by dot blot assay for affinity and specificity. The #3 aptamer sequence was found to have no affinity to AIV H7N2 and was possibly either a non-specific fragment that managed to make it through the selection process or specific to an epitope on the HA molecule that was not readily available for binding onto viral HA. The #2 aptamer sequence showed only slight affinity towards AIV H7N2. It was found the heating the aptamer sequence before using it in the dot blot assay increased its affinity, due to the relaxation of the secondary structure. The #1 aptamer sequence showed the best affinity for the H7 protein, having a visible color change at the 1 HAU concentration. No heating was required to obtain good affinity so the aptamer was chosen for further evaluation. The #1 aptamer sequence was seen to have no non-specific interaction with non-target AIV

#### **4.5 Conclusion**

Three aptamer sequences were obtained after 12 cycles of SELEX. Of the three sequences gathered, one (#3) showed no affinity to the target virus. This aptamer could possibly be a fragment which bound non-specifically to the filter membrane. Another possibility is that

the aptamer bound specifically to the recombinant HA molecule at an epitope that was either hidden or non-existent on the viral HA molecule. This suggests that at some point in the selection process whole virus should be used as the target to select against aptamers that are unable to bind the target molecule in its native form. This was done by Wang et al. (2013) in a previous aptamer selection though for a different reason, as they were selecting for an aptamer that would specifically bind at the junction of the H5 and N1 proteins. The #2 aptamer sequence isolated showed good affinity for H7 but only when heated before performing the dot blot. One explanation for this phenomenon is that the aptamers most thermodynamically stable structure does not have high affinity to H7 but some less thermodynamically probable form. A similar secondary structure for the #2 aptamer was found to have an extra hairpin loop near the 3' end. It is possible that heating the aptamer before use allowed a higher percentage of the extra hairpin loop structure to exist, contributing to the increased affinity for H7. Because the purpose of this research was to develop an aptamer for use in biosensor research, where heating the aptamer before each use would be impractical, it was decided this aptamer did not meet the research goals. The #3 aptamer was found to have good affinity for H7 even without heating before use and therefore met the objectives of the research.

Future aptamer selection should take into account the end use of the developed aptamers so as to not waste time and resources. When developing an aptamer for an end use in which it would be impractical to heat the aptamer before use the heating step before mixing could be reduced or eliminated. Other factors such as end use pH and ion content should also be taken into consideration when developing aptamers.



## 4.6 References

- Bai, H., Wang, R., Hargis, B., Lu, H., Li, Y., 2012. *Sensors (Basel)* 12, 12506-12518.
- Brockman, L., Lum, J., Wang, R., Li, Y., 2013. *Open J. Appl. Biosens.* 2, 97-103.
- Cheng, C., Dong, J., Yao, L., Chen, A., Jia, R., Huan, L., Guo, J., Shu, Y., Zhang, Z., 2008. *Biochem. Biophys. Res. Commun.* 366, 670-674.
- Gopinath, S.C., Misono, T.S., Kawasaki, K., Mizuno, T., Imai, M., Odagiri, T., Kumar, P.K., 2006a. *J. Gen. Virol.* 87, 479-487.
- Gopinath, S.C., Misono, T.S., Kawasaki, K., Mizuno, T., Imai, M., Odagiri, T., Kumar, P.K., 2006b. *J. Gen. Virol.* 87, 479-487.
- Iliuk, A.B., Hu, L., Tao, W.A., 2011. *Anal. Chem.* 83, 4440-4452.
- Jeon, S.H., Kayhan, B., Ben-Yedidia, T., Arnon, R., 2004. *J. Biol. Chem.* 279, 48410-48419.
- Koopmans, M., Wilbrink, B., Conyn, M., Natrop, G., van der Nat, H., Vennema, H., Meijer, A., van Steenbergen, J., Fouchier, R., Osterhaus, A., Bosman, A., 2004. *Lancet.* 363, 587-593.
- Park, S.Y., Kim, S., Yoon, H., Kim, K.B., Kalme, S.S., Oh, S., Song, C.S., Kim, D.E., 2011. *Nucleic Acid Ther.* 21, 395-402.
- Tuerk, C., Gold, L., 1990. *Science* 249, 505-510.
- Wang, R., Li, Y., 2013. *Biosens. Bioelectron.* 42, 148-155.
- Wang, R., R., Zhao, J., Jiang, T., Kwon, Y., Lu, H., Jiao, P., Liao, M., Li, Y., 2013. *J. Virol. Methods.* 189, 362-369.
- WHO, 2013. [http://www.who.int/influenza/human\\_animal\\_interface/influenza\\_h7n9/03\\_ReportWebH7N9Number.pdf](http://www.who.int/influenza/human_animal_interface/influenza_h7n9/03_ReportWebH7N9Number.pdf). Accessed April 25, 2013.

## **5. An impedance aptasensor with microfluidic chips for rapid and specific detection of avian influenza viruses H5N1 and H7N2**

### **5.1 Abstract**

Avian influenza virus (AIV) subtypes H5 and H7 have been historically associated with high pathogenic influenza outbreaks in poultry. Current methods for detecting them are very time consuming and expensive, and require specialized facilities and trained personnel. In this research two DNA aptamers, which were selected through SELEX (systematic evolution of ligands by exponential enrichment) to be specific against AIV H5N1 and AIV hemagglutinin (HA) subtype H7N2, respectively, were used as alternative reagents to monoclonal antibodies in an impedance biosensor utilizing a microfluidics flow cell and an interdigitated microelectrode for the rapid and specific detection of AIV H5N1 and AIV H7N2 subtypes. The gold surface of interdigitated microelectrode embedded in a microfluidics flow cell was modified using streptavidin. Biotinylated aptamer against either H5N1 or H7N2 was then immobilized on the electrode surface using biotin-streptavidin binding. A sample of AIV H5N1 or H7N2 was injected and the impedance measurement was taken and compared to that of a control sample. The DNA aptamers were not only more stable and less expensive than monoclonal antibodies but also their smaller size and uniformity gave the developed aptasensor higher sensitivity and repeatability compared to equivalent immunosensors. The aptasensor had a detection time of 30 min and the lower detection limit for both subtypes was determined to be  $2^7 \times 10^{-4}$  hemagglutinin units (HAU). The developed aptasensor offers a portable, rapid, low-cost alternative to current methods with the same sensitivity and specificity.

## 5.2 Introduction

The two important H5 and H7 subtypes of avian influenza virus (AIV) have caused major high pathogenic avian influenza (HPAI) outbreaks in poultry and H5N1 fatal cases of human infection. These outbreaks not only cost the poultry industry millions of dollars in lost revenue but also threaten human health. The new HPAI H5N1 virus, which originally emerged in south east Asia in late 1990's, cost the poultry industry an estimated \$10 billion between 1997 and 2008 (Burns et al., 2008). Since 2003, there have been 615 H5N1 human cases with 364 deaths, for a mortality rate of 60% (WHO, 2013). A HPAI H7N7 virus began showing up on poultry farms in the Netherlands in 2003, leading to multiple outbreaks in poultry flocks and an outbreak in humans, causing 83 infections and 1 death (CDC, 2013). Rapid and specific detection of these viruses is needed to monitor current outbreaks and prevent future outbreaks (Lu et al., 2012). Laboratory diagnosis of HPAI takes 2-3 days, during which time the virus may have spread. A rapid, specific, and simple method for the detection of avian influenza viruses in the field is needed.

Currently virus isolation and real-time RT-PCR are the gold standard methods of AIV detection, though these are time-consuming, expensive and require specialized facilities and personnel. Commercially available rapid detection assays such as ELISA and immunochromatographic strip tests lack the required sensitivity and specificity to compete with the gold standard methods (Dhumpa et al., 2011). Biosensors, which combine a target-specific biological element with a transducer and signal processing unit, have shown great promise in their applications to pathogen detection for food safety, environmental monitoring, and clinical diagnostics. Some biosensors have been reported for the detection of AIV using methods such as surface plasmon resonance (Estmer-Nilsson et al., 2010; Bai et al., 2012; Suenaga et al., 2012;

Kim et al., 2009; Chang et al., 2010), quartz crystal microbalance (Peduru Hewa et al., 2009; Li et al., 2011; Owen et al., 2007; Wang and Li, 2013), fluorescence (Nguyen et al., 2012; Yun et al., 2007), optical interferometry (Xu et al, 2007), imaging ellipsometry (Qi et al., 2010), and electrochemistry (Lai et al., 2012; Diouani et al., 2008; Kamikawa et al., 2010). These developed sensors have shown potential but are not suitable for rapid, in-field testing due to either lack of specificity, high complexity, are too time-consuming or expensive, or are not practical for use on site or in field conditions.

Impedance biosensors measure changes in the electrochemistry of a sample to detect a specific analyte. They have several advantages over conventional AIV detection methods and also other types of the biosensors developed for AIV detection. They can be easily miniaturized and have a low cost and simple design. Combining an impedance biosensor with an interdigitated microelectrode gives further advantages of low ohmic drop, rapid establishment of steady state, rapid reaction kinetics, increased signal to noise ratio, and reduced sample size and detection time due to rapid response time (Varshney and Li, 2009). The addition of microfluidics to biosensors allows for precise control of small sample volumes, faster detection times due to the proximity of the sample to the transducer, and high surface area to volume ratio. The ability to work with a small sample size allows for the concentration of a larger sample, resulting in more sensitive detection, and also means that a person performing the test is exposed to less of potentially dangerous pathogens (Whitesides, 2006)

DNA aptamers are single-stranded oligonucleotides that can be selected to bind to specific targets such as proteins, carbohydrates, lipids, small organic and inorganic molecules, and metal ions. They have been looked to as alternatives to antibodies due to a number of advantages such as high thermal and chemical stability, chemical selection that allows for a great

deal of freedom in the selection pressures, and chemical synthesis, which results in low cost and no batch-to-batch variation (Iliuk et al., 2011). This study also suggested that aptamers have added advantages when used in impedance biosensors in that their small size and uniformity result in low noise and high repeatability.

Several impedance biosensors have previously been developed for the detection of AIV subtype H5 or H5N1. A non-Faradic impedance biosensor was investigated in combination with a microfluidic flow cell containing an embedded interdigitated microelectrode array and immunomagnetic separation using anti-H5 antibody-coated magnetic nanobeads, and a lower detection limit of  $10^3 \text{ EID}_{50} \text{ ml}^{-1}$  was achieved specific for the H5 subtype (Li et al., 2006; Wang et al., 2011). The second non-Faradic biosensor developed for the detection of AIV H5N1 used immunomagnetic separation with anti-H5 antibody-coated magnetic nanobeads, a microfluidic flow cell with an embedded interdigitated microelectrode that was coated in anti-N1 antibody and chicken red blood cell (RBC) labels for amplification (Lum et al., 2012). This biosensor was capable of specifically detecting AIV subtype H5N1 at  $10^3 \text{ EID}_{50} \text{ ml}^{-1}$  but had a detection time of 2 h and required multiple steps in the detection protocol. A Faradic impedance biosensor was developed using an open interdigitated microelectrode array with immobilized polyclonal antibody against H5, and when RBC amplification was used the sensor had a lower detection limit of  $10^3 \text{ EID}_{50} \text{ ml}^{-1}$  (Wang et al., 2009).

Several aptamer-based biosensors have been developed for the detection of AIV. Bai et al. (2012) reported a surface plasmon resonance aptasensor for the detection of AIV H5N1. The developed aptasensor had a detection time of 1.5 h and a lower detection limit of  $2^7 \times 10^{-4}$  HAU. A hydrogel-based QCM aptasensor was able to detect AIV H5N1 at  $2^7 \times 10^{-4}$  HAU in 30 min (Wang and Li, 2013). Though the developed aptasensor was both rapid and sensitive, it is not

practical for in-field use due to QCM's predisposition to environmental noise (Spangler et al., 2001). Cui et al. (2011) investigated a method of labeling AIV particles with aptamer-coated quantum dots, but no detection limit or detection time was given.

In this study, a non-Faradic impedance biosensor was developed for the detection of AIV H5N1 and H7N2 using a microfluidic flow cell with an embedded interdigitated microelectrode coated with aptamers specific for either AIV H5N1 or AIV H7N2. The microelectrode surface was modified using streptavidin and biotin-labeled aptamer was immobilized through biotin-streptavidin binding. Target AIV was captured on the microelectrode surface, causing an increase in impedance magnitude. The specificity of the aptasensors was tested with non-target AIV subtypes. Scanning electron microscopy was used to confirm the binding of AIV on the electrode surface.

### **5.3 Materials and methods**

#### **5.3.1 Materials**

Phosphate buffered saline (PBS, 10 mM, pH 7.4) was purchased from Sigma-Aldrich (St. Louis, MO). Streptavidin was purchased from Rockland Immunochemicals Inc. (Gilbertsville, PA) and reconstituted in PBS to a concentration of 0.2 mg ml<sup>-1</sup>. Biotinylated single-stranded DNA aptamers against H5N1 (73 nt; 5'-GTG TGC ATG GAT AGC ACG TAA CGG TGT AGT AGA TAC GTG CGG GTA GGA AGA AAG GGA AAT AGT TGT CCT GTT G-3') (Wang et al., 2013) and H7N2 (80 nt; 5'-CCG AAT TCG AAG GAC AAG AGG CGA AAA GAT TTA AAG TAA TCA AAG ACT GAG CAA CTC TTA TCT TTT ATG CTA CGT CCC GC-3') (Lum et al., 2013) were purchased from Integrated DNA Technologies (Coralville, IA) and reconstituted in PBS to a concentration of 220 µg ml<sup>-1</sup>. Washing solution (0.04 M imidazole

buffered saline with 0.4% Tween 20) was purchased from KPL, Inc. (Gaithersburg, MD) and diluted with Milli-Q water (18.2 MΩ cm, Millipore, Bedford, MA) to 1:200,000 dilution for use as a measuring buffer.

Inactivated avian influenza subtypes H5N1 (Scotland/59) and H7N2 were provided by the USDA/APHIS National Veterinary Services Lab (Ames, IA) and the Animal Diagnostics Laboratory at Pennsylvania State University (University Park, PA), respectively. The stock concentration of both viruses was  $2^7$  hemagglutination units (HAU)  $50 \mu\text{l}^{-1}$ . All use of HAU will refer to HAU  $50 \mu\text{l}^{-1}$ . Non-target AIV subtypes H1N1 and H2N2 were also provided by the Animal Diagnostics Laboratory at Pennsylvania State University (University Park, PA). All viruses were inactivated by the providers using  $\beta$ -propiolactone, eliminating infectivity while preserving hemagglutination activity (Goldstein and Tauraso, 1970). Sterile PBS was used for virus dilutions.

### **5.3.2 Microfluidics biochips with embedded interdigitated microelectrodes**

A microfluidics biochip with an embedded gold interdigitated microelectrode was designed and fabricated using the method described by Varshney et al. (2007). A microfluidic channel (40  $\mu\text{m}$  deep and 100  $\mu\text{m}$  wide) with an oval-shaped microfluidics chamber (40  $\mu\text{m}$  deep, 500  $\mu\text{m}$  wide and 1723  $\mu\text{m}$  long; 34.5 nl volume) was molded from polydimethylsiloxane (PDMS) and fixed to an interdigitated microelectrode chip with a glass substrate. Each electrode consisted of 25 pairs of 10  $\mu\text{m}$  wide electrode fingers spaced 10  $\mu\text{m}$  apart.

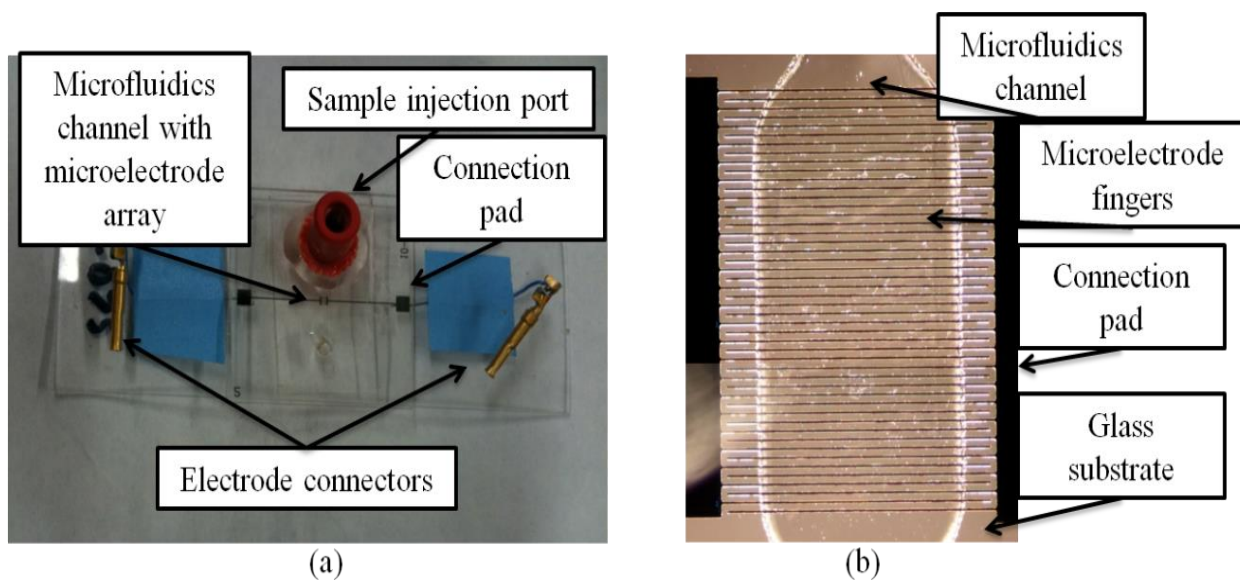


Fig 5.1. (a) Microfluidics biochip with an embedded gold interdigitated array with electrode connections and sample injection port. (b) Close up of interdigitated microelectrode array with PDMS microfluidics flow chamber.

### 5.3.3 Aptamer immobilization

The experimental protocol consisted of immobilization of a specific aptamer onto the microelectrode surface followed by capture of influenza virus and impedance measurement as shown in Fig. 5.1. After each immobilization/capture step, the microfluidic chip was washed for 2 min with measuring buffer at a rate of  $16.7 \mu\text{l min}^{-1}$  to remove any unbound particles. The pump was then stopped and the impedance was measured after 2 min incubation. All incubations and measurements were done at room temperature.

The microfluidic chip was cleaned by pumping Milli-Q water (Milli-Q,  $18.2 \text{ M}\Omega \text{ cm}$ , Bedford, MA) for 15 min at a rate of  $16.7 \mu\text{l min}^{-1}$ . Streptavidin ( $0.2 \text{ mg ml}^{-1}$ ) was injected into the microfluidic chip and incubated for 30 min. The streptavidin was immobilized through direct adsorption onto the gold electrode. Biotin-labeled aptamer specific for either H5N1 or H7N2 was



injected and incubated for 30 min, allowing the aptamer to be immobilized through streptavidin-biotin binding ( $K_d=10^{-14}$  M).

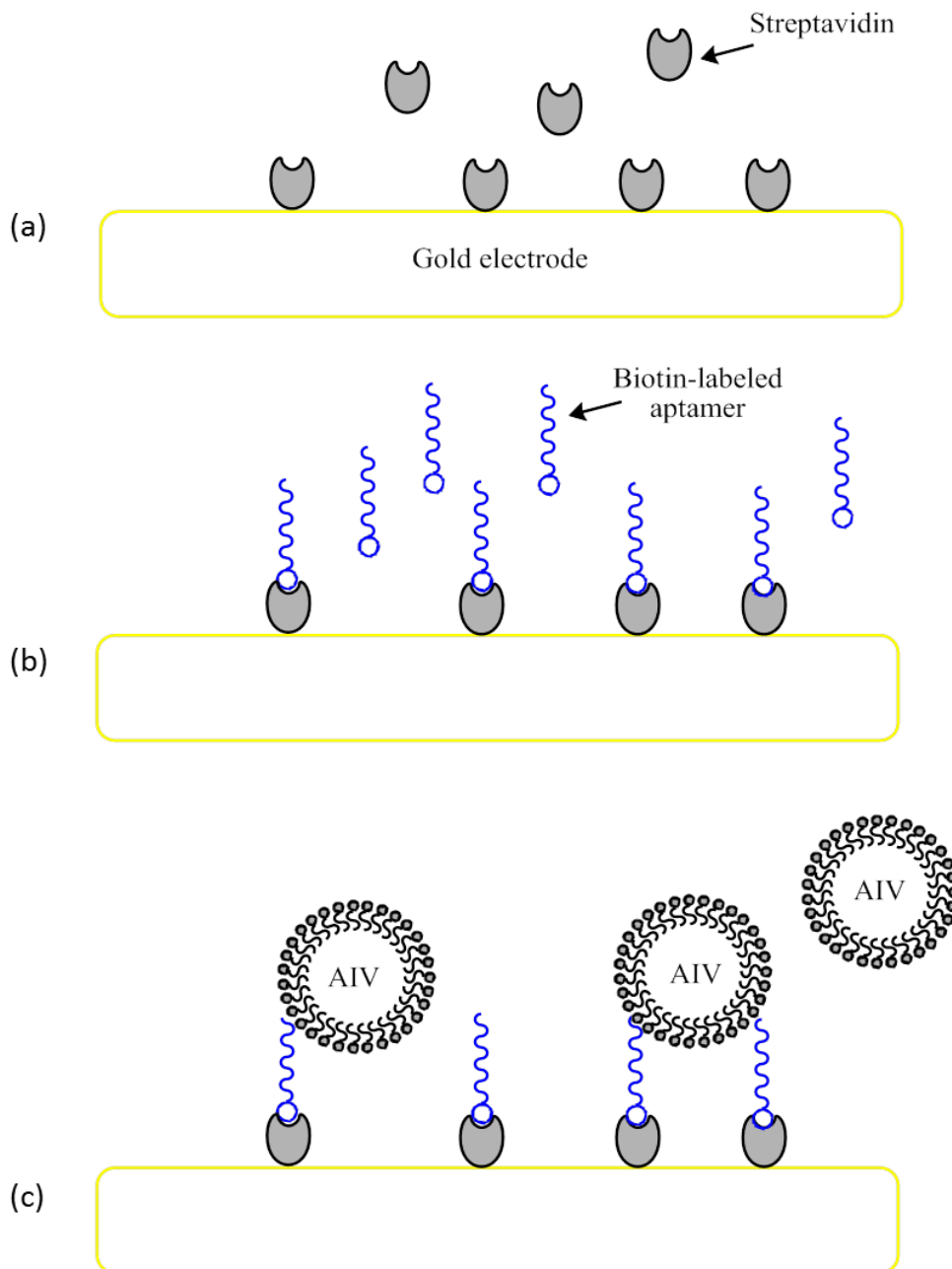


Fig. 5.2. Design of the impedance aptasensors for the detection of AIV subtype H7N2 and AIV H5N1. (a) The microelectrode surface was modified using streptavidin. (b) Biotin-labelled aptamer was then immobilized through biotin-streptavidin binding. (c) Target AIV was captured and the impedance was measured. After each step the flow cell was washed to remove unbound particles.

### **5.3.4 AIV detection**

Impedance measurements were taken using an IM-6 impedance analyzer with IM-6/Thales 2.49 software (BAS, West Lafayette, IN). The connecting wires of the microfluidic chip were attached to the test-sense and counter-reference probes of the impedance analyzer. In all impedance measurements a sinusoidal AC potential of 100 mV was applied. 100 mV was used in the study to overcome noise while impedance is still linearly measured (Varshney et al., 2007). Impedance magnitude and phase angle were measured at 54 points in the frequency range from 1 Hz to 1 MHz. All impedance measurements were done in the presence of measuring buffer.

A virus sample was injected into the microfluidic flow cell and incubated for 30 min. After washing the impedance was measured. The impedance change was calculated as the virus impedance minus the impedance of the aptamer immobilization. AIV H7N2 or H5N1 with titers in the range of  $2^7 \times 10^{-1}$  HAU and  $2^7 \times 10^{-5}$  HAU were measured. Triplicate tests were conducted at each virus concentration to determine the effect of virus concentration on the impedance change and to form a calibration curve for the sensor. A PBS sample containing no virus was used as a negative control.

Non-target AIV including subtypes of H1N1 and H2N2 were also used to determine the specificity of the aptasensor.

### **5.3.5 Electron microscopy**

Environmental scanning electron microscopy (ESEM) was used to confirm the binding of AIV on the electrode surface. Samples for ESEM were prepared by modifying the electrode surface with aptamer against H5N1 as described in Section 5.3.3. AIV H5N1 was then injected at

a concentration of  $2^7 \times 10^{-1}$  HAU and incubated for 30 min. Deionized water was then pumped into the flow cell at a rate of  $16.7 \mu\text{l min}^{-1}$  for 10 min to remove excess salts from the sample. The PDMS flow cell was removed from the electrode and the sample was allowed to dry in a fume hood overnight. . No critical point drying or sputter coating was used to prepare the samples. A Philips FEI XL-30 environmental scanning electron microscope (FEI, Hillsboro, OR) was used to take electron micrographs under a vacuum.

### **5.3.6 Statistical analysis**

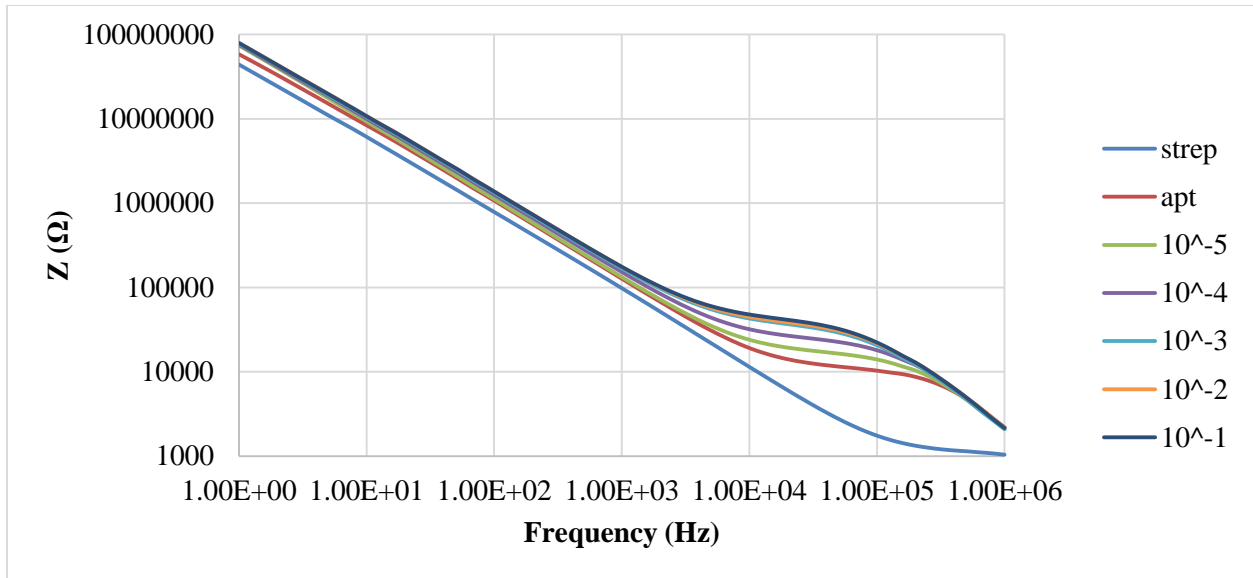
Microsoft Excel (Microsoft, Redmond, VA) was used for all statistical analysis of data and preparation of graphs. Means and standard deviations were calculated based on triplicate tests for each concentration. Lower detection limits were determined as a signal/noise ratio of 3, where noise was defined as the standard deviation of the negative PBS control. Statistically significant differences were determined using t-tests ( $\alpha=0.05$ ).

## **5.4 Results and Discussion**

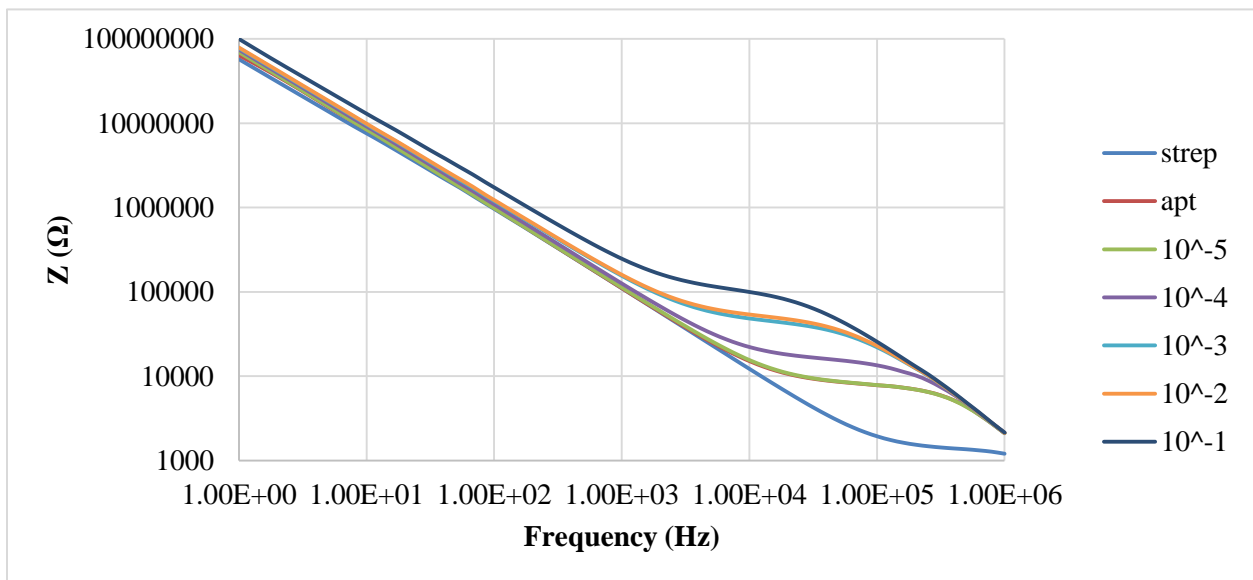
### **5.4.1 Characterization of impedance data**

Fig. 5.3 (a) and (b) show the impedance magnitude of each step of the aptamer immobilization and AIV capture of the aptasensors for the detection of H7N2 and H5N1, respectively. The physical adsorption of streptavidin onto the electrode surface caused a large decrease in impedance as compared to pure measuring buffer. An increase in impedance was seen after incubation with aptamers indicating successful immobilization of aptamers through biotin-streptavidin binding. The capture of AIV onto the modified electrode surface further increased impedance, with the increase in impedance correlated to the virus concentration. Fig.

5.4 (a) and (b) show the phase angle data of each step of the aptamer immobilization and AIV capture of the aptasensors for the detection of H7N2 and H5N1, respectively. At the frequency at which the greatest amount of impedance magnitude is seen (25.8 kHz, determined by percent change), the phase angle approaches zero, suggesting that the real component of the impedance plays a major role in the impedance change as compared to the imaginary component.

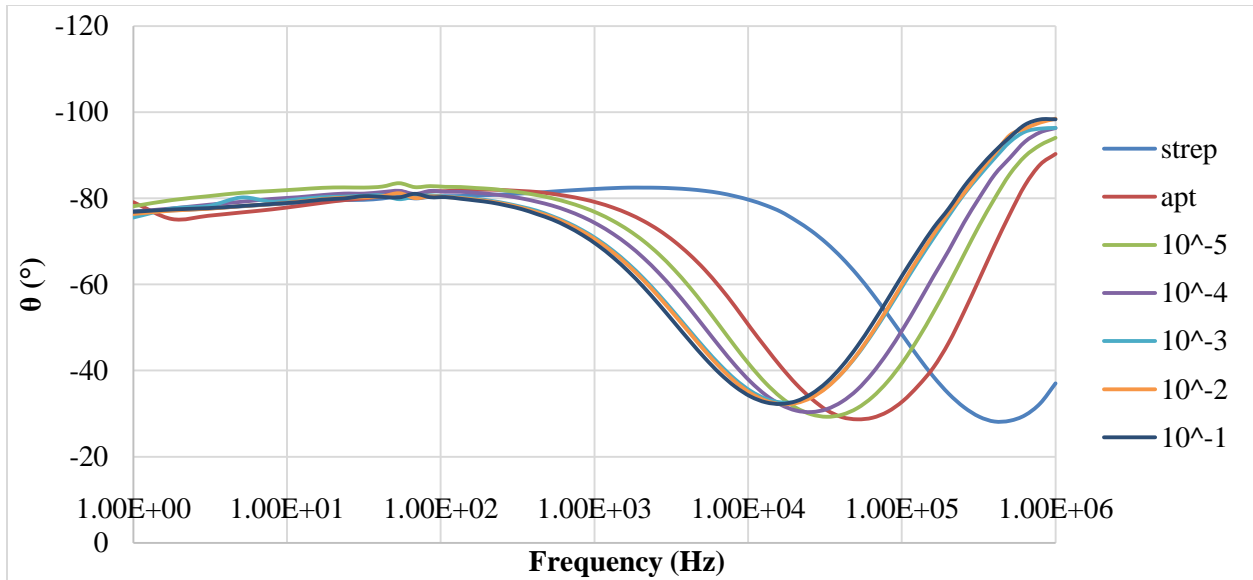


(a)

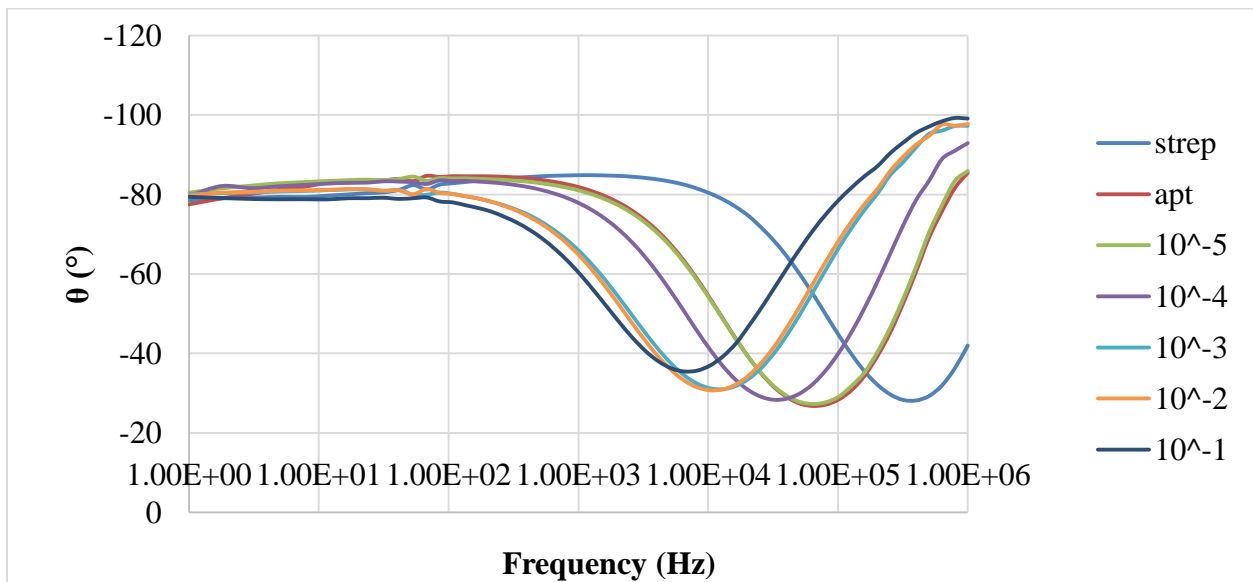


(b)

Fig. 5.3. Typical impedance magnitude data of the tests on (a) AIV H7N2 and (b) AIV H5N1. Data labels correspond to serial dilution value of  $2^7$  HAU virus sample ( $2^7 \times 10^{-1} \dots 2^7 \times 10^{-5}$ ). Frequency range was from 1 Hz to 1 MHz. Amplitude of voltage, 100 mV.



(c)



(d)

Fig. 5.4. Typical phase angle data of the tests on (c) AIV H7N2 and (d) AIV H5N1. Data labels correspond to serial dilution value of  $2^7$  HAU virus sample ( $2^7 \times 10^{-1} \dots 2^7 \times 10^{-5}$ ). Frequency range was from 1 Hz to 1 MHz. Amplitude of voltage, 100 mV.

The roles of the real and imaginary components were confirmed by constructing an equivalent circuit model as shown in Fig. 5.5 (a). The circuit consisted of two resistor elements,  $R_{sol}$  and  $R_{pdms}$ , and two capacitive elements,  $C_g$  and  $C_{dl}$ . The resistor elements corresponded to the resistance of the electrolyte solution ( $R_{sol}$ ) and the resistance of the PDMS layer connecting the electrode fingers ( $R_{pdms}$ ), while  $C_g$  and  $C_{dl}$  corresponded to the geometric capacitance of the electrolyte solution and the double layer capacitor formed by the ions near the electrode surface, respectively. This equivalent circuit was found to hold true for both H7N2 and H5N1 detection.

Fig. 5.5 (b) shows the measured experimental data compared to the simulated data from the equivalent circuit model gathered using the IM-6/Thales software. Data collected from the detection of  $2^7 \times 10^{-1}$  HAU AIV H7N2 and H5N1 was used for fitting analysis. 54 points from the experimental data were chosen by the software to fit a simulated impedance spectrum. The mean error between the experimental and simulated spectrums was 2.1% for the impedance magnitude and  $0.9^\circ$  for the phase angle, while the maximum error was 12.9% for impedance magnitude and  $13^\circ$  for the phase angle.



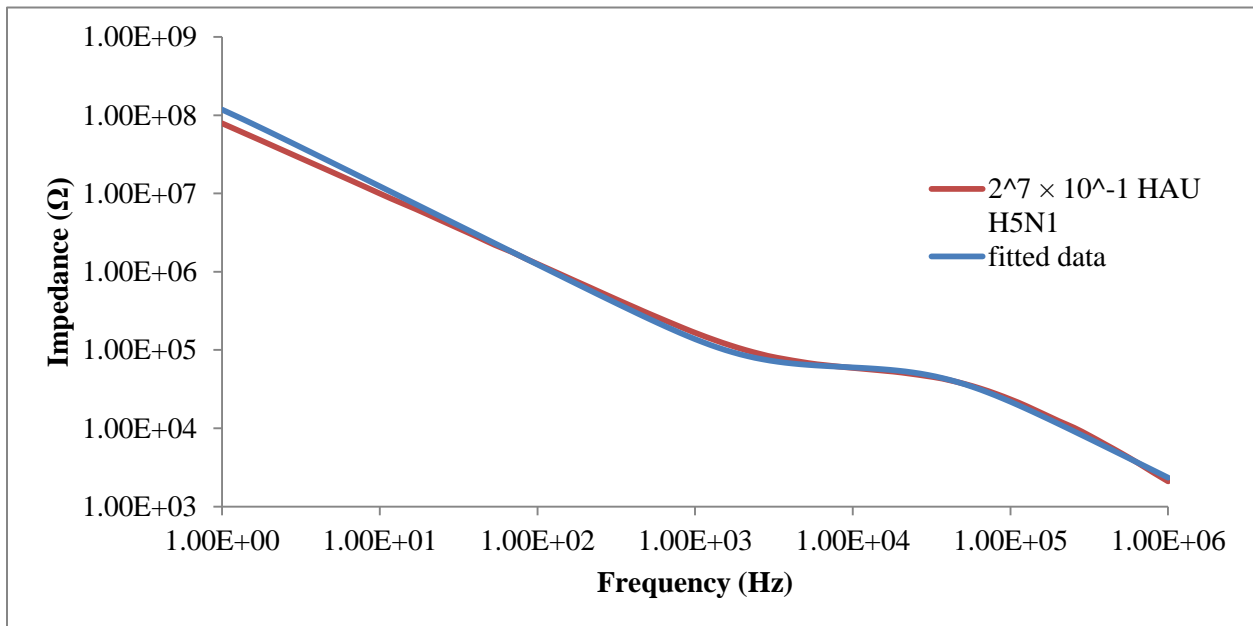
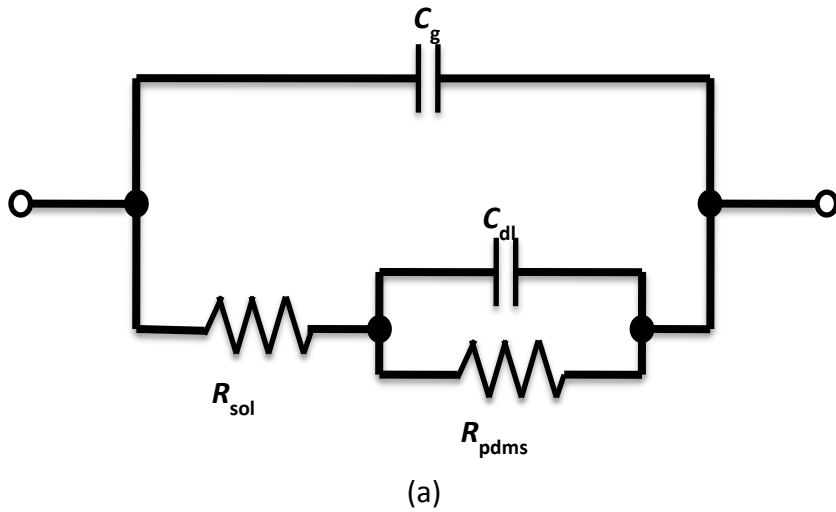


Fig. 5.5. (a) Equivalent circuit used for data analysis. The equivalent circuit components were resistance of the solution ( $R_s$ ), resistance of PDMS ( $R_{pdms}$ ), double layer capacitance ( $C_{dl}$ ), and geometrical capacitance ( $C_g$ ). (b) Bode diagram of measured impedance data and simulated impedance data generated by curve fitting of equivalent circuit. Measured data taken with  $2^7 \times 10^{-1}$  HAU H5N1 virus sample.

The role of each equivalent circuit element was further investigated to understand the phenomenon causing the impedance changes. Two elements were found to contribute to the impedance change,  $R_{sol}$  and  $C_{dl}$ . Their contribution to the impedance magnitude value, as calculated from the simulated values from the equivalent circuit model, is shown in Table 5.1. The  $C_{dl}$  element accounted for only 1 k $\Omega$  (1.8%) of the total impedance magnitude change, while the  $R_{sol}$  element accounted for 54.7 k $\Omega$  (98.2%) of the impedance magnitude change. The  $R_{pdlms}$  and  $C_g$  elements contributions to the impedance magnitude change were negligible. The  $R_{sol}$  and  $C_{dl}$  contributions to the impedance magnitude change confirm what was suggested by the phase angle data, that the real component, specifically  $R_{sol}$ , dominates at the frequency at which the greatest impedance magnitude change is seen. Due to the importance of  $R_{sol}$  to the impedance magnitude change it can be assumed that the largest factor in the system is the flow of ions between the electrode fingers, which was obstructed by the capture of virus onto the electrode surface. The capture of virus onto the electrode surface also affects the ability to form a double layer capacitor on the surface of the electrode, resulting in a small but non-negligible change in the impedance magnitude.

Table 5.1. Contributions of the elements in the equivalent circuit to the impedance magnitude. Impedance magnitude values were calculated using simulated data from fitting the equivalent circuit to measured data gathered in the detection of  $2^7 \times 10^{-1}$  HAU of AIV H5N1 and H7N2.

	$R_{sol}$ (k $\Omega$ )	$R_{pdms}$ ( $\Omega$ )	$C_{dl}$ (nF)	$C_g$ (pF)
<i>H5N1 detection</i>				
Aptamer	9.4	282	1.486	73.55
Virus	64.1	388	0.870	65.98
% of change	582	37.6	-41.5	-10.3
<i>H7N2 detection</i>				
Aptamer	12.8	246	1.378	98.86
Virus	49.6	308	1.064	67.69
% change	287	25.2	-22.8	-31.5

The immobilization of the H7N2 aptamer caused an 8.3 k $\Omega$  impedance increase at 25.8 kHz while the immobilization of the H5N1 aptamer only caused a 5 k $\Omega$  increase. This may be explained by the differences in sequence and secondary structures between the two aptamers. Changes in the structure and shape of a DNA oligonucleotide may affect its electrochemical properties (Wang, 2008). The H7N2 aptamer sequence has a lower G-C content (41.3%) than the H5N1 aptamer sequence (47.9%). The H7N2 aptamer's secondary structure also has a lower melting temperature ( $T_m = 36.4$  °C) than the H5N1 aptamer secondary structure ( $T_m = 49.6$  °C).

The secondary structures of the two aptamers differ in shape and melting temperature. The H7N2 aptamer structure consists of a large central circle with two small circles and one long finger ending in a small circle compared to the H5N1 aptamer structure which consisted of a central circle with two fingers ending in similar sized circles.

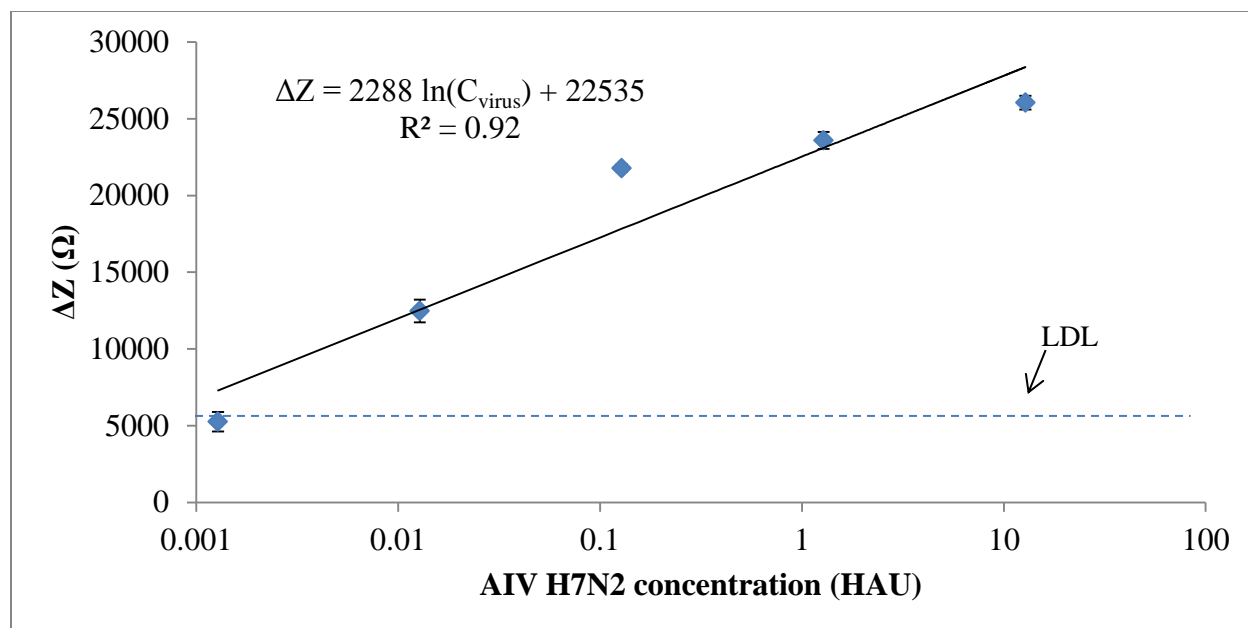
The equivalent circuit model was used to investigate the reason for the difference in impedance values between the two aptamers. While the  $R_{sol}$  value for increased after the both aptamers were immobilized (H5N1 aptamer,  $\Delta R_{sol} = 8 \text{ k}\Omega$ ; H7 aptamer,  $\Delta R_{sol} = 10 \text{ k}\Omega$ ), the effect on capacitance by the two aptamers was very different. The immobilization of the H5N1 aptamer caused a small increase in the  $C_{dl}$  value ( $\Delta C_{dl} = 0.024 \text{ nF}$ ) and a decrease in the  $C_g$  value ( $\Delta C_g = -15.14 \text{ pF}$ ), while the H7N2 aptamer caused a large decrease in the  $C_{dl}$  value ( $\Delta C_{dl} = -0.297 \text{ nF}$ ) and a decrease in the  $C_g$  value ( $\Delta C_g = -26.75 \text{ pF}$ ). This indicates the immobilization of the H7N2 aptamer disrupted the both the double layer capacitance and the geometric capacitance. More studies could be conducted to further investigate the role of aptamer sequence and structure on impedance values.

The equivalent circuit investigation also showed that the capture of the  $2^7 \times 10^{-1}$  HAU H7N2 caused a 0.314 nF decrease in the  $C_{dl}$  element while the capture of  $2^7 \times 10^{-1}$  HAU H5N1 caused a decrease of 0.616 nF. This difference could be because the immobilization of the H7N2 aptamer had already disrupted the double layer capacitance. This knowledge could affect how future aptamers are developed for use in electrochemical sensing techniques.

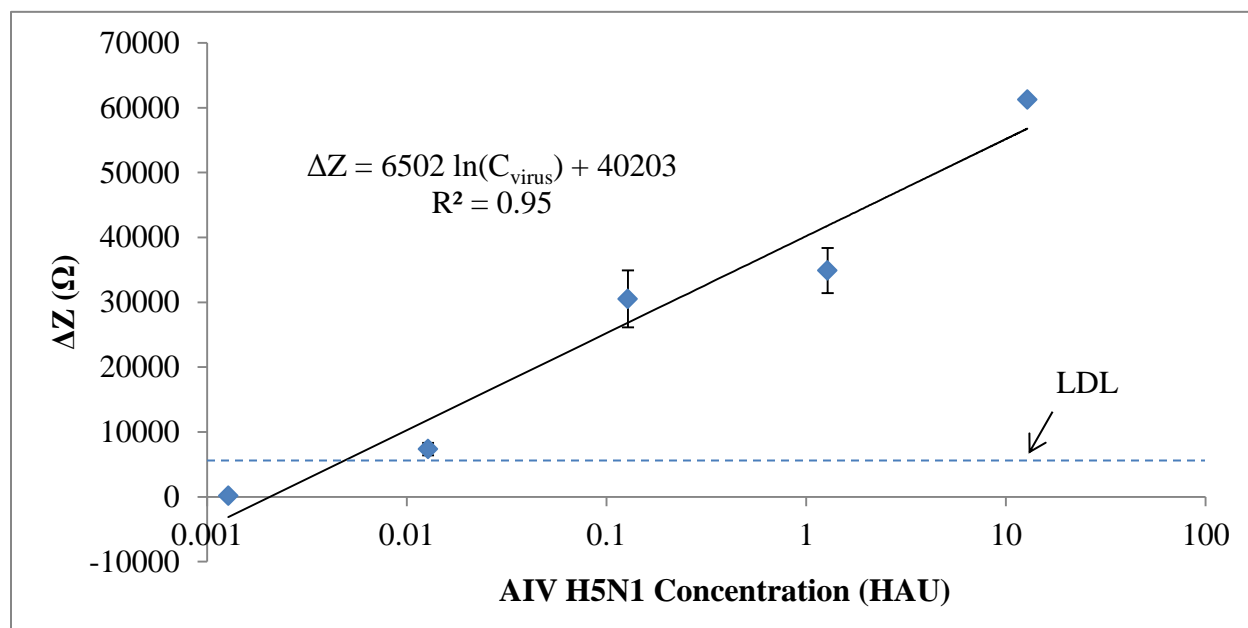
#### **5.4.2 Detection of AIV H7N2 and H5N1**

Figures 5.6 (a) and (b) show the impedance magnitude change at 25.8 kHz plotted for each concentration from  $2^7 \times 10^{-1}$  to  $2^7 \times 10^{-5}$  HAU for H7N2 and H5N1, respectively. As stated

in Section 3.1, 25.8 kHz was found to be the point at which the greatest impedance magnitude change was seen for both the H7N2 and H5N1.



(a)



(b)

Fig. 5.6. Average impedance change caused by different concentrations of (a) AIV H7N2 and (b) AIV H5N1. The values of horizontal axis correspond to serial dilution value of  $2^7$  HAU virus sample ( $2^7 \times 10^{-1} \dots 2^7 \times 10^{-5}$ ). Error bars based on the standard deviation of means in triplicate tests. LDL line was determined by signal/noise ratio of 3. The impedance was measured at the frequency of 25.8 kHz.

For the detection of AIV H7N2 a logarithmic relationship was found between the impedance change,  $\Delta Z$  in  $\Omega$ , and the virus concentration,  $C_{\text{virus}}$  in  $\log(\text{HAU})$ , in the range of  $2^7 \times 10^{-1}$  to  $2^7 \times 10^{-5}$  HAU ( $\Delta Z = 2288 \ln(C_{\text{virus}}) + 22535$ ;  $R^2=0.92$ ) and the lower detection limit was determined to be  $2^7 \times 10^{-4}$  HAU. A linear relationship was also seen for the detection of AIV H5N1 ( $\Delta Z = 6502 \ln(C_{\text{virus}}) + 40203$ ;  $R^2=0.95$ ) and the lower detection limit was found to be the same as that for the detection of H7N2,  $2^7 \times 10^{-4}$  HAU. In Fig. 5.6 (a), it can be seen that the  $\Delta Z$  values begin to plateau after between  $2^7 \times 10^{-3}$  and  $2^7 \times 10^{-1}$  HAU. This suggests that the carrying capacity of the electrode surface may have begun to reach its limit after these concentrations. Fig. 5.6 (b) shows larger error bars in the detection of H5N1 as compared to that in the detection H7N2 and a lower  $\Delta Z$  for  $2^7 \times 10^{-4}$  HAU. This may be explained by the binding site of the H5N1 aptamer, which requires a combination of both the H5 and N1 proteins in the correct orientation for efficient binding. The experimental data fits the hypothesis that capture of H5N1 by the H5N1 aptamer may be less efficient and therefore more erratic than the capture of H7N2 by the H7N2 aptamer, which requires only one protein to be present and has no restrictions on orientation with other proteins. Since the H7N2 aptamer was designed to target the H7 protein, it has ~400-500 hemagglutinin molecules to attach to on the virus surface, likely allowing a single virus to be captured by multiple aptamers on the electrode surface, resulting in high avidity and efficient capture of the virus. The H5N1 aptamer was designed to specifically target only the H5N1 subtype. This requires that the aptamer recognize a site at a junction between a H5 molecule and N1 molecule (~100-150 per virus) in the correct orientation, limiting the number of binding sites available. While a single H5N1 aptamer may have a high affinity to its target, the limited number of binding sites results in less avidity and less efficient capture on the electrode surface. This results in the larger standard deviation seen when detecting AIV H5N1. The high

$\Delta Z$  and small error bar at the  $2^7 \times 10^{-1}$  HAU concentration may reflect a saturation of the virus onto the electrode surface, which resulted in forced binding of the virus to the aptamer.

In the detection of AIV H5N1, a higher  $\Delta Z$  was seen as compared the detection of H7N2. This may result from the differences in the aptamer binding kinetics discussed above. Since the H7N2 aptamer can easily bind multiple sites on the virus surface, it is possible that fewer virus particles can bind on the electrode surface. This is due to a single virus binding multiple aptamers on the electrode surface, leaving fewer binding sites on the electrode and limiting the number of virus particles that can be captured. The larger  $\Delta Z$  values seen in the H5N1 detection may also be due to the binding kinetics of the H5N1 aptamer. Because the binding sites are limited on the virus surface, fewer binding sites on the electrode surface are taken up by one virus. This may mean that more virus particles can be bound on the electrode, resulting in larger  $\Delta Z$  values. Though more virus particles may have been bound to the electrode when detecting H5N1, the capture of the virus was less efficient which resulted in larger standard deviations. When detecting H7N2, multiple aptamers are likely bound to a single virus particle, giving high avidity and capture efficiency and therefore low standard deviations.

Some differences in  $\Delta Z$  values may also be due to differences in the H5N1 and H7N2 virus particles, which may differ in lipid and protein content.

The lower detection limit of the aptasensor was the same as a previously described impedance immunosensors (Wang et al., 2009; Lum et al., 2012) for the detection of H5N1, though the aptasensors were capable of detecting AIV and formulating a linear calibration curve without the use of labels or pre-concentration, decreasing the detection time and resources needed. The total detection time from injection of a virus sample to impedance measurement was



30 min, a fourth of the time the previous immunosensor required (Lum et al., 2012). The small size and uniformity of the aptamers meant that the impedance aptasensors were more sensitive and had higher repeatability compared to equivalent impedance immunosensors. The use of DNA aptamers also meant that a blocking step was not needed, saving time and resources (Willner and Zayats, 2007). The lack of a blocking step likely increased the sensitivity of the aptasensor due to the lack of noise caused by a blocking layer.

The developed impedance aptasensor had a lower detection limit and shorter detection time compared to the SPR aptasensor by Bai et al. (2012). The QCM aptasensor developed by Wang and Li (2013) had the same lower detection limit and detection time as the developed impedance aptasensor but the impedance aptasensor is a more practical format for rapid, in-field testing because impedance biosensors are easily miniaturized, low energy requirements, and simple design.

Fig. 5.7 (a) shows the electrode surface with streptavidin and aptamers immobilized before virus capture. Fig. 5.7 (b) shows the electrode surface after capture of AIV H5N1.

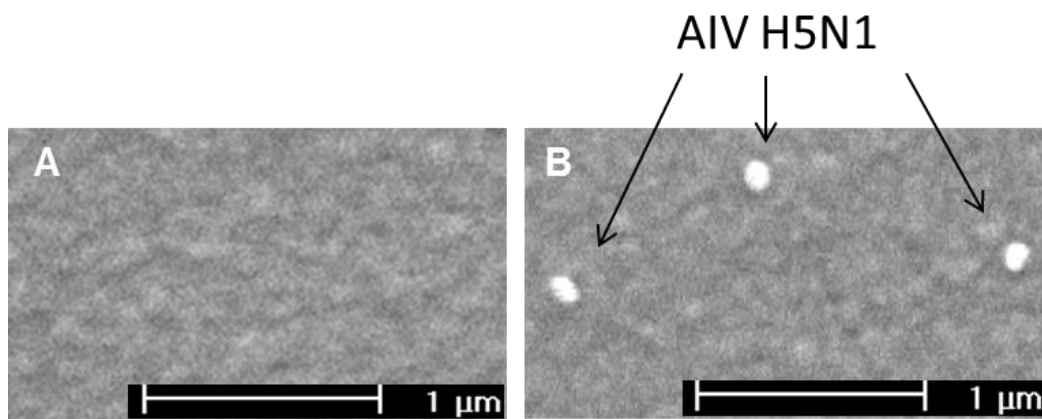
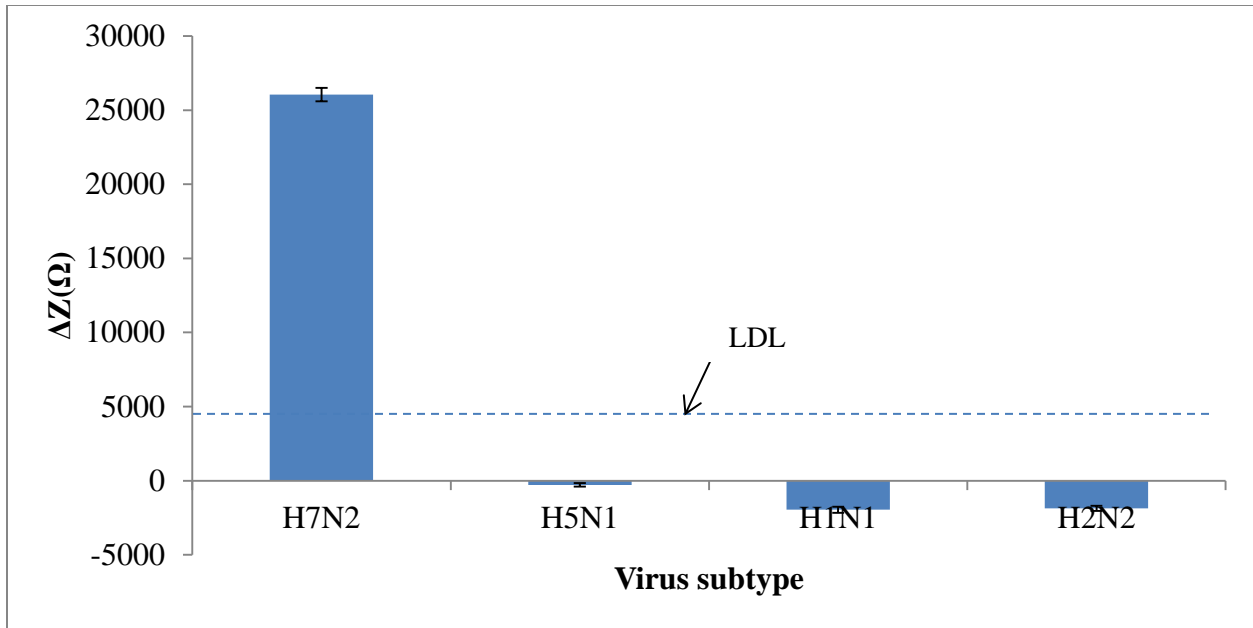


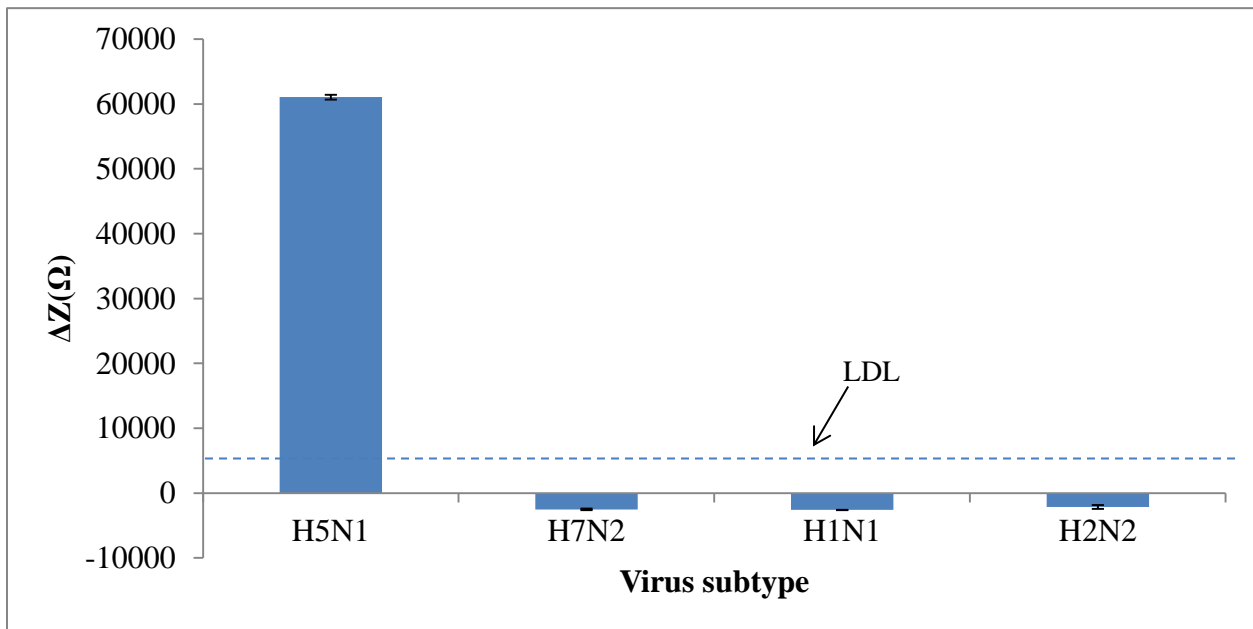
Fig. 5.7. ESEM micrographs of the electrode surface with immobilized aptamers (a) before and (b) after AIV capture.

### 5.4.3 Specificity of the aptasensor in detection of AIV H7N2 and H5N1

Figures 5.8 (a) and (b) show the  $\Delta Z$  at 25.8 kHz for the target viruses compared to the non-target virus for the detection of H7N2 and H5N1, respectively. Each virus was tested using three non-target virus subtypes at the concentration of  $2^7 \times 10^{-1}$  HAU. Both tests showed a negative impedance change after incubation with non-target AIV subtypes, indicating no non-specific interaction. The average impedance decrease for both tests was  $\sim 2$  k $\Omega$  except for the measurement of non-target AIV H5N1 when using the H7N2 aptamer, which resulted in an average impedance decrease of  $\sim 300$   $\Omega$ . Prior testing of the H5N1 aptamer specificity with multiple H5 subtype AIVs was done in two previous studies (Wang et al., 2013; Bai et al., 2012). The specificity of the H7N2 aptamer was also discussed in a previous study (Lum et al., 2013).



(a)



(b)

Fig. 5.8. Average impedance change caused by  $2^7 \times 10^{-1}$  HAU target and three non-target virus at 25.8 kHz in the detection of (a) H7N2 and (b) H5N1. Error bars based on the standard deviation of mean in triplicate tests. LDL line was determined by signal/noise ratio of 3.

The negative  $\Delta Z$  values seen for the non-target virus subtypes may be due to the removal of some of the immobilized aptamers and streptavidin by bombardment by the non-target virus particles. This effect could be of concern if the aptamer-coated electrode were used in multiple negative field samples, where the complex media may wash away the immobilized streptavidin and aptamers. Chemical immobilization, which typically results in a stronger attachment to the electrode surface, could be used to lessen this effect.

The smaller impedance decrease for the non-target AIV H5N1 when using the H7N2 aptamer could possibly be due to some very minor non-specific interaction between AIV H5N1 and the H7N2 aptamer. A small amount of non-specific binding could have slightly offset the impedance decrease caused by the removal of the immobilized elements. This effect was very small though and far below the threshold for detection. Though previous studies have tested the specificity of the H7 aptamer and found no non-specific interaction, those tests were not as sensitive as the developed impedance biosensor and so a very small amount of non-specific interaction would have gone unnoticed.

## **5.5 Conclusion**

An impedance aptasensor was developed using microfluidic flow cells with interdigitated electrodes for the rapid and specific detection of AIV subtypes H5N1 and H7N2. The aptasensor was capable of detecting AIV at concentrations as low as  $2^7 \times 10^{-4}$  HAU in 30 min. The developed aptasensor was capable of matching the detection limit of previously developed impedance immunosensors for AIV detection without label amplification or sample pre-concentration, while reducing the detection time and required resources. Compared to previously

developed aptasensors for AIV detection, the impedance aptasensor was either more or as sensitive and was a more practical design for in-field tests.

Future research may involve taking advantage of aptamer's high stability to prepare electrodes far in advance of AIV detection. This would make the developed aptasensor even more practical for rapid, in-field tests.

The two aptamers were evaluated in this study for their applications in detection of AIV using biosensing techniques. The highly specific H5N1 aptamer was able to give higher subtype specificity than the less specific H7N2 aptamer, though at the cost of small standard deviations. From the experimental results it can be suggested that an aptamer targeting only a single protein should be more useful, due to the higher repeatability, for the majority of rapid detection techniques unless high subtype specificity is needed.

## 5.6 References

- Bai, H., Wang, R., Hargis, B., Lu, H., Li, Y., 2012. *Sensors* 12, 12506-12518.
- Burns, A., van der Mensbrugge, D., Timmer, H., 2008. World Bank Report. [http://siteresources.worldbank.org/EXTAVIANFLU/Resources/EvaluatingAHIEconomics\\_2008.pdf](http://siteresources.worldbank.org/EXTAVIANFLU/Resources/EvaluatingAHIEconomics_2008.pdf) (accessed 1.23.13)
- CDC, 2013. <http://www.cdc.gov/flu/avian/h7n7-netherlands.htm> (accessed 2-14-2013).
- Chang, Y., Wang, S., Huang, J.C., Su, L., Yao, L., Li, Y., Wu, S., Chen, Y.A., Hsieh, J., Chou, C., 2010. *Biosens. Bioelectron.* 26, 1068-1073.
- Chen, L., Sheng, Z., Zhang, A., Guo, X., Li, J., Han, H., Jin, M., 2010. *Luminescence* 25, 419-423
- Cui, Z.Q., Ren, Q., Wei, H.P., Chen, Z., Deng, J.Y., Zhang, Z.P., Zhang, X.E., 2011. *Nanoscale* 3, 2454-2457.
- Dhumpa, R., Handberg, K.J., Jørgensen, P.H., Yi, S., Wolff, A., Bang, D.D., 2011. *Diagn. Microbiol. Infect. Dis.* 69, 258-265.

- Diouani, M.F., Helali, S., Hafaid, I., Hassen, W.M., Snoussi, M.A., Ghram, A., Jaffrezic-Renault, N., Abdelghani, A., 2008. *Mater. Sci. Eng. C.* 28, 580-583.
- Estmer Nilsson, C., Abbas, S., Bennemo, M., Larsson, A., Hämäläinen, M.D., Frostell-Karlsson, Å., 2010. *Vaccine* 28, 759-766.
- Goldstein, M.A., Tauraso, N.M., 1970. *Appl. Microbiol.* 19 (2), 290–294.
- Iliuk, A.B., Hu, L., Tao, W.A., 2011. *Anal. Chem.* 83, 4440-4452.
- Kamikawa, T.L., Mikolajczyk, M.G., Kennedy, M., Zhang, P., Wang, W., Scott, D.E., Alocilja, E.C., 2010. *Biosens. Bioelectron.* 26, 1346-1352.
- Kim, S., Kim, S., Lee, S., Park, T., Byun, K., Kim, S., Shuler, M., 2009. *J. Opt. Soc. Korea.* 13(3), 392-397.
- Lai, W., Lin, C., Yang, Y., Lu, M.S., 2012. *Biosens. Bioelectron.* 35, 456-460.
- Li, Y., Hargis, B., Tung, S., Berghman, L., Bottje, W., Wang, R., Ye, Z., Varshney., M., Srinivasan, B., 2006. US Patent Applications 60/876,919.
- Li, D., Wang, J., Wang, R., Li, Y., Abi-Ghanem, D., Berghman, L., Hargis, B., Lu, H., 2011. *Biosens. Bioelectron.* 26, 4146-4154.
- Lu, H., Lin, L., Wang, R., Li, Y., Scheuchenzuber, B., Liu, J., Xie, Z., Rosebrook, J., 2012. *Health.* 4, 923-926.
- Lum, J., Wang, R., Jiang, T., Li, Y., 2013. *J. Virol. Meth.* (in review)
- Lum, J., Wang, R., Lassiter, K., Srinivasan, B., Abi-Ghanem, D., Berghman, L., Hargis, B., Tung, S., Lu, H., Li, Y., 2012. *Biosens. Bioelectron.* 38, 67-73.
- Nguyen T, Ung T, Vu T, Tran T, Dong V, Dinh, Nguyen, Q., 2012. *Adv. Nat. Sci.: Nanosci. Nanotechnol.* 3, 035014.
- Owen, T., Al-Kaysi, R., Bardeen, C., Cheng, Q., 2007. *Sens. Actuators B.* 126, 691-699.
- Peduru Hewa, T.M., Tannock, G.A., Mainwaring, D.E., Harrison, S., Fecondo, J.V., 2009. *J. Virol. Methods* 162, 14-21.
- Qi, C., Tian, X., Chen, S., Yan, J., Cao, Z., Tian, K., Gao, G.F., Jin, G., 2010. *Biosens. Bioelectron.* 25, 1530-1534.
- Spangler, B.D., Wilkinson, E.A., Murphy, J.T., Tyler, B.J., 2001. *Anal. Chim. Acta.* 444, 149-161.
- Suenaga, E., Mizuno, H., Penmetcha, K.K.R., 2012. *Biosens. Bioelectron.* 32, 195-201.

- Varshney, M., Li, Y., 2009. *Biosens Bioelectron.* 24, 2951-2960.
- Varshney, M., Li, Y., Srinivasan, B., Tung, S., 2007. *Sens. Actuators B.* 128, 99-107.
- Wang, J., 2008. *Phys. Rev. B.* 78, 245304.
- Wang, R., Li, Y., 2013. *Biosens. Bioelectron.* 42, 148-155.
- Wang, R., Li, Y., Hargis, B., Tung, S., Bottje, W., Lassiter, K., Brewer, R., Srinivasan, B., 2007. ASABE Paper No. 077112.
- Wang, R., Lin, J., Lassiter, K., Srinivasan, B., Lin, L., Lu, H., Tung, S., Hargis, B., Bottje, W., Berghman, L., Li, Y., 2011. *J. Virol. Methods* 178, 52-58.
- Wang, R., R., Zhao, J., Jiang, T., Kwon, Y., Lu, H., Jiao, P., Liao, M., Li, Y., 2013. *J. Virol. Methods.* 189, 362-369.
- Wang, R., Wang, Y., Lassiter, K., Li, Y., Hargis, B., Tung, S., Berghman, L., Bottje, W., 2009. *Talanta* 79, 159-164.
- Whitesides, G.M., 2006. *Nature* 442, 368-373.
- WHO, 2013.  
[http://www.who.int/influenza/human\\_animal\\_interface/EN\\_GIP\\_20130201CumulativeNumberH5N1cases.pdf](http://www.who.int/influenza/human_animal_interface/EN_GIP_20130201CumulativeNumberH5N1cases.pdf) (accessed 2-14-2013)
- Willner, I., Zayats, M., 2007. *Angew. Chem. Int. Ed Engl.* 46, 6408-6418.
- Xu, J., Suarez, D., Gottfried, D., 2007. *Anal. Bioanal. Chem.* 389, 1193-1199.
- Yun, Z., Zhengtao, D., Jiachang, Y., Fangqiong, T., Qun, W., 2007. *Anal. Biochem.* 364, 122-127.

## **6. A label-free impedance biosensor using screen-printed interdigitated electrodes and magnetic nanobeads for the detection of *E. coli* O157:H7**

### **6.1 Abstract**

*Escherichia coli* O157:H7 is one of the most dangerous foodborne pathogens, infecting an estimated 90,000 people in the US each year and having an infective dose as low as 10 cells. In this study an impedance biosensor based on the use of magnetic nanobeads and screen-printed interdigitated electrodes was developed for the rapid detection of *E. coli* O157:H7. Magnetic nanobeads coated with anti-*E. coli* antibody were mixed with an *E. coli* sample and used to isolate and concentrate the bacterial cells. The sample was suspended in redox probe and placed on to a screen-printed interdigitated electrode. A magnetic field was applied to concentrate the cells on the surface of the electrode and the impedance was measured. The impedance biosensor could detect *E. coli* O157:H7 at a concentration of  $10^{4.45}$  cfu ml<sup>-1</sup> (corresponding to ~1400 bacterial cells) in less than 1 h. A linear relationship between bacteria concentration and impedance value was seen between  $10^5$  cfu ml<sup>-1</sup> and  $10^7$  cfu ml<sup>-1</sup>. Though impedance measurement was carried out in the presence of a redox probe, analysis of the equivalent circuit model showed that the impedance change was primarily due to two elements: double layer capacitance and resistance due to electrode surface roughness. Computer simulation with COMSOL Multiphysics software was used to confirm the necessity of the magnetic field.



## 6.2 Introduction

*E. coli* O157:H7 is one of the most dangerous foodborne pathogens, infecting an estimated 63,000 people in the US each year, including 20 deaths, and having an infective dose as low as 10 cells (FDA, 2012; Scallan et al., 2011). Infection of *E. coli* O157:H7 may cause a life-threatening complication known as hemolytic uremic syndrome in 10-15% of patients with hemorrhagic colitis. *E. coli* O157:H7 infections have primarily been associated with ground beef and leafy green produce but increased integration of the food supply chain has resulted in *E. coli* O157:H7 contamination of unusual food products, such as cookie dough and hazelnuts (Miller et al., 2012). Contaminated food products not only threaten human health but also cost food producers millions of dollars in economic loss (Rekow et al., 2011). As such, a method to rapidly detect *E. coli* O157:H7 in food products is needed.

Bacterial culture and plating and polymerase chain reaction are the traditional methods for *E. coli* O157:H7 detection, but these methods are time-consuming and require trained personnel and specialized laboratories and equipment. Results may take days, during which food products may have been shipped to consumers or to other producers. Biosensors have attracted attention in the field of foodborne pathogen detection due to their speed, simplicity, and low cost. Several types of biosensors have been developed for the detection of *E. coli* O157:H7 including quartz crystal microbalance (Shen et al., 2011; Poitras and Tufenkji, 2009; Liu et al., 2007; Jiang et al., 2011), surface plasmon resonance (Waswa et al., 2007; Wang et al., 2011; Eum et al., 2010; Subramanian et al., 2006) and electrochemistry (Varshney and Li, 2007; Chowdhury et al., 2012; Chan et al., 2012; Radke and Alocilja, 2005; Varshney et al., 2007; Varshney and Li, 2008; Lin et al., 2008; Settingington and Alocilja, 2011, Santos et al., 2013). Many of the developed biosensors relied on immobilization of antibodies on the sensing surface to

concentrate and hold the bacterial cells close enough to the sensing surface for measurement. This method has the problem of low capture efficiency, often being as low as 35% even after extensive optimization (Gehring et al., 2006). A method not reliant on antibody immobilization should be used to overcome the problem of low capture efficiency.

Magnetic nanoparticles have been used extensively in biosensors for bacterial detection though usually for immunomagnetic separation of the bacteria from a sample (Varshney and Li, 2007; Chowdhury et al., 2012; Chan et al., 2012) or as labels to increase the sensitivity of the biosensor (Liu et al., 2007; Jiang et al., 2011). Magnetic nanoparticles may also be used to concentrate the bacterial cells onto the sensing surface, as done by Varshney and Li (2007), where a magnetic field was applied under the electrode to pull the bacteria close to an interdigitated microelectrode array for sensitive detection. The interdigitated microelectrode arrays used by Varshney and Li (2007), while being highly sensitive, were time-consuming and expensive to produce, making them impractical for commercial use. Screen printed interdigitated electrodes are capable of being produced at a much lower cost and in high volume, making them practical for use in commercialized rapid tests.

In this study, an impedance biosensor for the detection of *E. coli* O157:H7 was developed using antibody-coated magnetic nanobeads and screen printed interdigitated electrodes. In the research the antibody-coated magnetic nanobeads served three roles: (1) to specifically separate *E. coli* O157:H7 cells from media and place them in redox probe for measurement, (2) to concentrate the separated *E. coli* O157:H7 into a smaller volume, and (3) to concentrate the *E. coli* O157:H7 cells onto the surface of the screen printed electrode. An equivalent circuit model was developed to understand the phenomenon involved in the impedance measurement.

## **6.3 Materials and methods**

### **6.3.1 Bacterial culture**

*Escherichia coli* O157:H7 was purchased from American Type Culture Collection (ATCC 43888) and stored in brain heart infusion broth (BHI, Remel Inc., Lenexa, KS) at -80 °C. The culture was grown in brain heart infusion broth BHI at 37 °C for 18 h. For enumeration the culture was serially diluted in phosphate buffered saline (PBS; 0.01 M; pH 7.4; Sigma-Aldrich, St. Louis, MO) and plated on sorbitol MacConkey agar (SMAC, Remel Inc., Lenexa, KS) incubated at 37 °C for 22-24 h. Due to biosafety concerns, the bacteria was killed by boiling for 10 min before use in biosensor tests.

### **6.3.2 Biological and chemical reagents**

Phosphate buffered saline (PBS; 0.01 M; pH 7.4) was purchased from Sigma Aldrich (St. Louis, MO). Biotin-labeled anti-*E. coli* antibody was purchased from Meridian Life Science (Memphis, TN) and diluted to 0.4-0.5 mg ml<sup>-1</sup> with PBS for use in tests. All solutions were prepared with deionized water from Millipore (Milli-Q, 18.2 MΩ cm, Bedford, MA).

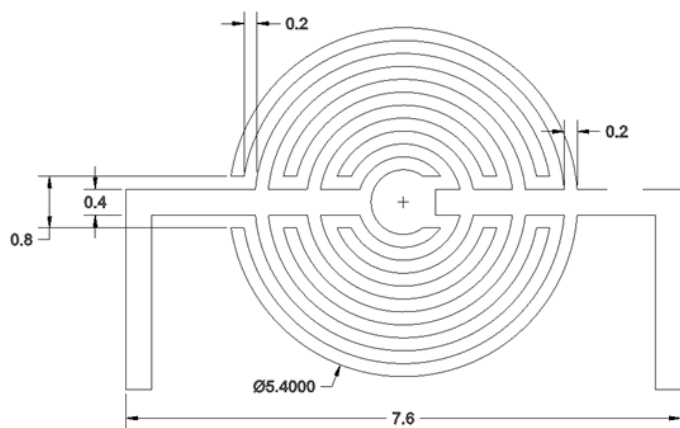
### **6.3.3 Screen-printed interdigitated electrodes and magnetic nanobeads**

Gold screen-printed interdigitated electrodes were provided by Aibit, LLC (Jiangyin, China). The interdigitated electrode consisted of 3 pairs of 200 μm wide electrodes spaced 200 μm apart arranged in a circular array printed on a ceramic substrate. The outer diameter of the array was 5.4 mm. Fig. 6.1 (a) and (b) show a photograph of the screen-printed interdigitated electrode and a drawing of the interdigitated electrode.

Magnetic nanobeads ( $\text{Fe}_3\text{O}_4$ ; ~150 nm diameter) were purchased from R&D Systems (Minneapolis, MN) and used at the stock concentration.



(a)



(b)

Fig. 6.1. (a) A photograph of the screen printed electrode and (b) drawing of the interdigitated electrode. Dimensions are given in millimeters.

#### **6.3.4 Impedance measurement**

Impedance measurements were performed using an IM-6 impedance analyzer with IM-6/Thales software (BAS, West Lafayette, IN). Test-sense and counter-reference probes were connected to the electrode. An AC potential of 50 mV was used for all impedance measurements. Impedance magnitude and phase angle were measured at 38 points in the frequency range of 10 Hz to 100 kHz. All impedance measurements were done in the presence of a redox probe consisting of 5 mM  $[\text{Fe}(\text{CN})_6]^{3-/4-}$  (1:1 ratio) mixture in PBS.

#### **6.3.5 Immunomagnetic separation of *E. coli* O157:H7**

Antibody-coated nanobeads were prepared by mixing 20  $\mu\text{l}$  of magnetic nanobeads with 20  $\mu\text{l}$  of anti- *E. coli* O157:H7 antibody in 200  $\mu\text{l}$  of PBS for 45 min in a rotating mixer at 5 rpm. A magnetic field ( $\sim 0.7$  T) was applied using a magnetic separator consisting of six permanent magnets (Aibit LLC, Jiangyin, China) for 4 min and the bead/antibody complexes were washed twice with 200  $\mu\text{l}$  of PBS. The nanobeads were split into two tubes. A 200  $\mu\text{l}$  sample of *E. coli* O157:H7 was added to one tube and 200  $\mu\text{l}$  of PBS was added to one as a negative control sample. The samples were mixed for 45 min in a rotating mixer at 5 rpm. The samples were then magnetically separated for 4 min and washed twice with redox probe and each suspended in 100  $\mu\text{l}$  of redox probe for impedance measurement. All mixing was done at room temperature.

#### **6.3.6 Detection of *E. coli* O157:H7**

Screen-printed interdigitated electrodes were cleaned using 1 M NaOH for 3 min. The electrode was then washed with deionized water and dried with nitrogen.

Impedance detection of *E. coli* O157:H7 was done by placing a 25  $\mu$ l drop of a prepared sample from immunomagnetic separation onto the electrode surface. A magnetic field (0.4 T) (neodymium rare earth magnet, CMS Magnetics, Garland, TX) was applied using a permanent magnetic (neodymium rare earth magnet, CMS Magnetics, Garland, TX) and used to draw the bacteria/nanobead complexes to the electrode surface for 10 min before impedance measurement. The impedance was measured while the magnetic field was still being applied. The impedance of the control sample prepared in parallel with the bacterial sample was measured first to gather a baseline for detection. The impedance of each bacteria sample was compared to the control sample prepared in parallel to it. Fig. 6.2 shows diagrams the immunomagnetic separation and detection protocols.

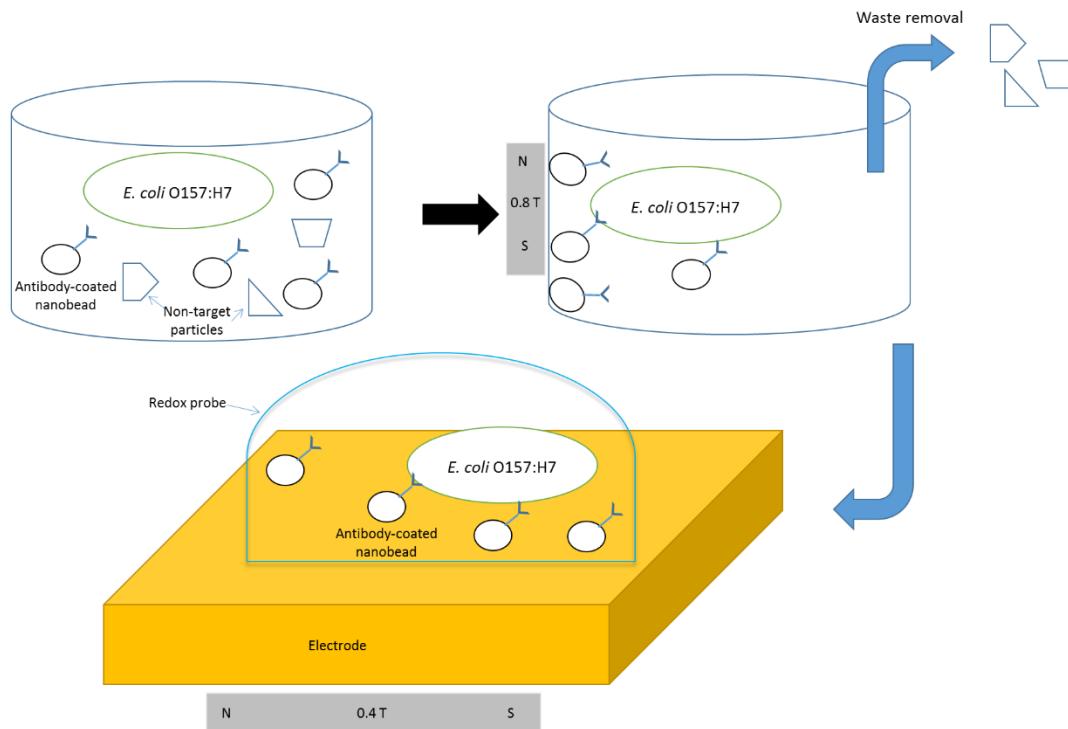


Fig. 6.2. Immunomagnetic separation of *E. coli* O157:H7 from media using the antibody-coated nanobeads and the concentration of bacteria on the electrode surface using a magnetic field.

### **6.3.7 Equivalent circuit modeling and statistical analysis**

An equivalent circuit was built and evaluated using IM-6/Thales software. Statistical analysis of data and preparation of graphs was done using Microsoft Excel (Microsoft, Redmond, VA).

*Escherichia coli* O157:H7 at concentrations of  $10^4$  to  $10^7$  cfu ml<sup>-1</sup> were measured. Means and standard deviations were calculated based on triplicate tests. Lower detection limits were determined as a signal/noise ratio of 3, where noise was defined as the standard deviation of the negative PBS control. Statistically significant differences were determined using t-tests ( $\alpha=0.05$ ).

### **6.3.8 Electron microscopy**

Electron scanning electron microscopy was done using a Philips XL30 ESEM (Environmental Scanning Electron Microscope, FEI, Hillsboro, OR) to confirm binding of the antibody-coated nanobeads to the *E. coli* O157:H7 cells. A sample was prepared using the protocol described in Section 6.3.5. Fixation was done using Karnovsky's fixative followed by dehydration with successive ethanol washes.

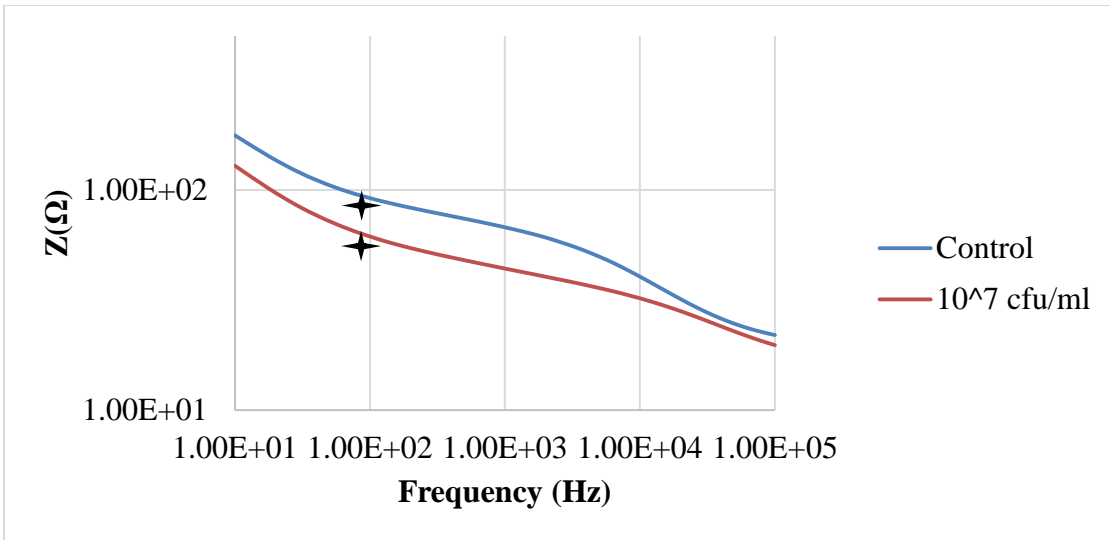
## **6.4 Results and Discussion**

### **6.4.1 Characterization of impedance spectrum data**

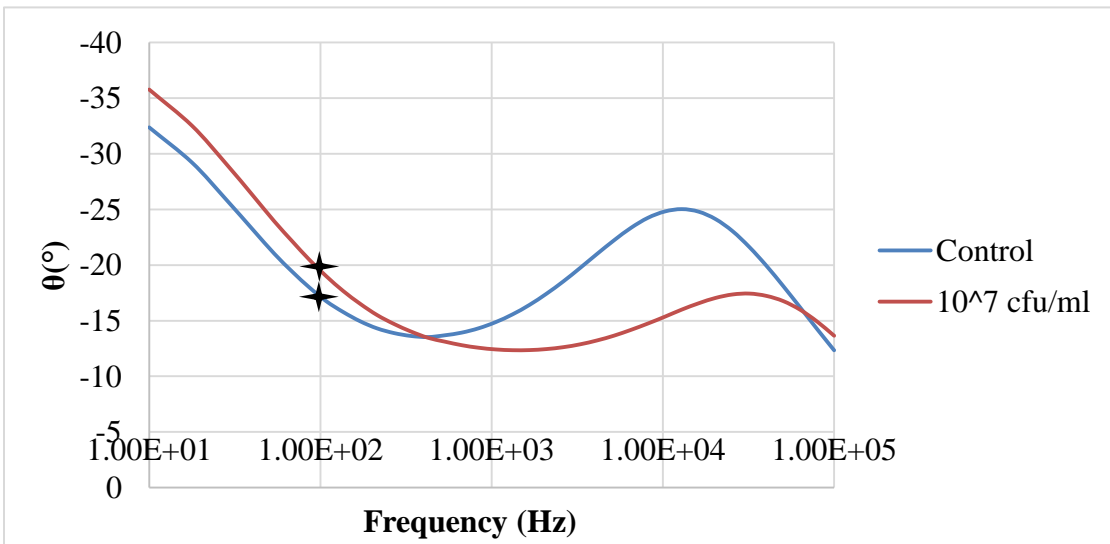
Impedance magnitude for the detection of a sample containing  $10^7$  cfu ml<sup>-1</sup> *E. coli* O157:H7 and a negative control sample are shown in Fig. 6.3 (a). The presence of bacteria resulted in a decrease in impedance magnitude and the maximum decrease occurred at 100 Hz. Fig. 6.3 (b) shows the phase angle data for the detection a sample containing  $10^7$  cfu ml<sup>-1</sup> *E. coli*



O157:H7 and a negative control sample. The phase angle describes the contribution of the resistance and capacitance elements to the impedance value. A current passing through a capacitor is phase shifted by  $-90^\circ$  with respect to the voltage while a current passing through a resistor is in phase with the voltage, therefore having a phase angle of  $0^\circ$ . A phase angle between  $-90^\circ$  and  $0^\circ$  indicates that the impedance value is affected by a combination of resistance and capacitive elements. The phase angles for both the bacterial and control samples decreased in the middle frequency around 500 Hz to 1 kHz and in the high frequency range nearing 100 kHz. In the higher frequency range between 10 kHz and 30 kHz the phase angle for both samples increased, though the bacterial sample phase angle was lower than the control sample's. At the lower frequency range (10 Hz to 500 Hz), the phase angle of the bacterial sample was higher than the control sample's. The phase angle data suggests that the presence of bacteria disrupted a capacitance element at the higher frequencies while creating a capacitance element in the low frequency range. An equivalent circuit model was built and evaluated to better understand the impedance spectrum data.



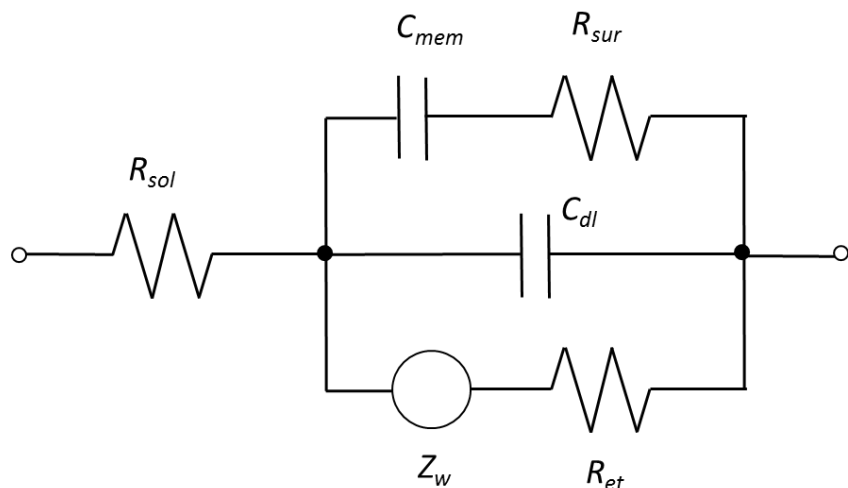
(a)



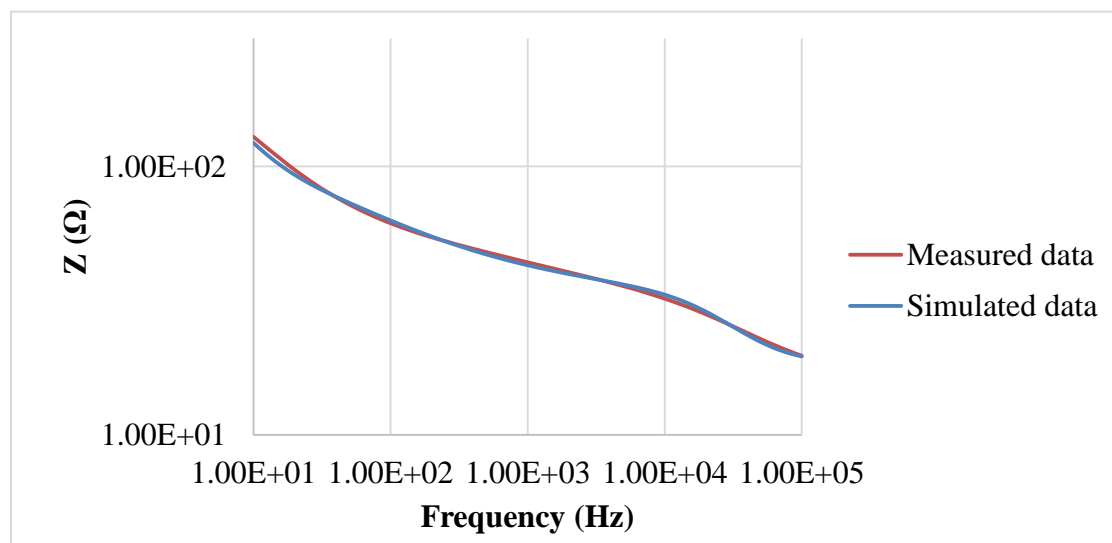
(b)

Fig. 6.3. A typical Bode plot of the measured impedance data of the control and *E. coli* O157:H7 at a concentration of  $10^7$  cfu ml<sup>-1</sup>. (a) Impedance magnitude and (b) Phase angle. Frequency range was 10 Hz to 100 kHz. The amplitude of voltage applied was 50 mV.

The equivalent circuit shown in Fig. 6.4 (a) contained three resistance elements corresponding to bulk electrolyte resistance ( $R_{sol}$ ), electron transfer resistance ( $R_{et}$ ) and resistance due to surface roughness ( $R_{sur}$ ), two capacitance elements corresponding to double layer capacitance ( $C_{dl}$ ) and capacitance of bacterial cells ( $C_{mem}$ )<sup>23</sup>, and a Warburg impedance element ( $Z_w$ ). A fitting analysis showed that the equivalent circuit fit the measured data with an average error of 0.4% and a maximum error of 4.6% for the impedance magnitude and an average error of 0.2° and a maximum error of 3.1° for the phase angle as shown in Fig. 6.4 (b).



(a)



(b)

Fig. 6.4. (a) Equivalent circuit used for data analysis. The equivalent circuit components were bulk electrolyte ( $R_{sol}$ ), electron transfer resistance ( $R_{et}$ ), resistance due to surface roughness ( $R_{sur}$ ), double layer capacitance ( $C_{dl}$ ), capacitance of bacterial cells ( $C_{mem}$ ), and a Warburg impedance element ( $Z_w$ ). (b) Bode diagram of measured impedance data and simulated impedance data generated by curve fitting of equivalent circuit. Measured data was taken with a sample containing  $10^7$  cfu ml<sup>-1</sup> *E. coli* O157:H7.

Two capacitance elements,  $C_{mem}$  and  $C_{dl}$ , were looked at to better understand the phase angle data. The  $C_{dl}$  element decreased by 53 nF between the control and the sample containing  $10^7$  cfu ml<sup>-1</sup> cells, showing that the presence of bacteria disrupting the formation of a double layer capacitor on the electrode surface. The  $C_{mem}$  element increased 13  $\mu$ F between the control and the sample containing  $10^7$  cfu ml<sup>-1</sup> cells, suggesting that the presence of the bacterial cells formed a capacitance element in the system (Santos-Sacchi, 2004). From this information, it can be implied that the presence of bacteria disrupted the double layer capacitance in the high frequency range while producing a capacitance element in the low frequency ranges. This would explain the pattern seen in the phase angle data.

The  $R_{sur}$  element decreased 76  $\Omega$  between the control and the sample containing  $10^7$  cfu ml<sup>-1</sup> cells. The decrease in resistance may be explained by an increase in the electrode surface roughness due to the presence of nanobeads and nanobead/bacteria clusters on the electrode. The addition of the beads and clusters likely had the effect of increasing the conductive surface area of the electrode, thereby reducing the resistance of electrical flow. The nanobead/bacteria clusters may have also formed “bridges” between the electrode fingers, further reducing the resistance. The resistance of the electron transfer decreased 21  $\Omega$  between the control and the bacteria sample, indicating the bacteria did not form a large enough layer on the electrode surface to impede electron transfer from the surface of the electrode.  $R_{sol}$  only decreased 3  $\Omega$  between the bacterial and control samples.

#### **6.4.2 Detection of *E. coli* O157:H7**

The impedance magnitude at 100 Hz was determined to be the best indicator of bacterial presence. Fig. 6.5 shows the average impedance decrease for each *E. coli* O157:H7

concentration. A linear relationship ( $R^2=0.94$ ) was found to exist between log value of *E. coli* concentration ( $C_{\text{bact}}$ ) in  $\text{cfu ml}^{-1}$  and impedance change ( $\Delta Z$ ) in ohms between control and bacteria samples that corresponded to  $\Delta Z = 13.6C_{\text{bact}} - 50.8$ . The lower detection limit was calculated to be  $10^{4.45}$   $\text{cfu ml}^{-1}$ . This corresponded to a final bacteria count of  $\sim 1400$  cells. The reproducibility of the biosensor was shown to be high, with small standard deviations at each bacteria concentration. The capture of the bacteria by the antibody-coated nanobeads was confirmed by ESEM as shown in Fig. 6.6. The concentrations of  $10^6$  and  $10^7$   $\text{cfu ml}^{-1}$  were not found to be significantly different, indicating that the upper detection limit of the biosensor may have been reached at  $10^6$   $\text{cfu ml}^{-1}$  and the biosensor may not be precise at concentrations above  $10^6$   $\text{cfu ml}^{-1}$ . The  $10^5$   $\text{cfu ml}^{-1}$  concentration was significantly different from  $10^4$  and  $10^6$   $\text{cfu ml}^{-1}$ .

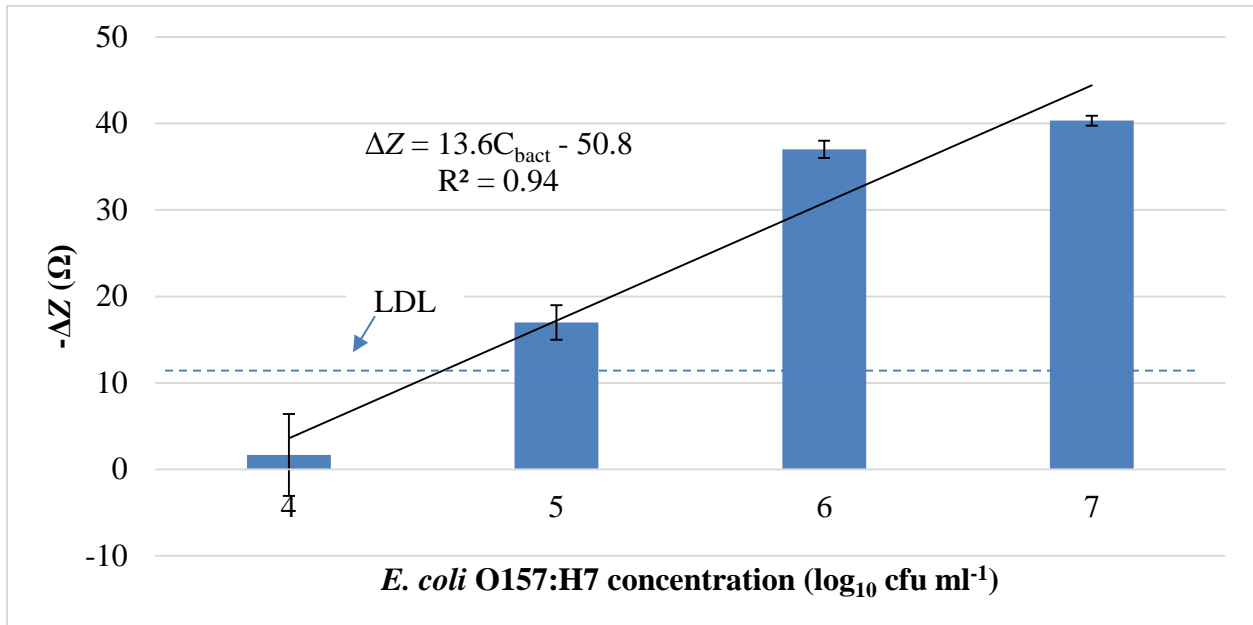


Fig. 6.5. Average impedance change between the control and bacteria measurements at 100 Hz for *E. coli* O157:H7. Error bars were based on the standard deviation of means in triplicate tests. LDL line was determined by signal/noise ratio of 3.

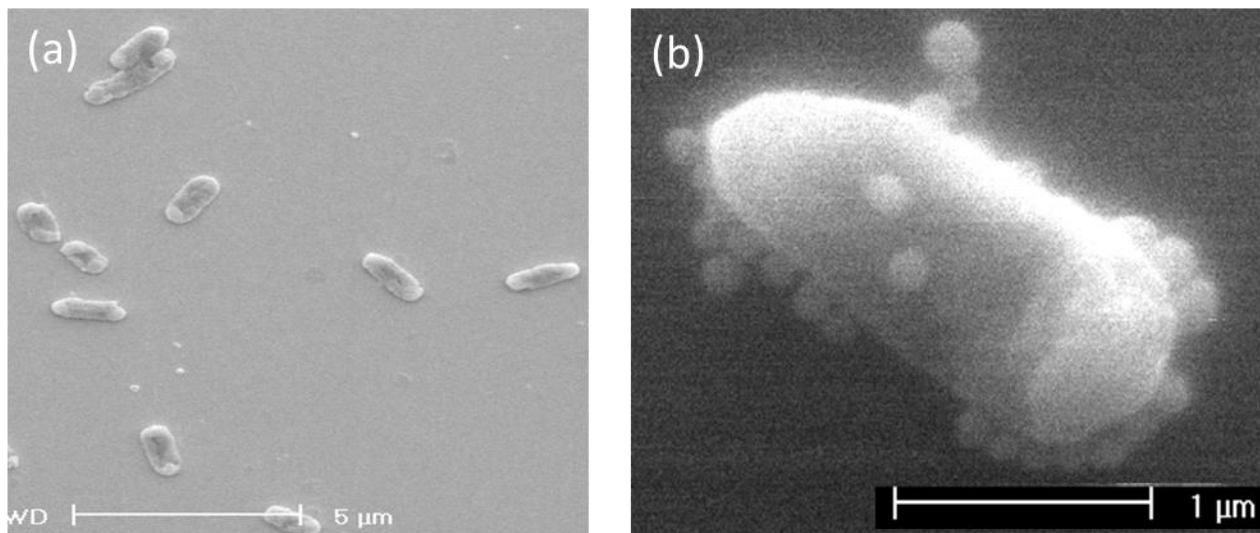


Fig. 6.6. ESEM photographs of (a) free *E. coli* O157:H7 cells and an *E. coli* O157:H7 cell captured by antibody-coated nanobeads.

The  $Z$  and  $\Delta Z$  values were in the low  $\Omega$  range due to the use of 5 mM  $[\text{Fe}(\text{CN})_6]^{3-/4-}$  (1:1 ratio) mixture in PBS as a measurement solution. The use of this high electrolyte solution was needed to provide stability to the biosensor. Previous tests with low electrolyte solutions had very low repeatability. It was hypothesized that the diffusion of ionic species from the interior of the bacteria was affecting these tests and so a high electrolyte solution was used to negate the effect of those ions. This resulted in lower  $Z$  and  $\Delta Z$  values but much higher repeatability.

The sensitivity of the biosensor could be potentially be improved by removing the free beads from the measurement sample. The presence of the free beads introduced noise into the system which may obscure the impedance measurement of *E. coli* O157:H7 at lower concentrations. Removal of free beads could be accomplished using a magnetophoretic separation device as described by Huang et al. (2011).

While a reduction in the initial amount of nanobeads used in the test would likely reduce the noise of the system, previous unpublished research has shown that a reduction in the amount of nanobeads used in the test would result in a loss of capture efficiency as shown in Fig. 6.7.

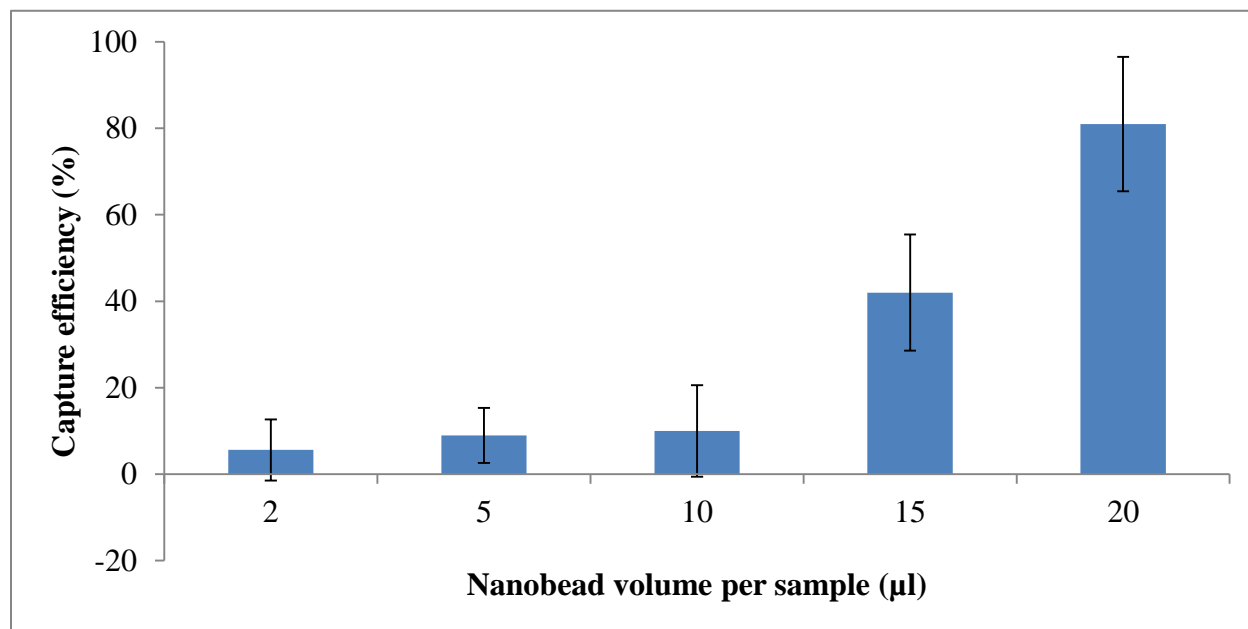


Fig. 6.7. Capture efficiency of  $10^5$  cfu ml<sup>-1</sup> *E. coli* O157:H7 using different amounts of antibody-coated magnetic nanobeads.

The magnetic nanobeads were determined to be necessary for detection by both experimental analysis and computer simulation. *Escherichia coli* cells without magnetic nanobeads were suspended in a redox probe and a drop of the sample was placed on a screen-printed and the impedance was measured after 10 min. No detectable signal could be seen for *E. coli* cells only in a redox probe. Also *E. coli* samples were prepared as described in Section 6.3.5 but no magnetic field was applied after placing the samples on the electrode. Again, no detectable signal was seen. The results of these tests are shown in Fig. 6.8. The impedance change caused by antibody-coated magnetic nanobeads without *E. coli* cells is also shown.



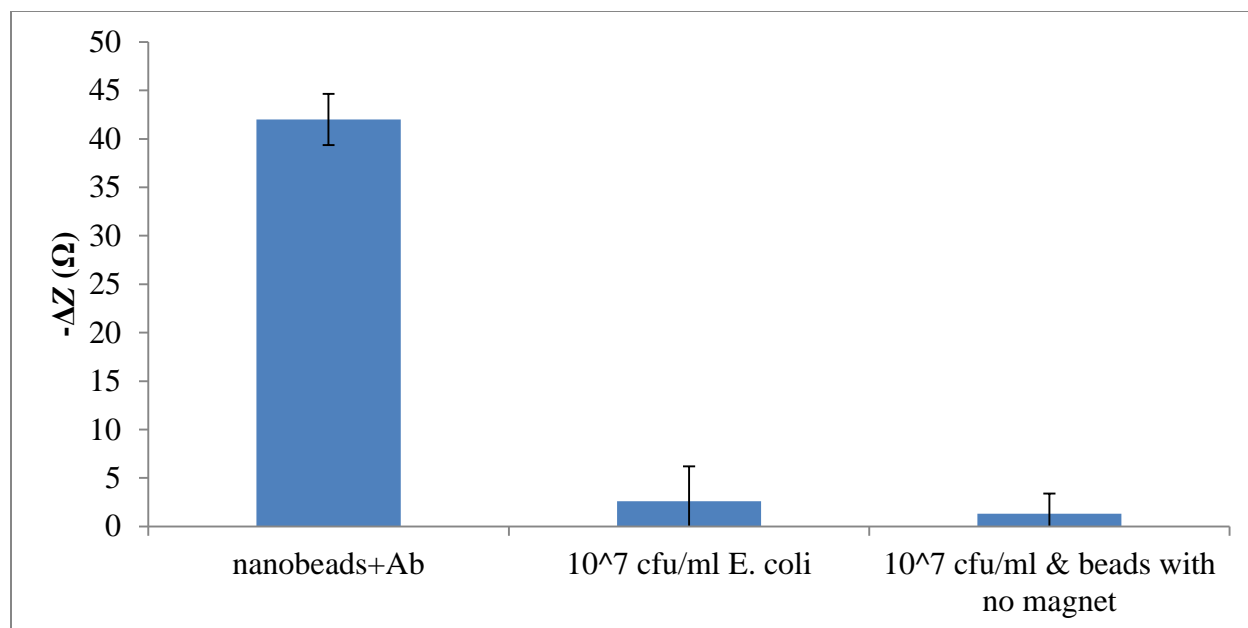
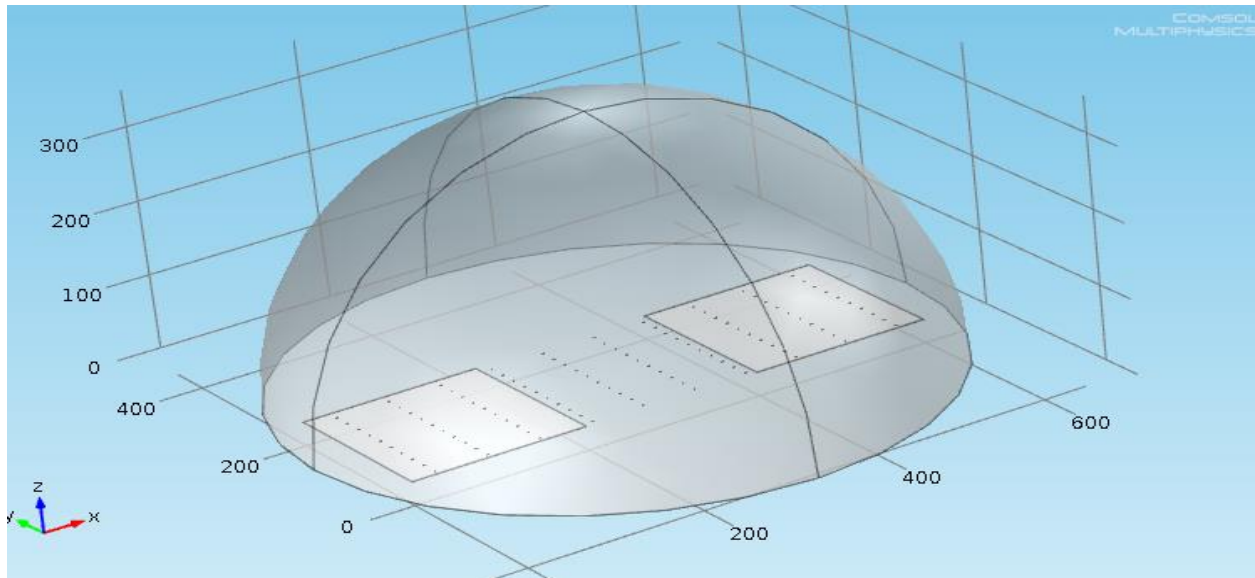


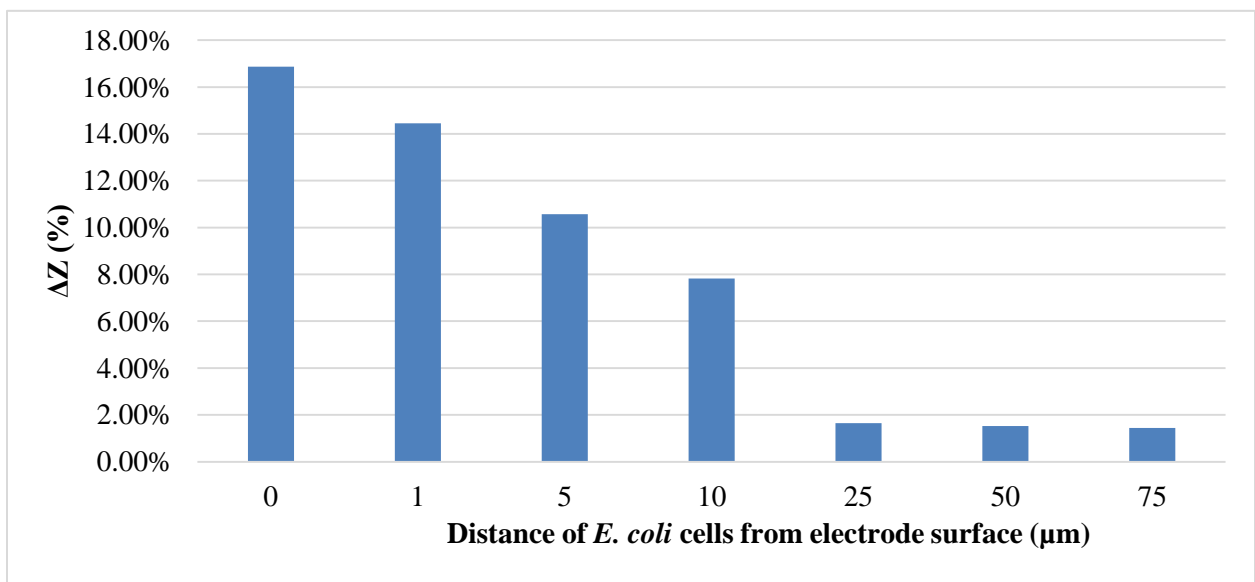
Fig. 6.8. Average impedance change between the pure redox probe and pure antibody-coated nanobeads under a magnetic field and pure *E. coli* O157:H7 and average impedance change between a control sample and *E. coli* O157:H7 and nanobeads with a magnetic field at 100 Hz. Error bars were based on the standard deviation of means in triplicate tests. LDL line was determined by signal/noise ratio of 3, where noise was defined as the standard deviation of the pure redox probe measurements.

Comsol Multiphysics (Comsol Inc., Burlington, MA) software was used to develop a computer model of the biosensor system. A simplified model consisting of a pair of electrodes ( $200\ \mu\text{m} \times 200\ \mu\text{m}$ ) spaced  $200\ \mu\text{m}$  apart and 100 cells of *E. coli* O157:H7 was used to study the effect of distance of the *E. coli* cells from the electrode surface on impedance measurement, as shown in Fig. 6.9(a). The *E. coli* O157:H7 cells were modeled as ellipsoids with a length of  $1.5\ \mu\text{m}$  and a width of  $1\ \mu\text{m}$  and were evenly distributed over the electrodes and the space between. Electrical conductivity and relative permittivity values for the gold electrodes ( $4.1 \times 10^7\ \text{S m}^{-1}$  and 1, respectively) and *E. coli* O157:H7 cells ( $0.5\ \text{S m}^{-1}$  and 60, respectively) were taken from the study of Srinivasan et al (Srinivasan et al., 2006). The measurement environment was set as a hemisphere with a radius of  $350\ \mu\text{m}$ . The electrical conductivity and relative permittivity were

set to  $0.0001 \text{ S m}^{-1}$  and 80, respectively. The impedance was simulated at 100 Hz with a voltage of 100 mV. It was found that the impedance change (17%) was largest when the *E. coli* cells were on the surface of the electrode. The amount of impedance change decreased as the distance between the *E. coli* cells and the electrode surface increased as shown in Fig. 6.9(b). When the cells were 1, 5, and 10  $\mu\text{m}$  from the electrode surface the percent change of impedance change decreased to 14.4%, 10.6%, and 7.8%, respectively. At the distances of 25  $\mu\text{m}$  and larger the impedance change was found to be negligible ( $<1.6\%$ ). The computer simulation confirmed that the magnetic nanobeads and magnetic field was needed for detection of *E. coli* O157:H7 due to the increased impedance change when the *E. coli* cells were close to the electrode surface.



(a)



(b)

Fig. 6.9. (a) COMSOL model of simplified biosensor system with a pair of electrodes and 100 cells of *E. coli* evenly distributed on the electrode surfaces and the space between and (b) simulated impedance magnitude percent changes at different distances between the electrode surface and the *E. coli* cells.

## 6.5 Conclusion

In this study an impedance biosensor for the rapid detection of *E. coli* O157:H7 using antibody-coated magnetic nanobeads and screen printed interdigitated electrodes. The antibody-coated magnetic nanobeads were successfully served multiple roles in the impedance biosensor including isolation and concentration of the bacterial sample and concentration of bacteria on the electrode surface. The impedance biosensor was capable of detecting ~1400 *E. coli* O157:H7 cells in less than 1 h. Both experimental data and computer simulation showed that the magnetic nanobeads and magnetic field were needed for detection of *E. coli* O157:H7.

## 6.6 References

- Asami, K., Hanai, T., Koizumi, N., 1980. *Biophys. J.* 31, 215-228.
- Chan, K.Y., Ye, W.W., Zhang, Y., Xiao, L.D., Leung, P.H.M., Li, Y., Yang, M., 2013. *Biosens. Bioelectron.* 41, 532-537.
- Chowdhury, A.D., De, A., Chaudhuri, C.R., Bandyopadhyay, K., Sen, P., 2012. *Sens. Actua. B: Chem.* 171-172, 916-923.
- dos Santos, M.B., Aguil, J.P., Prieto-Simón, B., Sporer, C., Teixeira, V., Samitier, J., . *Biosens. Bioelectron.*
- Eum, N., Yeom, S., Kwon, D., Kim, H., Kang, S., 2010. *Sens. Actua. B: Chem.* 143, 784-788.
- FDA, “Bad Bug Book: Foodborne Pathogenic Microorganisms and Natural Toxins Handbook,” 2012.  
<http://www.fda.gov/downloads/Food/FoodSafety/FoodborneIllness/FoodborneIllnessFoodbornePathogensNaturalToxins/BadBugBook/UCM297627.pdf>
- Gehring, A.G., Albin, D.M., Bhunia, A.K., Reed, S.A., Tu, S.I., Uknalis, J., 2006. *Anal. Chem.* 78, 6601-6607.
- Huang, H., Ruan, C., Lin, J., Li, M., Cooney, L., Oliver, W., Li, Y. and Wang, A., *Trans. ASABE*, 2011, 54, 1015-1024
- Jiang, X., Wang, R., Wang, Y., Su, X., Ying, Y., Wang, J., Li, Y., 2011. *Biosens. Bioelectron.* 29, 23-28.

- Lin, Y., Chen, S., Chuang, Y., Lu, Y., Shen, T.Y., Chang, C.A., Lin, C., 2008. *Biosens. Bioelectron.* 23, 1832-1837.
- Liu, F., Li, Y., Su, X., Slavik, M., Ying, Y., Wang, J., 2007. *Sens. Instrument. Food Qual. Safe.* 1, 161-168.
- Miller, B.D., Rigdon, C.E., Ball, J., Rounds, J.M., Klos, R.F., Brennan, B.M., Arends, K.D., Kennelly, P., Hedberg, C., Smith, K.E., 2012. *J. Food Prot.* 75, 320-327.
- Poitras, C., Tufenkji, N., 2009. *Biosens. Bioelectron.* 24, 2137-2142.
- Radke, S.M., Alocilja, E.C., 2005. *Biosens. Bioelectron.* 20, 1662-1667.
- Rekow, C.L., Brashears, M.M., Brooks, J.C., Loneragan, G.H., Gragg, S.E., Miller, M.F., 2011. *Meat Sci.* 87, 361-365.
- Santos-Sacchi, J., 2004. *Biophys. J.* 87, 714-727.
- Scallan, E., Hoekstra, R., Angulo, F., Tauxe, R., Widdowson, M., Roy, S., Jones, J., Griffin, P., 2011. *Emerging infectious diseases.* 17, 7-15.
- Settingington, E.B., Alocilja, E.C., 2011. *Biosens. Bioelectron.* 26, 2208-2214.
- Shen, Z., Wang, J., Qiu, Z., Jin, M., Wang, X., Chen, Z., Li, J., Cao, F., 2011. *Biosens. Bioelectron.* 26, 3376-3381.
- Srinivasan, B., Tung, S., Li, Y., and Varshney, M., *Proc. COMSOL Users Conf.*, 2006.
- Subramanian, A., Irudayaraj, J., Ryan, T., 2006. *Biosens. Bioelectron.* 21, 998-1006.
- Varshney, M., Li, Y., 2008. *Talanta.* 74, 518-525.
- Varshney, M., Li, Y., 2007. *Biosens. Bioelectron.* 22, 2408-2414.
- Varshney, M., Li, Y., Srinivasan, B., Tung, S., 2007. *Sens. Actuat. B: Chem.* 128, 99-107.
- Wang, H., Li, Y., Wang, A., Slavik, M., 2011. *J. Food Prot.* 74, 2039-2047.
- Wang, Y., Ye, Z., Si, C., Ying, Y., 2011. *Sensors (Basel).* 11, 2728-2739.
- Waswa, J., Irudayaraj, J., DebRoy, C., 2007. *LWT - Food Sci. Tech.* 40, 187-192.

## **7. An impedance aptasensor for rapid detection of *E. coli* O157:H7 using screen-printed interdigitated electrodes and Gox/Con A-labeled gold nanoparticles**

### **7.1 Abstract**

*Escherichia coli* O157:H7 is one of the most dangerous foodborne pathogens, infecting an estimated 73,000 people in the US each year and having an infective dose as low as 10 cells. A rapid and sensitive method is needed to detect *E. coli* O157:H7 in complex matrices such as food and clinical samples. Therefore, an impedance aptasensor using screen-printed interdigitated electrodes and Gox/ConA-labeled gold nanoparticles was developed in this study. Aptamer-coated magnetic nanobeads were mixed with *E. coli* O157:H7 and a magnetic field (0.8 T) was used to isolate the target bacteria. Gold nanoparticles labeled with glucose oxidase (GOx) and Concanavalin A (ConA), a carbohydrate-binding protein, were mixed with the sample, binding to the captured *E. coli* cells. The sample was then suspended in a 10 mM glucose solution and measured at 0 and 30 min using the screen-printed interdigitated electrode. The change in impedance between the two times was correlated to *E. coli* concentration. Specificity of the aptasensor was tested using non-target bacteria. The aptasensor was capable of specifically detecting *E. coli* O157:H7 within 1.5 h with a lower detection limit of 8 *E. coli* O157:H7 cells (S/N=3).

## 7.2 Introduction

*E. coli* O157:H7 is one of the most dangerous foodborne pathogens, infecting an estimated 63,000 people in the US each year, including 20 deaths, and having an infective dose as low as 10 cells (FDA, 2012; Scallan, 2012). Infection of *E. coli* O157:H7 may cause a life-threatening complication known as hemolytic uremic syndrome in 10-15% of patients with hemorrhagic colitis. *E. coli* O157:H7 infections have primarily been associated with ground beef and leafy green produce but increased integration of the food supply chain has resulted in *E. coli* O157:H7 contamination of unusual food products, such as cookie dough and hazelnuts (Miller et al., 2012). Contamination of food products not only threaten human health but also cost food producers millions of dollars in economic loss. Therefore, a rapid, sensitive, and specific detection method for *E. coli* O157:H7 is needed.

Traditional methods of *E. coli* O157:H7 detection include bacterial culture and polymerase chain reaction (PCR). These methods are time consuming and require highly trained personnel and specialized facilities. Results from suspected samples may take days, during which process lines may be shut down, resulting in economic loss from downtime, or possibly contaminated products may be shipped out. A positive sample can result in expensive product recalls and a loss of consumer trust (Rekow et al., 2011). Biosensors have attracted attention in the food protection field as a possible alternative to traditional bacterial detection methods due to their speed, sensitivity, specificity, and simplicity. Many biosensors have been developed for the detection of *E. coli* O157:H7 such as quartz crystal microbalance (Shen et al., 2011; Poitras and Tufenkji, 2009; Lui et al., 2007; Jiang et al., 2011), surface plasmon resonance (Subramanian et al., 2006; Eum et al., 2010; Wang et al., 2011), and electrochemistry (Chan et al., 2013; Chowdhury et al., 2012; Radke and Alocilja, 2005; Varshney and Li, 2007; Varshney et al.,

2007; Varshney and Li, 2008; Lin et al., 2008; Settingington and Alocilja, 2011; Santos et al., 2013). Impedance biosensors are especially promising due to their high sensitivity, low cost, and ease of use and miniaturization. Two of the previously developed impedance biosensors have been shown to be capable of extreme sensitivity. Chan et al. were able to detect 10 *E. coli* O157:H7 cells using immunomagnetic separation and concentration and a nanoporous alumina membrane coated with antibody. Santos et al. developed a highly sensitive biosensor based on antibody-coated electrodes and impedance measurement in the presence of a redox probe that was able to detect 2 *E. coli* O157:H7 cells. While the developed biosensors were highly sensitive, the fabrication and use of both biosensors was complex and time consuming, making them impractical for rapid in-field use. An amperometric biosensor developed by Settingington and Alocilja used screen-printed carbon electrodes, immunomagnetic separation, and electroactive polyaniline labels to detect *E. coli* O157:H7 at a lower detection level of 7 cells in 70 min. Their biosensor was highly sensitive, easy to use, and reusable though it was limited in that the detection was not quantitative.

Most of the previously developed biosensors depended on antibodies as the biological recognition element, which have a limited shelf life, are prone to thermal degradation, and can be costly. DNA aptamers are single stranded oligonucleotides that can be selected to bind to a variety of targets including proteins, carbohydrates, lipids, whole cells and viruses, chemicals, and metal ions (Song et al., 2008). Aptamers function similar to antibodies and have several advantages over antibodies in that they have greater thermal and chemical stability, high uniformity, and low cost (Pendergrast et al., 2005). A few aptamer-based biosensors have been developed for the detection of *E. coli* O157:H7. Wu et al. (2012a) developed a colorimetric biosensor based on aptamer-labeled nanoscale polydiacetylene vesicles. Upon binding to the



target *E. coli* O157:H7 the vesicles displayed a color shift that was read using absorbance spectroscopy. The detection limit of the aptasensor was  $10^4$  colony forming units (cfu)  $\text{ml}^{-1}$ . Wu et al. (2012b) developed a biosensor based on aptamer modified gold nanoparticles which produced a color shift upon aggregation onto the target *E. coli* O157:H7 and had a detection limit of  $10^5$  cfu  $\text{ml}^{-1}$ . So et al. (2008) was able to detect a concentration of  $10^3$  cfu  $\text{ml}^{-1}$  *E. coli* using aptamer-functionalized single-walled carbon nanotube field-effect transistors, though the *E. coli* strain used was DH5 $\alpha$ , not O157:H7, and the fabrication of the biosensor was costly, time consuming, and labor intensive.

Several of the previously developed electrochemical biosensors for *E. coli* O157:H7 relied on gold microelectrode interdigitated arrays (IDAMs), which are time consuming and costly to fabricate and can easily be damaged. In contrast, screen-printed gold interdigitated electrodes are inexpensive and easy to mass produce, characteristics necessary for a rapid in-field test. Also many of the biosensors required immobilization of the biological recognition element on the electrode surface for sensitive detection. This not only increases the time and resources required but also makes regeneration and reuse of the electrodes difficult or impossible. A method that does not rely on immobilized elements on the electrode surface would greatly decrease cost and time per test.

In this study a DNA aptamer specific to *E. coli* O157:H7 was used as the biological recognition element in an impedance biosensor based on screen-printed interdigitated electrodes, magnetic nanobeads, and gold nanoparticles coated with glucose oxidase/Concanavalin A. Magnetic nanobeads coated in aptamer against *E. coli* O157:H7 were used to capture and concentrate the bacterial cells. Gold nanoparticles coated with glucose oxidase/Concanavalin A were then bound to the cells for use as labels. The labeled bacterial cells were suspended in a low

ionic glucose solution and the impedance was measured using a screen printed interdigitated electrode at  $t=0$  min and  $t=30$  min. The impedance decrease after 30 min was correlated with the log value of the *E. coli* O157:H7 concentration.

### **7.3 Materials and methods**

#### **7.3.1 Culture and plating of bacteria**

*Escherichia coli* O157:H7 was purchased from American Type Culture Collection (ATCC 43888) and stored in brain heart infusion broth (BHI, Remel Inc., Lenexa, KS) at  $-80$  °C. The culture was grown in brain heart infusion broth BHI at  $37$  °C for 18 h. For enumeration the culture was serially diluted in phosphate buffered saline (PBS; 0.01 M; pH 7.4; Sigma-Aldrich, St. Louis, MO) and plated on sorbitol MacConkey agar (SMAC, Remel Inc., Lenexa, KS) incubated at  $37$  °C for 22-24 h. Due to biosafety concerns, the bacteria was killed by boiling for 10 min before use in biosensor tests.

#### **7.3.2 Materials**

Phosphate buffered saline (PBS; 0.01 M; pH 7.4) was purchased from Sigma Aldrich (St. Louis, MO). Streptavidin-coated magnetic nanobeads ( $\text{Fe}_3\text{O}_4$ ;  $\sim 150$  nm diameter) were purchased from R&D Systems (Minneapolis, MN) and used at the stock concentration. All solutions were prepared with deionized water ( $\text{dH}_2\text{O}$ ) from Millipore (Milli-Q,  $18.2$  M $\Omega$  cm, Bedford, MA). Glucose oxidase (GOx; type II from *Aspergillus niger*, 100-250 kU  $\text{g}^{-1}$ ) and Concanavalin A (Con A; type VI from *Canavalia ensiformis*) were purchased from Sigma–Aldrich (St. Louis, MI). Con A is a carbohydrate-binding protein that binds nonspecifically to various sugars, glycolipids, and glycoproteins. It contains four binding sites, a feature utilized in

this study to bind both GOx and lipopolysaccharide membrane (O-antigen) of the *E. coli* O157:H7.

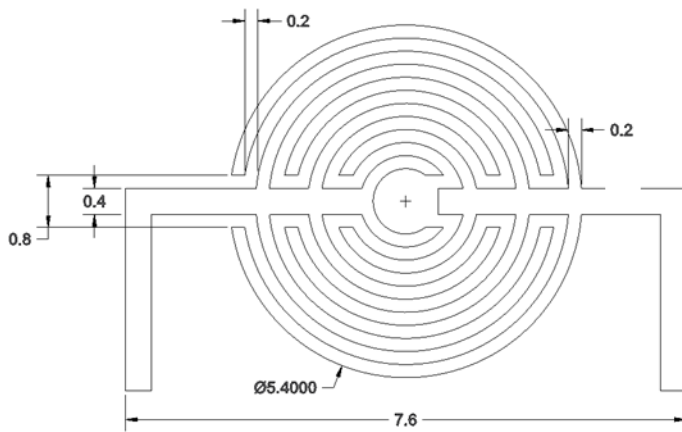
Biotin-labeled ssDNA aptamer (37 nt; 5'-AT CAA ATG TGC AGA TAT CAA GAC GAT TTG TAC AAG AT -3') was purchased from Integrated DNA Technologies (IDT, Coralville, IA).

### **7.3.3 Screen-printed interdigitated electrodes**

Gold screen-printed interdigitated electrodes were designed by Aibit, LLC (Jiangyin, China). The interdigitated electrode consisted of 3 pairs of 200  $\mu\text{m}$  wide electrodes spaced 200  $\mu\text{m}$  apart arranged in a circular array printed on a ceramic substrate. The outer diameter of the array was 5.4 mm. Fig. 7.1 (a) and (b) show a photograph of the screen-printed interdigitated electrode and a drawing of the interdigitated electrode.



(a)



(b)

Fig. 7.1. (a) A photograph of the screen printed electrode and (b) drawing of the interdigitated electrode. Dimensions are given in millimeters.

### **7.3.4 Preparation of GOx/ConA gold nanoparticles**

Gold nanoparticles were prepared using the Frens' methods (Zhu et al., 2003). Gold nanoparticles (0.5 ml; ~12-20 nm diameter; 21 nM) were centrifuged at 12,000 rpm for 30 min and the supernatant was discarded. The nanoparticles were resuspended in 0.5 ml of dH<sub>2</sub>O and mixed with 0.5 ml glucose oxidase solution in dH<sub>2</sub>O (10 mg ml<sup>-1</sup>) for 2 h at 5 rpm. After mixing the sample was split into two tubes and 1 ml of PBS was added to each. The samples were centrifuged for 20 min at 8,000 rpm, washed with 200 µl of dH<sub>2</sub>O and 800 µl of PBS, and centrifuged again for 20 min at 8,000 rpm. The supernatant was removed and 0.98 ml of Concanavalin A in PBS (4 mg ml<sup>-1</sup>), 10 µl of CaCl<sub>2</sub> (100 mM), and 10 µl of MgCl<sub>2</sub> (100 mM) was added to the gold nanoparticles and mixed for 1 h at 5 rpm. The samples were centrifuged for 10 min at 3,000 rpm and washed with 1 ml of PBS and centrifuged again for 10 min at 3,000 rpm. The GOx/ConA gold nanoparticles were resuspended in 1 ml of PBS with 1% bovine serum albumin and stored at 4 °C. Before use the suspension was shaken and let stand for 1 h. The supernatant was sonicated for 5 s and used for tests.

The concentration of the final concentration of the GOx/ConA gold nanoparticles was measured by enzyme catalysis activity, which was determined to be equivalent to the enzymatic activity of 0.16 mg ml<sup>-1</sup> of pristine glucose oxidase.

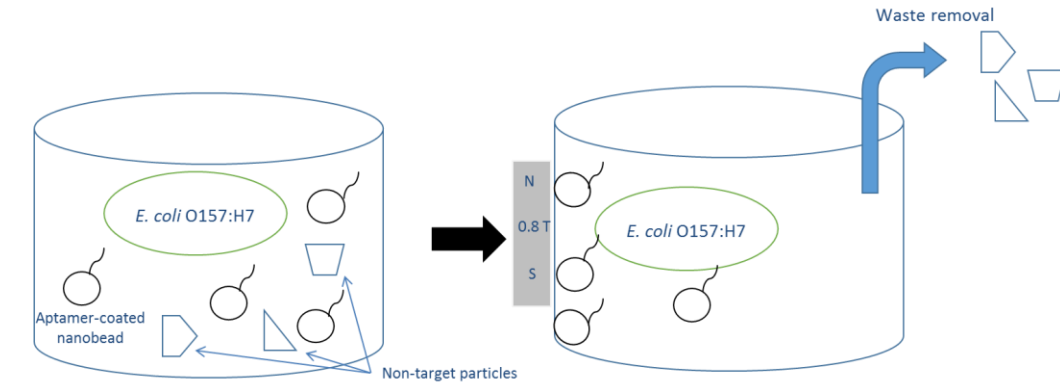
### **7.3.5 Magnetic separation of *E. coli* O157:H7 with aptamer-coated beads**

Streptavidin-coated nanobeads were washed by vortexing 10 µl of nanobeads with 100 µl of PBS and magnetically separating for 4 min and discarding the waste. 180 µl of PBS and 20 µl of anti-*E. coli* O157:H7 aptamer were mixed with the nanobeads for 60 min at 5 rpm. The sample was magnetically separated for 4 min and the waste was removed. The sample was

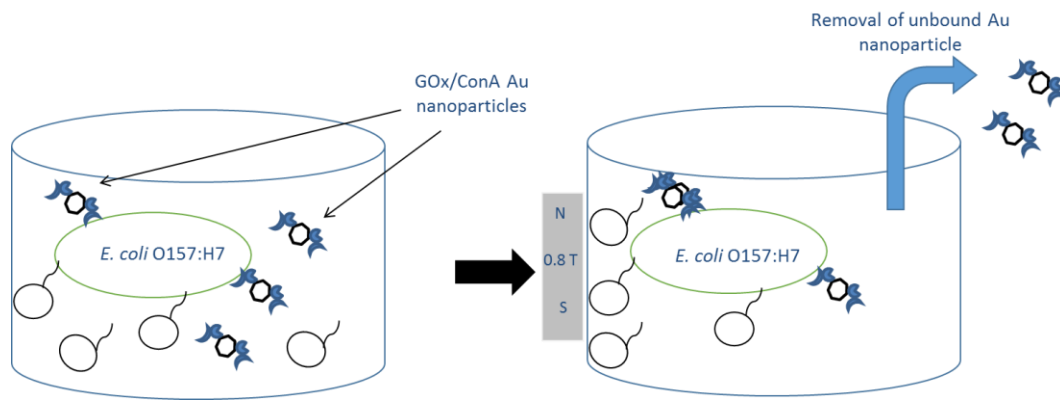
washed once with 200  $\mu$ l of PBS. 200  $\mu$ l of an *E. coli* O157:H7 sample was added to the nanobead/aptamer complexes and mixed for 45 min. A negative control was prepared using PBS without *E. coli* O157:H7. After mixing the samples were magnetically separated for 4 min and washed twice with 200  $\mu$ l of PBS. The sample was resuspended in 190  $\mu$ l of PBS. A negative control was prepared using PBS without *E. coli* O157:H7.

### **7.3.6 Detection of *E. coli* O157:H7 using GOx/ConA gold nanoparticle labels**

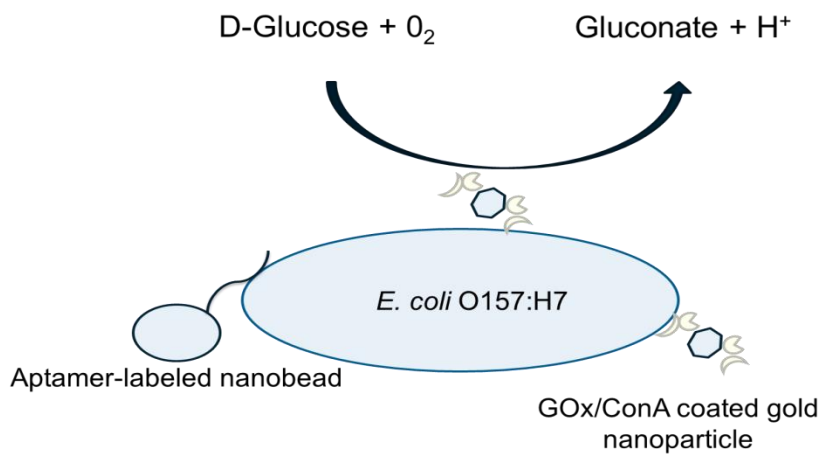
The previously prepared *E. coli* O157:H7 sample was mixed with 10  $\mu$ l of GOx/ConA gold nanoparticles, 2  $\mu$ l of CaCl<sub>2</sub> (100 mM), and 2  $\mu$ l of MgCl<sub>2</sub> (100 mM) for 10 min at 5 rpm. The sample was then magnetically separated for 4 min and washed with 200  $\mu$ l of 0.1 % Tween-20 in PBS. The sample was washed three times with 100  $\mu$ l 10 mM glucose in dH<sub>2</sub>O. The sample was suspended in 100  $\mu$ l of 10mM glucose solution and the impedance was measured immediately by placing a 50  $\mu$ l drop on the screen-printed interdigitated electrode. After impedance measurement the sample was returned to the tube and left open for 30 min and measured again. The impedance change between 0 min and 30 min was correlated to *E. coli* O157:H7 concentration. A diagram of the magnetic separation with aptamer-coated beads, labeling of *E. coli* O157:H7 cells with GOx/ConA gold nanoparticles, and impedance measurement is shown in Fig. 7.2 (a), (b), and (c).



(a)



(b)



(c)

Fig. 7.2. Diagram of the (a) magnetic separation with aptamer-coated beads, (b) labeling of *E. coli* O157:H7 cells with GOx/ConA gold nanoparticles, and (c) impedance measurement.

Impedance measurements were performed using an IM-6 impedance analyzer with IM-6/Thales software (BAS, West Lafayette, IN). Test-sense and counter-reference probes were connected to the electrode. An AC potential of 5 mV was used for all impedance measurements. Impedance magnitude and phase angle were measured at 38 points in the frequency range of 10 Hz to 100 kHz. An equivalent circuit model was built and evaluated using IM-6/Thales SIM software, with simulated being compared to 38 measured data points.

*E. coli* O157:H7 was measured at concentrations between  $10^1$  and  $10^6$  cfu ml<sup>-1</sup> to formulate a calibration curve for the biosensor. Means and standard deviations were calculated based on triplicate tests conducted at each concentration. A lower detection limit was determined as a signal/noise ratio of 3, where noise was defined as the standard deviation of the negative control tests. Significant differences between treatment groups were determined using t-tests ( $\alpha=0.05$ ). All statistical analysis and graphs were produced using Microsoft Excel (Redford, VA).

The specificity of the biosensor was evaluated by testing with non-target *E. coli* K12, *Listeria monocytogenes*, and *Salmonella* Typhimurium. Triplicate tests using bacteria at  $10^6$  cfu ml<sup>-1</sup> were used to determine the specificity of the biosensor.

### **7.3.7 Environmental scanning electron microscopy**

Electron scanning electron microscopy was done using a Philips XL30 ESEM (Environmental Scanning Electron Microscope, FEI, Hillsboro, OR) to confirm binding of the antibody-coated nanobeads to the *E. coli* O157:H7 cells. A sample was prepared using the protocol described in Section 7.3.5. Fixation was done using Karnovsky's fixative followed by dehydration with successive ethanol washes.



## 7.4 Results and discussion

### 7.4.1 Characterization of impedance spectrum data

A Bode plot of the impedance spectrum for a  $10^5$  cfu ml<sup>-1</sup> *E. coli* O157:H7 sample is shown in Fig. 7.3. The impedance decreased between 0 min and 30 min due to the catalysis of glucose by the glucose oxidase labels attached to the *E. coli* O157:H7 cells. The binding of aptamer-coated nanobeads and GOx/Con A gold nanoparticles to the *E. coli* O157:H7 cells was confirmed using ESEM as shown in Fig. 7.4. The catalysis of glucose to hydrogen peroxide and D-glucono-1,5-lactone, which hydrolyzed to gluconic acid and H<sup>+</sup> ions, increased the ionic strength of the solution and caused the impedance of the solution to decrease. The impedance change between the two times was largest at 1 kHz, as determined by percent change. The phase angle data shows that the phase angle approached zero at this frequency (0 min, -5.39°; 30 min, -3.81°), indicating that resistance dominated at this point. The phase angle describes the contribution of the resistance and capacitance elements to the impedance value. A current passing through a capacitor is phase shifted by -90° with respect to the voltage, while a current passing through a resistor is in phase with the voltage, therefore having a phase angle of 0°. A phase angle between -90° and 0° indicates that the impedance value is affected by a combination of resistance and capacitive elements. At higher frequencies, the phase angle is larger though it quickly dropped between 100 kHz and 1 kHz. It began to increase again at frequencies below 100 Hz.

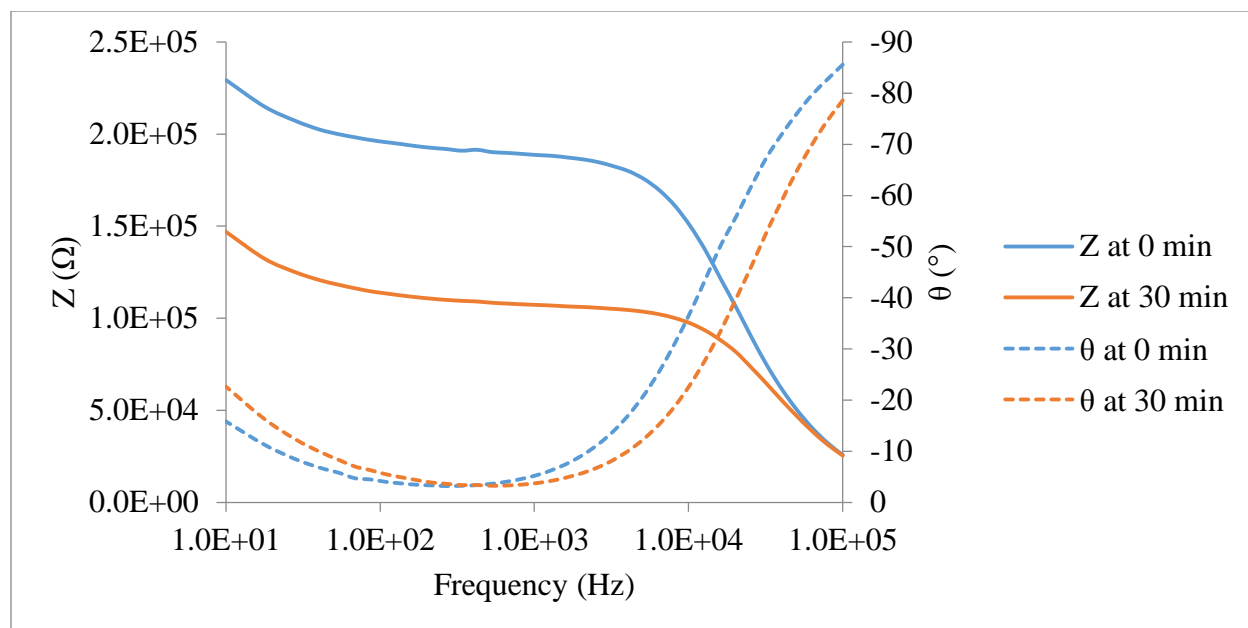
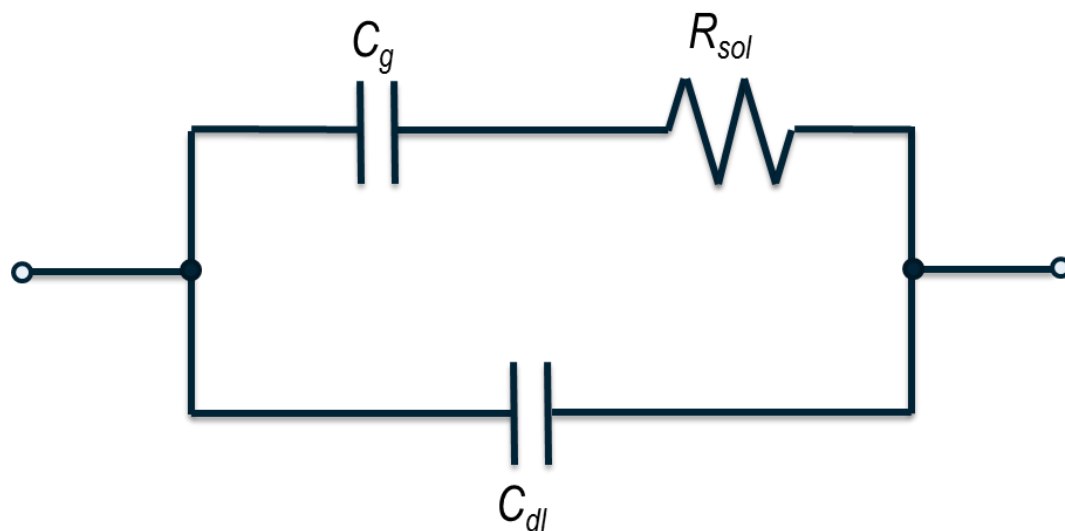
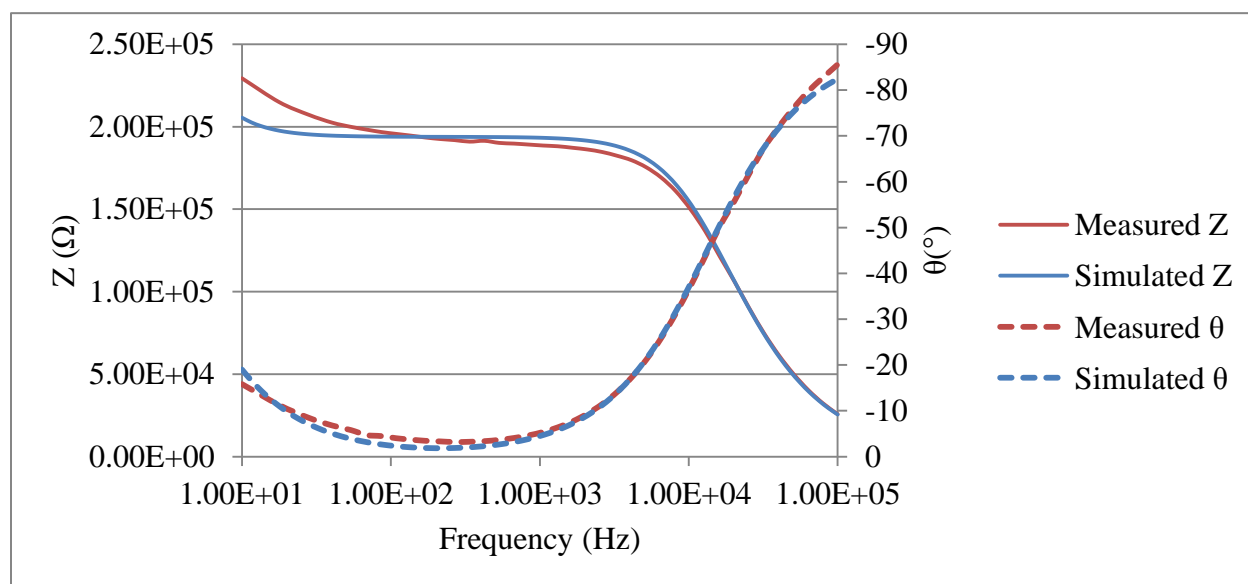


Fig. 7.3. Bode plot of impedance measurement of *E. coli* O157:H7 sample containing  $10^5$  cfu ml<sup>-1</sup> cells. 38 points were measured at frequencies from 100 kHz to 10 Hz. The voltage amplitude was 5 mV.

An equivalent circuit was built and evaluated to further investigate the impedance data. The equivalent circuit, shown in Fig. 7.5 (a), consisted of three elements: bulk electrolyte resistance ( $R_{sol}$ ), double layer capacitance ( $C_{dl}$ ), and geometric capacitance ( $C_g$ ). A simple equivalent was able to be used because of the simplicity of the biosensor design. No proteins, antibodies, or aptamers were immobilized on the electrode surface and, because the impedance was measured immediately after placing a drop on the electrode, it was likely no nanobeads or bacteria cells were on the electrode surface either. This allowed the use of a simple equivalent circuit, since the biosensor was primarily measuring the impedance of the solution.



(a)



(b)

Fig. 7.4 (a) Equivalent circuit model for impedance aptasensor. The equivalent circuit components were bulk electrolyte resistance ( $R_{sol}$ ), double layer capacitance ( $C_{dl}$ ), capacitance of solution ( $C_g$ ). (b) Bode plot of measured and fitted data. Measured data was taken using *E. coli* O157:H7 sample containing  $10^5$  cfu  $ml^{-1}$  cells.

A fitting analysis showed the equivalent circuit fit the measured data closely with an average error of 0.5% and a maximum error of 11.3% for the impedance magnitude and an average error of 0.2° and maximum error of 3.5° for the phase angle. The simulated impedance magnitude data deviates slightly from the measured data at frequencies below 300  $\Omega$  but matches the measured data closely at frequencies above 300  $\Omega$ , as seen in Fig. 7.5 (b).

The values of the equivalent circuit elements were investigated to understand the reasons behind the impedance change. The values for each equivalent circuit element are shown in Table 7.1. The  $R_{sol}$  element was found to play the largest role in the impedance change, decreasing from 194 k $\Omega$  to 110 k $\Omega$  between the 0 min and 30 min measurements for the detection of  $10^5$  cfu  $ml^{-1}$  *E. coli* O157:H7. The  $C_{dl}$  element also played small role in the impedance change, increasing from 235 nF to 270 nF between the 0 min and 30 min measurements. The increase in the  $C_{dl}$  element after 30 min was likely due to the increase in ions in the solution forming a better double layer capacitor at the electrode surface. The  $C_g$  element showed a very small decrease between 0 min and 30 min, only decreasing 0.7 pF between the two measurement times. The equivalent circuit evaluation supported what was seen in the phase angle data: that resistance played the largest role in determining the impedance value.

Table 7.1. Contributions of the elements in the equivalent circuit to the impedance magnitude. Impedance magnitude values were calculated using simulated data from fitting the equivalent circuit to measured data gathered in the detection of an *E. coli* O157:H7 sample containing  $10^5$  cfu ml<sup>-1</sup> cells.

	$R_{sol}$ (k $\Omega$ )	$C_{dl}$ (nF)	$C_g$ (pF)
T= 0 min	193.9	235.2	61.72
T= 30 min	110	270.7	60.9
% $\Delta$	-43	15	-1.3

#### 7.4.2 Detection of *E. coli* O157:H7

As stated in Section 7.4.1, the impedance change was found to be the largest at the frequency of 1 kHz. Fig. 7.6 shows the average impedance changes ( $\Delta Z = Z_{t=0} - Z_{t=30}$ ) for the detection of each *E. coli* O157:H7 concentration. A linear relationship ( $R^2 = 0.88$ ) was found between the log value of the bacteria concentration ( $C_{bact}$ ) and the impedance change in k $\Omega$  ( $\Delta Z$ ) that corresponded to  $\Delta Z = 17C_{bact} - 19.5$ . The calculated lower detection limit was determined to be  $10^{1.6}$  cfu ml<sup>-1</sup>. Only the concentrations of  $10^3$  and  $10^4$  cfu ml<sup>-1</sup> were found to not be significantly different, indicating the developed aptasensor was capable of quantitative measurement. The lower detection limit corresponded to the detection of only  $\sim 8$  *E. coli* O157:H7 cells in a 200  $\mu$ l sample, as calculated in equations 7.1 and 7.2.

$$\text{Cells per ml} = 10^{1.6} \approx 39 \text{ cells} \quad (7.1)$$

$$\text{Cells per sample} = 39/5 \approx 8 \text{ cells} \quad (7.2)$$

One other study has used aptamer-coated magnetic nanobeads and GOx/Con A gold nanoparticle labels to detect avian influenza virus (AIV) H5N1 (Fu et al., 2013). The GOx/Con A gold nanoparticles were the same that were used in this study, therefore it is possible to compare the two studies. The lower detection limit of that aptasensor was  $8 \times 10^{-4}$  HAU which corresponded to  $\sim 3200$  virus particles in the detection sample (Killian, 2008). Fu et al. (2013) showed that a GOx concentration of 1 pM decreased the impedance of a 100  $\mu\text{l}$  10 mM glucose solution by 14 k $\Omega$  after 30 min. Since the 100  $\mu\text{l}$  sample was known to contain  $6.02 \times 10^7$  GOx molecules it is possible to calculate the impedance change caused by 1 molecule of GOx, as shown in equation 7.3.

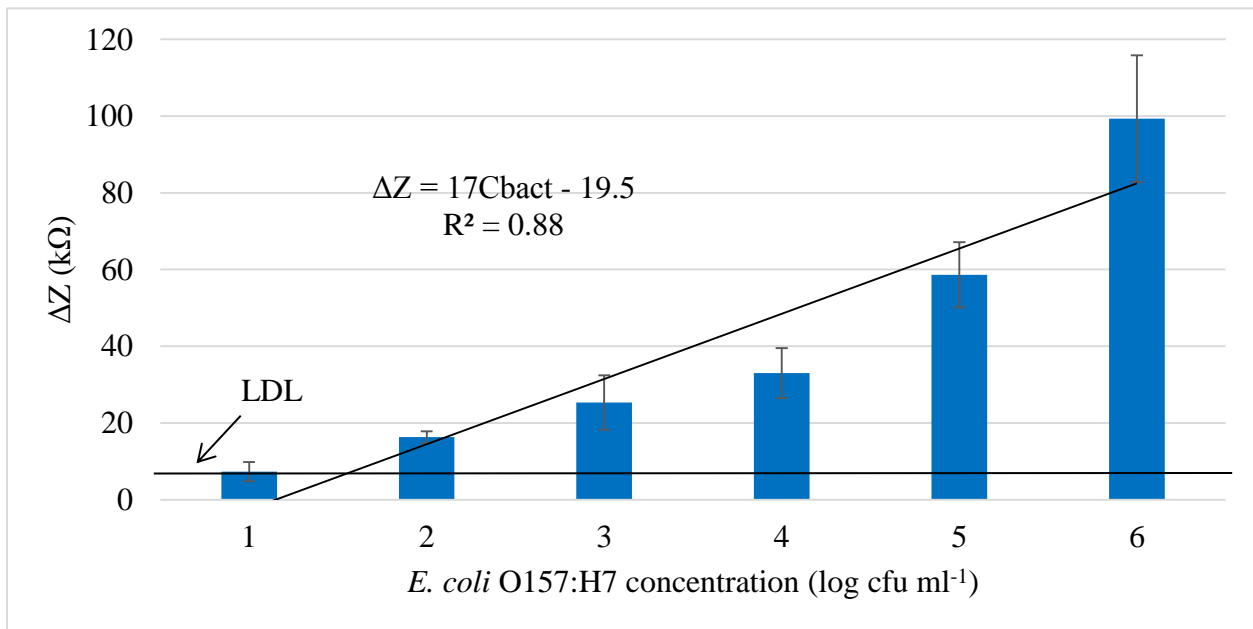


Fig. 7.5. Average impedance change at 1 kHz between 0 min and 30 min after introduction of glucose solution for detection of *E. coli* O157:H7. Error bars were based on the standard deviation of means in triplicate tests. LDL line was determined by signal/noise ratio of 3.

$$\Delta Z \text{ per GOx molecule} = 14000 \Omega / 6.02 \times 10^7 = 2.33 \times 10^{-4} \Omega \quad (7.3)$$

With this it was possible to calculate the number of glucose molecules present in the H5N1 and *E. coli* O157:H7 samples. A 7.5 k $\Omega$  decrease was seen for an *E. coli* O157:H7 sample containing 8 cells so the total GOx molecules and GOx per cell could be calculated as shown in equations 7.4 and 7.5, respectively.

$$\text{GOx molecules per sample} = 7500 \Omega / 2.325 \times 10^{-4} = 3.23 \times 10^7 \text{ GOx molecules} \quad (7.4)$$

$$\text{GOx molecules per bacteria} = 3.23 \times 10^7 / 8 = 4.03 \times 10^6 \text{ GOx molecules} \quad (7.5)$$

Since an AIV H5N1 sample containing 3200 virus particles caused a 4.088 k $\Omega$ , the number of GOx molecules present in the sample and on each virus could be calculated as shown in equations 7.6 and 7.7.

$$\text{GOx molecules per sample} = 4088 \Omega / 2.325 \times 10^{-4} = 1.76 \times 10^7 \text{ GOx molecules} \quad (7.6)$$

$$\text{GOx molecules per virus} = 1.76 \times 10^7 / 3200 = 5.5 \times 10^3 \text{ GOx molecules} \quad (7.7)$$

Though the number of H5N1 viruses needed for detection was 400 times higher than what was needed for detection of *E. coli* O157:H7, the total surface area available for GOx/Con A gold nanoparticle binding was very similar between the *E. coli* test (62.8  $\mu\text{m}^2$ ) and the AIV H5N1 test (64.3  $\mu\text{m}^2$ ), though the impedance decrease caused by the two was different. Since the similar surface area of AIV H5N1 caused a smaller impedance decrease it can be concluded that the virus particles could not bind as many GOx/Con A gold nanoparticles per unit of surface area as the bacteria, likely due to steric hindrance on the surface of the much smaller virus particle. Since the availability of surface area and steric hindrance of binding to that surface area

correlated to the impedance decrease it is not unreasonable to think that this biodetection method could be used to detect larger targets, such as cancer cells or parasitic protozoa, at the single cell level.

The difference between the detection thresholds of the two aptasensors (AIV H5N1, 4.088 k $\Omega$ ; *E. coli*, 7.5 k $\Omega$ ) could be explained by differences in the preparation of the aptamer-coated nanobeads. Fu et al. (2013) used a blocking step with bovine serum albumin (BSA) after coating the nanobeads with aptamer. A blocking step was not used in this study because a decrease in capture efficiency was seen when using a blocking step. This likely allowed a small amount of GOx to become bound on the magnetic nanobeads, resulting in a higher threshold for detection. The fact that BSA blocking worked for the AIV H5N1 aptasensor and not the *E. coli* O157:H7 may be explained by the length of the aptamers used. The AIV H5N1 aptamer was 73 nt long while the *E. coli* O157:H7 aptamer was 37 nt long. The extra length of the AIV H5N1 aptamer may have allowed it to reach past the BSA block to bind its target, while the shorter *E. coli* O157:H7 aptamer was unable to bind its target when being blocked by the BSA. Using a blocking agent with a smaller size could possibly improve the sensitivity of the aptasensor while preserving capture efficiency, though even if the detection threshold was as low as the AIV H5N1 aptasensor the developed aptasensors detection limit would only decrease to 5 cfu *E. coli* O157:H7. This small increase in sensitivity would likely not warrant the extra time and resources required to prepare the aptamer-coated magnetic nanobeads.

The ultimate goal of many biosensor studies is to develop a biosensor sensitive enough to detect a single cell, though the detection is limited by the noise of the biosensor system. The noise of the negative control samples was found to be 2.5 k $\Omega$ , while the noise of the pure 10 mM glucose solution was found to be 1.3 k $\Omega$ . Each *E. coli* O157:H7 cell caused an impedance



decrease of roughly 940  $\Omega$ , well below the S/N ratio of 3. It could be possible that the use of electrodes with much smaller dimensions could decrease the noise of the system and thereby increase the sensitivity of the aptasensor (Varshney and Li, 2009), though many of the advantages of this system, such as low cost and ease of electrode regeneration, would be lost.

Since no chemicals or proteins were immobilized on the electrode surface, the regeneration procedure consisted of simply rinsing the electrode with deionized water and drying with a nitrogen stream. The simple and gentle regeneration method meant that only two screen printed interdigitated electrodes were needed throughout the entire study, greatly reducing costs and resources.

#### **7.4.3 Specificity of the aptasensor**

The impedance aptasensor was evaluated for specificity with non-target bacteria species or strains using the same procedure described in Section 7.3.6. The average impedance change between 0 min and 30 min is shown in Fig. 7.7. No non-specific interaction was seen for the non-target bacteria species *L. monocytogenes* and *S. Typhimurium*. The non-target strain of *E. coli* K12 showed no non-specific interaction either, indicating the impedance aptasensor was strain specific.

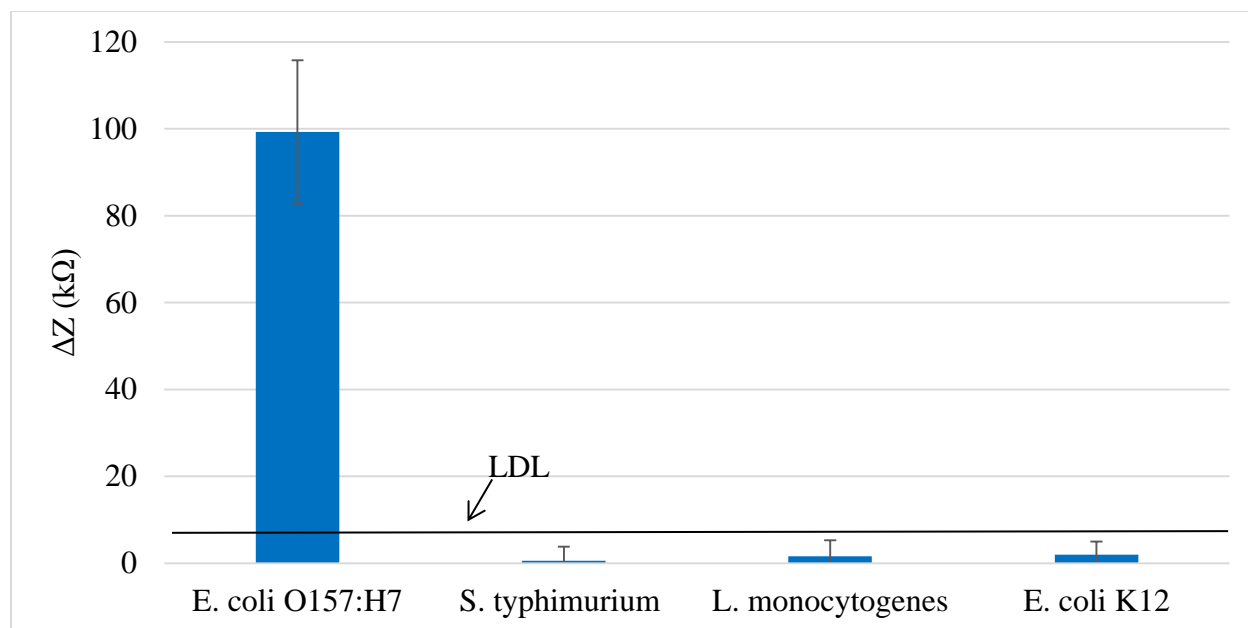


Fig. 7.6. Average impedance change at 1 kHz between 0 min and 30 min after introduction of glucose solution for specificity tests. Error bars based on the standard deviation of means in triplicate tests. LDL line was determined by a signal/noise ratio of 3.

## 7.5 Conclusion

In this study an impedance aptasensor was developed for the detection of *E. coli* O157:H7 using screen printed interdigitated electrodes, aptamer-coated magnetic nanobeads, and gold nanoparticles coated in GOx/Con A. The developed aptasensor was capable of specifically detecting *E. coli* O157:H7 within 1.5 h with a lower detection limit of 8 *E. coli* O157:H7 cells, a level below the estimated infectious dose. This detection limit was several orders of magnitude lower than previously designed aptasensors for *E. coli* O157:H7 detection and equal to the most sensitive antibody-based biosensors reported. Compared to the highly sensitive antibody-based biosensors, the fabrication and use of this aptasensor was much more simple and inexpensive.

The capability of this aptasensor to quantitatively detect *E. coli* O157:H7 was also an advantage over some other highly sensitive techniques.

The use of screen-printed interdigitated electrodes that could easily be regenerated and aptamers resulted in a highly cost effective detection method that could easily be used in an in-field setting. Since the aptasensor relied on the aptamer-coated nanobeads for specificity and used non-specific labels, this aptasensor design could conceivably be applied to any target that an aptamer has been developed for and has Con A binding sites available.

## 7.6 References

- Chan, K.Y., Ye, W.W., Zhang, Y., Xiao, L.D., Leung, P.H.M., Li, Y., Yang, M., 2013. *Biosens. Bioelectron.* 41, 532-537
- Chowdhury, A.D., De, A., Chaudhuri, C.R., Bandyopadhyay, K., Sen, P., 2012. *Sens. Actuators, B.* 171–172, 916-923
- Eum, N., Yeom, S., Kwon, D., Kim, H., Kang, S., 2010. *Sens. Actuators, B.* 143, 784-788
- FDA, “Bad Bug Book: Foodborne Pathogenic Microorganisms and Natural Toxins Handbook,” 2012.  
<http://www.fda.gov/downloads/Food/FoodSafety/FoodborneIllness/FoodborneIllnessFoodbornePathogensNaturalToxins/BadBugBook/UCM297627.pdf>. Accessed 2-19-2013.
- Fu, Y., Callaway, Z., Lum, J., Wang, R., Lin, J., Li, Y., 2014. *Anal. Chem.* 86, 1965-1971.
- Jiang, X., Wang, R., Wang, Y., Su, X., Ying, Y., Wang, J., Li, Y., 2011. *Biosens. Bioelectron.* 29, 23-28
- Killian, M.L., 2008. *Meth. Mol. Biol.* 436, 47-52
- Lin, Y., Chen, S., Chuang, Y., Lu, Y., Shen, T.Y., Chang, C.A., Lin, C., 2008. *Biosens. Bioelectron.* 23, 1832-1837
- Liu, F., Li Y., Su, X., Slavik, M., Ying, Y., Wang, J., *Sens. Instrum. Food Qual. Saf.*, 2007. 1, 161-168
- Miller, B.D., Rigdon, C.E., Ball, J., Rounds, J.M., Klos, R.F., Brennan, B.M., Arends, K.D., Kennelly, P., Hedberg, C., Smith, K.E., 2012. *J. Food Prot.* 75, 320-327

- Pendergrast, P.S., Marsh, H.N., Grate, D., Healy, J.M., Stanton, M., 2005. *J. Biomol. Tech.* 3, 224-234
- Poitras, C., Tufenkji, N., 2009. *Biosens. Bioelectron.* 24, 2137-2142
- Radke, S.M., Alocilja, E.C., 2005. *Biosens. Bioelectron.* 20, 1662-1667
- Rekow, C.L., Brashears, M.M., Brooks, J.C., Loneragan, G.H., Gragg, S.E., Miller, M.F., 2011. *Meat Sci.* 87, 361-365
- Santos, M.B., Aguil, J.P., Prieto-Simón, B., Sporer, C., Teixeira, V., Samitier, J., 2013. *Biosens. Bioelectron.* In Press.
- Scallan, E., Hoekstra, R., Angulo, F., Tauxe, R., Widdowson, M., Roy, S., Jones, J., Griffin, P., 2011. *Emerg. Infect. Dis.* 17, 7-15
- Settingington, E.B., Alocilja, E.C., 2011. *Biosens. Bioelectron.* 26, 2208-2214
- Shen, Z.Q., Wang, J.F., Qiu, Z.G., Jin, M., Wang, X.W., Chen, Z.L., Li, J.W., Cao, F.H., 2011. *Biosens. Bioelectron.* 26, 3376-3381
- So, H.M., Park, D.W., Jeon, E.K., Kim, Y.H., Kim, B.S., Lee, C.K., Choi, S.Y., Kim, S.C., Chang, H., Lee, J.O., 2008. *Small* 4, 197-201
- Song, S., Wang, L., Li, J., Fan, C., Zhao, J., 2008. *TrAC, Trends Anal. Chem.* 27, 108-117
- Subramanian, A., Irudayaraj, J., Ryan, T., 2006. *Biosens. Bioelectron.* 21, 998-1006
- Varshney, M., Li, Y., 2007. *Biosens. Bioelectron.* 22, 2408-2414
- Varshney, M., Li, Y., 2008. *Talanta* 74, 518-525
- Varshney, M., Li, Y., 2009. *Biosens. Bioelectron.* 24, 2951-2960
- Varshney, M., Li, Y., Srinivasan, B., Tung, S., 2007. *Sens. Actua. B.* 128, 99-107
- Wang, Y., Ye, Z., Si, C., Ying, Y., 2011. *Sensors (Basel)* 11, 2728-2739
- Wu, W., Zhang, J., Zheng, M., Zhong, Y., Yang, J., Zhao, Y., Wu, W., Ye, W., Wen, J., Wang, Q., Lu, J., 2012a. *PLoS One.* 7, e48999
- Wu, W.H., Li, M., Wang, Y., Ouyang, H.X., Wang, L., Li, C.X., Cao, Y.C., Meng, Q.H., Lu, J.X., 2012b. *Nanoscale Res. Lett.* 7, 658-276X-7-658

## 8. Conclusion

In this dissertation several avenues of research were conducted to develop impedance biosensors for both viral and bacterial targets. Avian influenza viruses H5N1 and H7N2 were chosen as the model viral targets for their significance to both the poultry industry and human health. *E. coli* O157:H7 was chosen as the model bacterial target due to its importance in food safety.

As part of developing an impedance biosensor for avian influenza virus H7N2, a DNA aptamer against avian influenza virus hemagglutinin H7 was developed using SELEX. Three aptamer sequences were obtained after 12 rounds of SELEX. Of the three, one (#3) had no affinity when used with whole virus, either due to it being a non-specific sequence that made it through selection or it being specific for an epitope not exposed on the viral hemagglutinin protein. Including whole virus into the selection process could help to eliminate aptamer sequences that bind to epitopes only found on the recombinant protein. A second aptamer sequence (#2) only showed good affinity when heated before binding. This suggests that the secondary structure that has the greatest affinity for the H7 protein is likely not the most thermodynamically stable structure. The #2 aptamer sequence is capable of forming a slightly different secondary structure with an extra hairpin loop near the 3' end. This form was only moderately less thermodynamically stable. It is possible that the extra hairpin loop contributed to the increase in affinity seen after heating the aptamer. Only one aptamer sequence (#1) was found to have good affinity for the H7 protein without any modification, such as heating. The #1 aptamer sequence fulfilled the objectives of the research to develop an aptamer for use in biosensors. In hindsight, several things could have been changed during the selection process to increase its efficiency. The whole virus could have been used as a selection target near the end of

SELEX to remove any aptamer sequences that bound to epitopes not present on the whole virus. The heating step between SELEX cycles could have been reduced or eliminated to select against aptamers that have low affinity in their lowest energy state. When developing aptamers for use in biosensors, care should be taken to consider how the aptamer will be used, and under which conditions it will be used.

The developed aptamer for H7 was applied alongside an existing DNA aptamer against AIV H5N1 in a microfluidics-based impedance biosensor for the detection of AIV H7N2 and H5N1. The small size of the aptamers allowed the developed aptasensor to have a lower detection level ( $2^7 \times 10^{-4}$  HAU) and higher repeatability than a similar previously designed biosensor based on antibodies. The developed aptasensor also did not require labels or sample pretreatment as the previous antibody-based biosensor, reducing the resources required and testing time. The total testing time for the biosensor was 30 min. Using the two aptamers in the same biosensor design allowed the comparison of the two aptamer binding strategies. The H7 aptamer targeted only the HA protein on the virus surface, of which there are ~400-500 present on each virus particle. The aptamer developed for detection of AIV H5N1 was designed to target only the H5N1 subtype and binds at a junction between the H5 and N1 proteins. Due to the fewer number of NA proteins on the viral surface and the requirement that the NA and HA proteins be in the correct orientation for binding, the number of available binding sites for the H5N1 aptamer was hypothesized to be lower than for the H7 aptamer and therefore more erratic. While a single H5N1 aptamer may have a high affinity to its target, the limited number of binding sites results in reduced avidity and capture efficiency. The experimental data supported this hypothesis in that the standard deviations for the detection of H5N1 were larger. The different binding schemes could also explain the differences seen in the  $\Delta Z$  values. Higher  $\Delta Z$  values were seen when

detecting AIV H5N1, possibly due to more virus being able to attach to the electrode surface. Since there were fewer binding sites on each virus it was plausible that an individual virus would take up less of the binding sites on the electrode surface, leaving binding sites open for other virus particles to attach. The aptamer against H7 had many more potential binding sites available on the virus surface, multiple aptamers on the electrode surface could bind a single virus particle, thus preventing those aptamers from binding more virus particles. While this may have reduced the  $\Delta Z$  values when detecting H7N2 it did reduce the standard deviations in those tests, due to higher avidity and a higher capture efficiency. This data suggests that aptamer binding schemes must be taken into consideration when developing and choosing which aptamers to use in an electrochemical biosensor, especially for influenza viruses. While a highly specific aptamer may be able to detect a single subtype, repeatability of the sensor may suffer. For a biosensor meant to be used for in-field tests an aptamer that only binds one protein may be a better choice.

The label-free biosensor for the detection of *E. coli* O157:H7 was capable of detecting ~1400 cells in less than 1 h using antibody-labeled magnetic nanobeads to concentrate the bacteria onto the surface of a screen-printed interdigitated electrode. When measuring impedance in the presence of a high ionic measuring solution the repeatability was high, with small standard deviations. A decrease in the amount of nanobeads used in the system would likely reduce noise and reduce the lower detection level but it was found that the capture efficiency would drop dramatically with a lower concentration of beads. Tests were also done to determine the necessity of the magnetic nanobeads. It was shown that the nanobeads were in fact necessary for the detection of *E. coli* O157:H7 cells. COMSOL Multiphysics software was used to build a computer model to confirm that the distance of the bacteria from the electrode surface was the primary factor in the impedance measurement. In the model it was shown that when the cells had

the greatest effect on impedance when less than 10  $\mu\text{m}$  from the electrode surface and had almost no effect when at distances greater than 25  $\mu\text{m}$ . While the designed biosensor did not have an impressively low lower detection limit, it did prove a proof of concept that inexpensive screen-printed interdigitated electrodes could be used in a simple biosensor to obtain highly repeatable results in a short amount of time.

A second impedance biosensor for the detection of *E. coli* O157:H7 was based on the same screen-printed electrodes described previously but also made use of aptamers and gold nanoparticles coated in GOx/Con A as labels. The biosensor was able to detect extremely low number of bacteria with a lower detection level of just 8 cells. This was equal to the most sensitive antibody-based reported in the literature and orders of magnitude more sensitive than any reported aptamer-based sensors. In addition to detect small numbers of cells the biosensor was also able to quantify bacteria at small concentrations, a feat unmatched by many other highly sensitive biosensing techniques. In comparing the *E. coli* O157:H7 sensor to a sensor for the detection of AIV H5N1 using the same method, it was found that the availability of binding sites for the nanoparticle labels was the primary sensitivity limitation. With this knowledge it is not unreasonable to suggest that a larger target, such as a cancer cell, could be detected on the single cell level. Because of the simple method described in the design of this biosensor it would be as simple as changing the aptamer specificity to modify the sensor to detect other targets. Another advantage of the designed biosensor was the reusability of the electrodes. A simple rinsing step was all that was needed to regenerate the electrode for another measurement. This would significantly reduce the cost of any commercialized biosensor based on this research.

The biosensors developed in this research for both viral and bacterial targets were shown to be viable concepts to expand upon for detection of other pathogens. The aptamer-based



biosensor for the detection of avian influenza virus H5N1 and H7N2 could easily be modified to detect other AIV subtypes and possibly other viruses simply by changing the aptamer specificity. Both of the biosensors for detection of *E. coli* O157:H7 were able to take advantage of inexpensive mass-produced screen-printed electrodes, dramatically lowering the cost per test and making biosensor use more feasible for everyday use.

## 9. Recommendations for Future Research

Further improvement on the biosensors could be accomplished by addressing several issues found during the research:

- a) For the aptamer-based biosensor for the detection of AIV, a shelf life study should be conducted to determine the feasibility of preparing electrodes beforehand. This would greatly reduce the required detection time and increase the practicality of the sensor as an in-field detection method.
- b) For the antibody-based biosensor for the detection of *E. coli* O157:H7, removal of the free nanobeads would likely increase the sensitivity of the biosensor. This could be accomplished using a magnetophoretic separation device or something similar, though this would increase the detection time and complexity.
- c) For the aptamer-based biosensor for the detection of *E. coli* O157:H7, it would be useful to expand the variety of potential targets by changing the specificity of the aptamer used.